Tectonics

RESEARCH ARTICLE
10.1029/2018TC005164

Reconstruction of Subduction and Back-Arc Spreading in the NW Pacific and Aleutian Basin: Clues to Causes of Cretaceous and Eocene Plate Reorganizations

Bram Vaes[1], **Douwe J. J. van Hinsbergen**[1], **and Lydian M. Boschman**[1]

[1]Department of Earth Sciences, Utrecht University, Utrecht, The Netherlands

Abstract The Eocene (~50–45 Ma) major absolute plate motion change of the Pacific plate forming the Hawaii-Emperor bend is thought to result from inception of Pacific plate subduction along one of its modern western trenches. Subduction is suggested to have started either spontaneously, or result from subduction of the Izanagi-Pacific mid-ocean ridge, or from subduction polarity reversal after collision of the Olyutorsky arc that was built on the Pacific plate with NE Asia. Here we provide a detailed plate-kinematic reconstruction of back-arc basins and accreted terranes in the northwest Pacific region, from Japan to the Bering Sea, since the Late Cretaceous. We present a new tectonic reconstruction of the intraoceanic Olyutorsky and Kronotsky arcs, which formed above two adjacent, oppositely dipping subduction zones at ~85 Ma within the north Pacific region, during another Pacific-wide plate reorganization. We use our reconstruction to explain the formation of the submarine Shirshov and Bowers Ridges and show that if marine magnetic anomalies reported from the Aleutian Basin represent magnetic polarity reversals, its crust most likely formed in an ~85- to 60-Ma back-arc basin behind the Olyutorsky arc. The Olyutorsky arc was then separated from the Pacific plate by a spreading ridge, so that the ~55- to 50-Ma subduction polarity reversal that followed upon Olyutorsky-NE Asia collision initiated subduction of a plate that was not the Pacific. Hence, this polarity reversal may not be a straightforward driver of the Eocene Pacific plate motion change, whose causes remain enigmatic.

Key Points:
- At 85-80 Ma, a plate reorganization occurred in the northern Pacific that included the formation of two subduction zones and the Kula plate
- Our reconstruction predicts that the Aleutian Basin crust formed between 85 and 60 Ma in a back-arc basin behind the Olyutorsky arc
- Subduction polarity reversal from Kamchatka to Sakhalin at ~50 Ma is not a straightforward driver of the Eocene Pacific plate motion change

Supporting Information:
- Supporting Information S1
- Table S1
- Data Set S1
- Data Set S2

Correspondence to:
B. Vaes,
b.vaes@uu.nl

Citation:
Vaes, B., van Hinsbergen, D. J. J., & Boschman, L. M. (2019). Reconstruction of subduction and back-arc spreading in the NW Pacific and Aleutian Basin: Clues to causes of Cretaceous and Eocene plate reorganizations. *Tectonics*, *38*, 1367–1413. https://doi.org/10.1029/2018TC005164

Received 30 MAY 2018
Accepted 4 MAR 2019
Accepted article online 12 MAR 2019
Published online 17 APR 2019

1. Introduction

A major event in the tectonic history of the Pacific region is a plate reorganization that occurred ~50 Ma (Müller et al., 2016; O'Connor et al., 2013; Seton et al., 2015; Torsvik et al., 2017; Whittaker et al., 2007). This reorganization is part of a wider, global plate motion change event which included changes in absolute plate motion of, for example, the Australian (Whittaker et al., 2007), South American (Oncken et al., 2006; Schepers et al., 2017), Caribbean (Boschman et al., 2014), and Indian plates (Copley et al., 2010; van Hinsbergen et al., 2011). For the Pacific plate, the sharp bend in the Hawaii-Emperor seamount chain dates the absolute plate motion change at ~47 Ma (Sharp & Clague, 2006; Torsvik et al., 2017; Whittaker et al., 2007). Recent studies based on numerical models suggested, however, that the bend may have resulted from a change in absolute plume motion relative to a continuously moving Pacific plate (e.g., Hassan et al., 2016; Tarduno et al., 2009). Although paleomagnetic data from the Emperor Seamounts indicate a southward drift of the Hawaiian hotspot from ~80 to 47 Ma (e.g., Tarduno et al., 2003), Torsvik et al. (2017) recently demonstrated that the formation of the Hawaii-Emperor bend cannot be explained without a significant change in absolute plate motion of the Pacific plate around 47 Ma.

The Eocene plate reorganization event holds key lessons on the driving mechanisms behind plate tectonics and is therefore widely studied. Current models invoke that the absolute plate motion change affecting the Pacific plate is the result of its first subduction along its modern western plate boundaries, including the Izu-Bonin-Marianas (Arculus et al., 2015; Ishizuka et al., 2011; Seton et al., 2015), and Aleutian and Kuril-Kamchatka Trenches (Domeier et al., 2017). Faccenna et al. (2012) postulated that the main driving force for the Pacific absolute plate motion change was the onset of slab pull acting on the Pacific plate following the inception of subduction of its western parts along the East Asia margin. This subduction has been postulated to have initiated (i) spontaneously at a transform plate boundary with an ill-defined plate whose relics are now preserved in the Philippine Sea plate (Arculus et al., 2015; Stern, 2004; Stern et al., 2012; Stern & Bloomer, 1992), (ii) after complete consumption of the conceptual Izanagi plate that contained

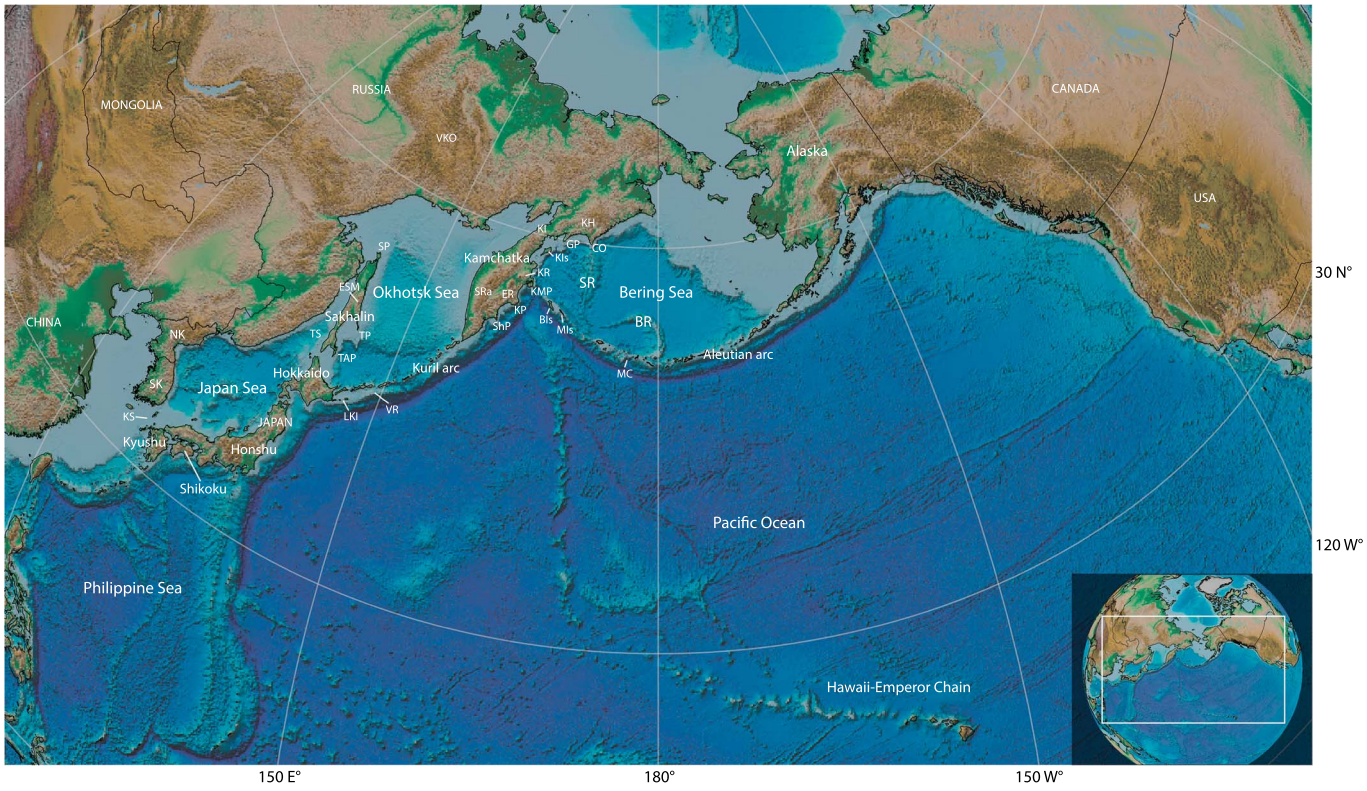

Figure 1. Geographic map of the northwest Pacific region. Country names are shown in capital letters. Key to abbreviations: BIs = Bering Island; BR = Bowers Ridge; CO = Cape Olyutorsky; ER = Eastern Ranges; ESM = East Sakhalin Mountains; GP = Govena peninsula; KH = Koryak Highlands; KI = Kamchatka isthmus; KIs = Karaginsky Island; KP = Kronotsky peninsula; KMP = Kamchatka Mys peninsula; KR = Kumroch Range; KS = Korea Strait; LKI = Lesser Kuril islands; MC = Murray Canyon; MIs = Medny Island; NK = North Korea; ShP = Shipunsky peninsula; SK = South Korea; SP = Schmidt peninsula; SR = Shirshov Ridge; SRa = Sredinny Range; TAP = Tonin-Aniva peninsula; TP = Terpeniya peninsula; TS = Tartary Strait; VKO = Verkhoyansk-Kolyma Orogen; VR = Vityaz Ridge.

the conjugate set of the marine magnetic anomalies preserved on the northwesternmost part of the Pacific plate (Seton et al., 2015; Whittaker et al., 2007), or (iii) after subduction polarity reversal following the collision of the Olyutorsky-East Sakhalin-Nemuro arc with NE Asia (Domeier et al., 2017). Domeier et al. (2017) proposed that this arc formed on the Pacific plate upon ~85–80 Ma intraoceanic subduction initiation at the Izanagi-Pacific ridge. This 85–80 Ma event itself is intriguing, since it is part of another Pacific-wide plate reorganization, including the formation of the Kula-Pacific and Pacific-Antarctica mid-ocean ridges (e.g., Mortimer et al., 2019; Wright et al., 2016).

The youngest marine magnetic anomalies preserved on the Pacific plate interpreted as conjugate to the Izanagi plate are Early Cretaceous in age, and all younger NW Pacific plate lithosphere has subducted (Seton et al., 2012). Timing of subduction of the Izanagi-Pacific ridge must thus be circumstantially inferred. Seton et al. (2015), for instance, inferred subduction of the Izanagi-Pacific ridge and the formation of a slab window below the east Asian margin from a disruption of arc magmatism in Korea and SW Japan from 55–50 to 43–42, and a gap in accretion in the Shimanto Belt of SW Japan between ~55 and 43 Ma, and extrapolated the thus inferred ridge subduction episode synchronously along the east Asian margin toward Kamchatka.

While continuous westward subduction below most of Japan throughout the Phanerozoic is well established from the Japanese accretionary prisms (Isozaki et al., 1990, 2010), the geology of the northwestern Pacific active margin hosts remnants of the long-recognized Late Cretaceous to Eocene Olyutorsky-East Sakhalin-Nemuro intraoceanic arc and ophiolites that are found on Kamchatka, Sakhalin, and East Hokkaido (Konstantinovskaya, 2001; Nokleberg et al., 2000; Parfenov et al., 2011; Shapiro & Solov'ev, 2009; Zharov, 2005; Figures 1 and 2). Paleomagnetic data indicate that formation of the island-arc rocks occurred at much lower paleolatitudes than expected for Eurasia and North America, suggesting that they

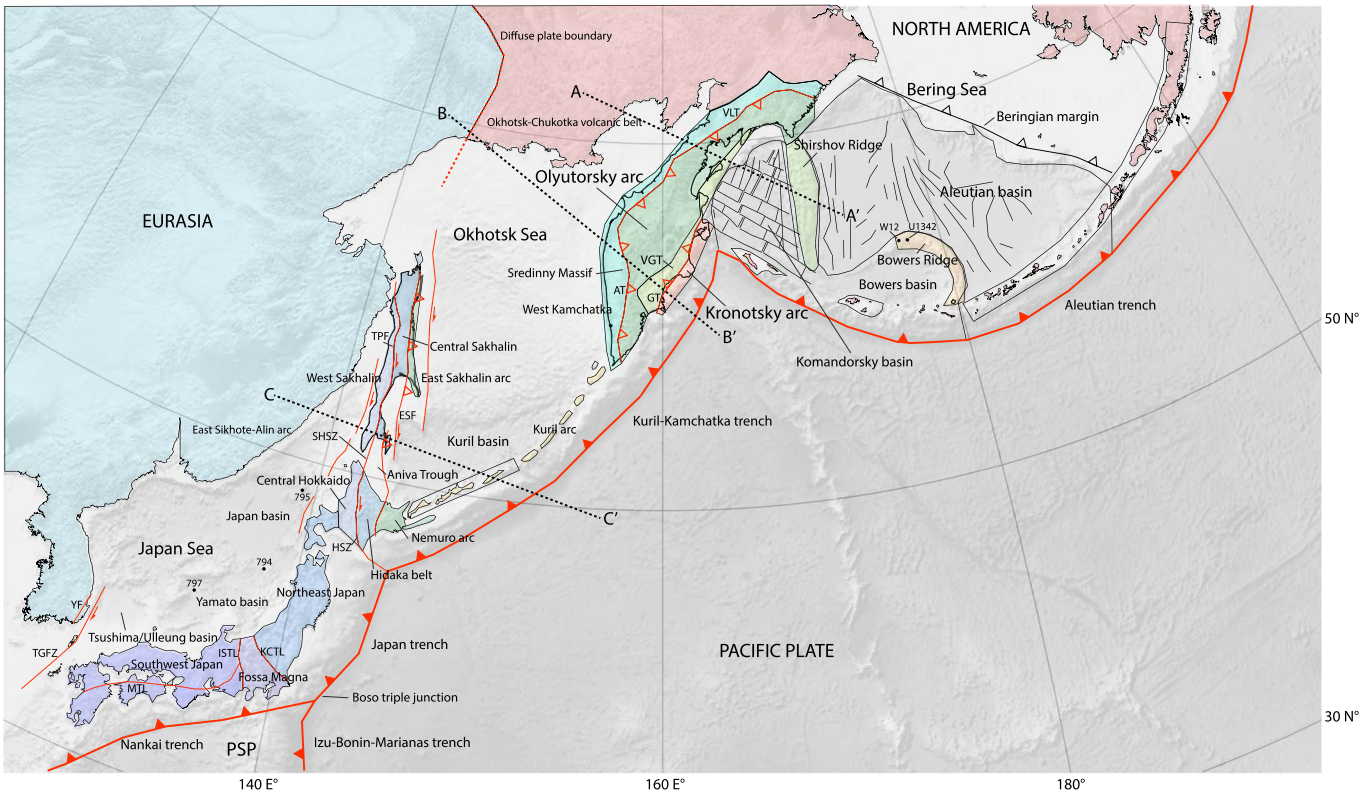

Figure 2. Simplified tectonic map of the northwest Pacific region. Major tectonic plates are given in capital letters. Colored polygons represent the tectonic blocks used in the reconstruction (see section 7 and Figures 9 and 10). Thick red lines with filled triangles indicate present-day subduction zones. Major faults are shown as thin red lines (after, e.g., Bogdanov & Khain, 2000; Fournier et al., 1994; Schellart et al., 2003). Key collisional sutures and extinct subduction zones are indicated with open triangles in red and black, respectively. Marine magnetic anomalies of the Komandorsky and Aleutian Basins used in this study are from the tectonostratigraphic terrane map of Nokleberg et al. (1996) and shown as thin black lines. These represent the magnetic anomaly patterns from Valyashko et al. (1993) for the Komandorsky Basin and Cooper et al. (1992) for the Aleutian Basin, respectively. Locations of drill sites are shown by black dots with a reference to the drill site number/code (see section 4; W12 = Wanke et al., 2012). Locations of cross-sections of Figure 3 are shown as dashed black lines. Abbreviations: AT = Andrianovka thrust; ESF = East Sakhalin fault; GT = Grechishkin thrust; HSZ = Hidaka Shear Zone; ISTL = Itoigawa-Shizuoka Tectonic Line; KCTL = Kashiwazaki–Choshi Tectonic Line; MTL = Median Tectonic Line; PSP = Philippine Sea plate; SHSZ = Sakhalin-Hokkaido Shear Zone; TGFZ = Tsushima-Goto fault zone; TPF = Tym-Poronaysk fault; VGT = Vetlovsky-Govena terrane; VLT = Vatyn-Lesnaya fault; YT = Yangsan fault.

must be exotic (e.g., Bazhenov et al., 1992; Konstantinovskaya, 2001; Shapiro & Solov'ev, 2009). These arcs are generally interpreted to have formed above southeastward-dipping, intraoceanic subduction within the northwest Pacific region, followed by a subduction polarity reversal in the Eocene (Domeier et al., 2017; Konstantinovskaya, 2001; Shapiro & Solov'ev, 2009). Domeier et al. (2017) recently noted that this intraoceanic subduction is not incorporated in the plate models that are used to investigate the cause of the Pacific plate motion change (e.g., Faccenna et al., 2012; Müller et al., 2016; Seton et al., 2012; 2015; Torsvik et al., 2017). Because geological data show that the Olyutorsky arc obducted onto the east Asian continental margin of Kamchatka from 55 to 45 Ma (Hourigan et al., 2009; Konstantinovskaya, 2001, 2011; Nokleberg et al., 2000; Shapiro et al., 2008; Shapiro & Solov'ev, 2009), and in the Middle Eocene on southern Sakhalin (Bazhenov et al., 2001; Zharov, 2005), conspicuously close to the timing of the Hawaii-Emperor bend, this subsequent subduction polarity reversal and inception of westward subduction at the modern Kuril-Kamchatka subduction zone at 50–45 Ma (Konstantinovskaya, 2001, 2011; Shapiro & Solov'ev, 2009) was therefore recently identified by Domeier et al. (2017) as a potential trigger of the Eocene plate reorganization and the formation of the Hawaii-Emperor bend.

Carefully restoring the Late Cretaceous-Eocene kinematic history of the plate that contained the Olyutorsky-East Sakhalin-Nemuro arc is thus key to assess whether the Pacific plate may have started subducting westward in the Eocene. However, several first-order observations have not been taken into account in kinematic reconstructions so far. First, the remnants of the Olyutorsky arc continue to north Kamchatka, well to the

north of the Aleutian subduction zone (Figure 2). Interestingly, subduction at the Aleutian subduction zone also started ~50 Ma, based on the oldest arc volcanic rocks in the Aleutians (Jicha et al., 2006; Layer et al., 2007). Initiation of this subduction is suggested to have trapped a fragment of oceanic crust, below the Aleutian Basin, that still lies east of the Olyutorsky arc below the Bering Sea (Figure 2), and may have been part of the same plate as the crust underlying the Olyutorsky arc (Scholl, 2007; Worrall, 1991) and thus hold clues to the NW Pacific plate motion history. Within the Bering Sea, the kinematic history of the Bowers and Shirshov Ridges, thought to be intraoceanic arc remnants, and the Komandorsky and Bowers Basins remain enigmatic (Chekhovich et al., 2012; Scholl, 2007; Shapiro & Solov'ev, 2009; Figure 2). Finally, a second, Kronotsky, intraoceanic island arc that formed ~85 Ma within the northwestern paleo-Pacific realm went extinct ~40 Ma, collided with Kamchatka ~10–5 Ma and is currently found structurally below the Olyutorsky arc (e.g., Konstantinovskaya, 2011; Shapiro & Solov'ev, 2009).

Between Kamchatka and Japan, the Sea of Okhotsk-Kuril back-arc basin opened after the Eocene arc-continent collision and disrupted the accreted Olyutorsky-East Sakhalin-Nemuro arc (Parfenov et al., 2011; Schellart et al., 2003). For the Sea of Japan back-arc basin, two competing models were proposed, either invoking trench-normal extension with oroclinal bending of the Japan arc (e.g., Martin, 2011; Otofuji et al., 1985), or transtensional opening with southward motion of Japan relative to Eurasia (e.g., Jolivet et al., 1994; Jolivet & Tamaki, 1992). The latter model would, if correct, significantly influence the restoration of the Nemuro arc.

To allow for quantitative analysis of NW Pacific plate motions, we first provide a detailed kinematic restoration of the post-accretionary deformation of the Olyutorsky-East Sakhalin-Nemuro arc due to back-arc basin formation and restore its links with the crust underlying the Bering Sea. We then use paleomagnetic data from the arc to further test whether the arc may have been part of the Pacific plate, as recently inferred (Domeier et al., 2017), or of a plate adjacent to the Pacific (e.g., Konstantinovskaya, 2011; Shapiro & Solov'ev, 2009). In addition, we restore the evolution of the Kronotsky arc and provide a new reconstruction of the kinematic evolution of the Bering Sea region, including the history of the Shirshov and Bowers Ridges and the spreading history of the oceanic crust of the Komandorsky and Bowers Basins. Our model covers the NW Pacific region from Japan to western Alaska (Figure 1). Finally, we compare the subduction evolution inferred by our reconstruction against the locations of subducted slabs in the mantle (e.g., van der Meer et al., 2018). We use our model to discuss the implications for the large-scale tectonic evolution of the Pacific realm, with an emphasis on the fate of the Izanagi-Pacific ridge and the possibility that the ~50 Ma NW Pacific arc-continent collision and polarity reversal drove the Pacific plate reorganization.

2. Approach

The present-day geological architecture of the NW Pacific region followed from the interplay between continent-hosting Eurasian and North American plates and several oceanic plates that originated in the Panthalassa Ocean. The relative motions between these large tectonic plates provide the boundary conditions for our plate-kinematic reconstruction of the region. Marine magnetic anomaly and fracture zone data from the Pacific plate were used to reconstruct major conceptual oceanic plates that contained the conjugate anomalies, including the Izanagi plate in the west and Farallon and Kula plates in the north and east (e.g., Engebretson, 1985; Müller et al., 2016; Seton et al., 2012; Woods & Davies, 1982; Wright et al., 2016). We develop our reconstruction in the GPlates plate reconstruction software (www.gplates.org; Boyden et al., 2011) and use the plate circuit of Seton et al. (2012), updated with Pacific reconstructions of Wright et al. (2016), as a basis. Our shape and rotation files are provided in the supporting information (Data Set S1).

As data input, we rely on available quantitative kinematic data, that is, data that provide information on the direction, magnitude, and/or timing of relative motion between geological units. We apply the following reconstruction hierarchy, adapted from Boschman et al. (2014). We first restore extensional records, as these provide the most complete geological record at the end of the deformation event. If available, we use marine magnetic anomaly-derived isochrons to constrain the direction and rate of seafloor spreading in an oceanic basin. Second, we use estimates of the amount and direction of continental extension. Third, we use transform and strike-slip fault displacements. Although the exact amount of displacement may not be determined, strike-slip and transform faults provide clear constraints on the orientation and direction of

relative motion between adjacent units. Next, we use records of contractional deformation. At the end of a collisional event, the minimum geological record is preserved, therefore only providing an estimate of the minimum amount of shortening. In the case of oceanic subduction, these records may be very incomplete, as shown by Isozaki et al. (1990) for the accretionary belts of the Japanese islands. We use stratigraphical or geochronological constraints to determine the timing of accretion of a geological unit from one tectonic plate onto another, and subsequently use the plate circuit to estimate the location of the unit in the period prior to the accretion event.

We fine-tune the reconstruction in such a way that for areas where limited kinematic data are available, geometrical consistency is ensured, that is, no overlaps or "gaps" between geological units should be present without geological evidence for extension or shortening. Any modifications to the reconstruction to make sure that it remains geometrically consistent are regarded as model predictions and will be clearly indicated in the reconstruction section. Also, our reconstruction should be in accordance with the basic rules of plate tectonics, stating that all tectonic plates are surrounded by plate boundaries that end in triple junctions (Cox & Hart, 2009). If relative motion between geological units is inferred, then there is a discrete fault or plate boundary between them.

After obtaining a tectonic model of the NW Pacific region based on quantitative geological data, we test our reconstruction twice with independent data sets. First, we test it against available paleomagnetic data. We use the thereto developed APWP tool by Li et al. (2017) that is integrated into the statistics portal of the n platform of Paleomagnetism.org (Koymans et al., 2016). This tool allows calculating a Global Apparent Polar Wander Path (whereby we used the version of Torsvik et al., 2012) in the coordinates for any element in the reconstruction. To this end, we calculate total reconstruction Euler poles of a tested element (e.g., polygon) in 10 Myr intervals relative to South Africa, using the global plate circuit of Seton et al. (2012), including the updates of Wright et al. (2016) for the Pacific region. This procedure allows for testing the paleomagnetic declinations and inclinations predicted by our reconstruction against published paleomagnetic data for key reconstructed elements, and iteratively adjusting our kinematic restorations where needed provided these remain consistent with available structural constraints.

Second, we test our updated kinematic reconstruction, consistent with paleomagnetism, against seismic tomography. Our tectonic model contains several (extinct) subduction zones, which can be compared with tomographic images of the upper and lower mantle (e.g., Domeier et al., 2017; van der Meer et al., 2018; www.atlas-of-the-underworld.org). Positive wave speed anomalies in the mantle may be linked to (detached) subducted plates, and therefore, to the locations of (former) subduction. To compare the locations of inferred slab remnants in the mantle with our reconstruction, we place the reconstruction in a global moving hotspot reference frame (Doubrovine et al., 2012) and we gain insight into the geodynamical assumptions of trench advance, retreat, or stationarity that are required to make our reconstruction consistent with the present-day mantle structure.

3. Plate Circuit and Marine Magnetic Anomaly-Based Isochrons

The tectonic framework for our reconstruction is provided by the relative motions of the Eurasian, North American, and Pacific plates, which are linked by a global plate circuit. The Euler rotation poles that quantitatively describe the motion between these and other major tectonic plates are calculated from records of past seafloor spreading, which are constrained by marine magnetic anomalies and transform fault/fracture zone data. The motion of the Pacific plate relative to Eurasia and North America is constrained by the plate circuit through Antarctica and Africa. We use the rotation poles of Wright et al. (2016), which include poles from Wright et al. (2015) and Croon et al. (2008), for the motion of the Pacific plate relative to West Antarctica, and the poles of Granot et al. (2013) for West Antarctica relative to East Antarctica. The motion of East Antarctica relative to Africa is constrained by combining the poles of Royer and Chang (1991), Bernard et al. (2005), and Cande et al. (2010), with minor motion between Somalia and South Africa restored according to Horner-Johnson et al. (2007) and Lemaux et al. (2002). We apply the reconstruction poles of Müller et al. (1999) for the relative motion of North America with respect to Africa. For Eurasia relative to North America we use recent reconstructions of the opening of the northern Atlantic based on the high-resolution rotation poles of DeMets et al. (2015) for the Neogene and the poles of Gaina et al. (2002) for older times. The motions of the oceanic Farallon, Kula, and Izanagi plates relative to the Pacific plate are

determined from the magnetic anomalies that are preserved on the Pacific plate. For our reconstruction we use the poles of Seton et al. (2012) for the Izanagi plate and the recent compilation of Wright et al. (2016) for the Kula and Farallon plates.

The northwest Pacific region includes a number of marginal basins that are (partly) underlain by oceanic crust. Following the reconstruction hierarchy outlined in the previous section, we would ideally base our reconstruction of these basins on available marine magnetic anomaly data. However, the marine magnetic anomalies in this region are often poorly constrained or poorly dated. We summarize the available observations for each basin below.

In the Japan Sea (Figure 1), several NW-SE oriented marine magnetic anomalies were identified in the eastern part of the Japan Basin (Isezaki, 1986; Seama & Isezaki, 1990), but no conclusive age correlation was made (Fukuma et al., 1998; Isezaki, 1986; Jolivet & Tamaki, 1992). No magnetic anomalies indicative of seafloor spreading have been observed in other basins in the Japan Sea despite their possible oceanic nature, perhaps owing to the formation of sill-sediment complexes (Fukuma et al., 1998). Marine magnetic lineations are also absent in the oceanic Kuril Basin (Figure 2). The Komandorsky Basin, located between Kamchatka and the Shirshov Ridge, contains NE-SW fossil spreading centers and magnetic anomalies and NW-SE striking fracture zones (Baranov et al., 1991; Cooper et al., 1976), with estimated age of formation between 10 and 20 Ma (Valyashko et al., 1993; Figure 2). We use these as input for our Komandorsky basin reconstruction.

Marine magnetic data of the Aleutian Basin (Figure 2) shows a set of roughly north-south-trending magnetic anomalies (see, e.g., Figure 4 in Cooper et al., 1992, or Figure DR1 in the supporting information of Steinberger & Gaina, 2007). These anomalies were initially correlated with the Early Cretaceous M1-M13 sequence (Cooper et al., 1976), that is, ~128–138 Ma (Ogg et al., 2016). Later, Cooper et al. (1992) cautioned that this age determination remains uncertain. Steinberger and Gaina (2007) tentatively suggested that the most prominent north-south-oriented magnetic lineations in the eastern part of the basin may correspond to chron 34 (~84 Ma) to chron 32 (~71 Ma). Although no definitive correlation with the magnetic polarity timescale has been made, the north-south-trending anomalies are generally interpreted as being formed by seafloor spreading (Cooper et al., 1976, 1992; Scheirer et al., 2016; Scholl, 2007; Steinberger & Gaina, 2007). In addition to the main set of N-S-trending anomalies, several enigmatic NE-SW oriented magnetic anomalies were traced on the northwest of the Aleutian Basin, interpreted by Cooper et al. (1992) to have formed in a Cenozoic back-arc spreading center. This structure, named the "Vitus arch," was instead interpreted by Chekhovich et al. (2012) as a large push-up structure formed along a large strike-slip fault during the Middle Eocene. However, a recent seismic study of the crustal structure of the Aleutian Basin across the Vitus Arch by Christeson and Barth (2015) found no evidence for Cenozoic spreading or push-up structures and we do not reconstruct significant Cenozoic deformation in this region.

Several north-south-oriented magnetic lineations have been observed in the eastern part of the Bowers Basin, separated from the Aleutian Basin by the Bowers Ridge (Cooper et al., 1976). No reliable match with published reversal time scales has been made so far. Cooper et al. (1976) initially suggested that the anomalies may correlate with the anomalies in the Aleutian Basin. In a later paper, however, Cooper et al. (1992) considered this correlation unlikely and suggested that the Bowers Basin formed in Eocene to Oligocene times by back-arc spreading behind the Bowers Ridge, due to eastward rollback of the Bowers subduction zone.

4. Review

4.1. General Outline

The northwest Pacific region, from Japan to Alaska, hosts a system of linked subduction zones located at the Japan, Kuril-Kamchatka, and Aleutian Trenches (Figure 2). These trenches form a continuous convergent plate boundary between the subducting oceanic Pacific plate and continental and oceanic lithosphere of the Eurasian and North American plates, which share a diffuse plate boundary through the Verkhoyansk-Kolyma orogen of NE Siberia (Figures 1 and 2). This present-day plate configuration is thought to have been established during Eocene times (~50–40 Ma, e.g., Domeier et al., 2017; Seton et al., 2012; Wright et al., 2016). Prior to this time, during the Early to mid-Cretaceous, the northern half of the proto-Pacific Ocean

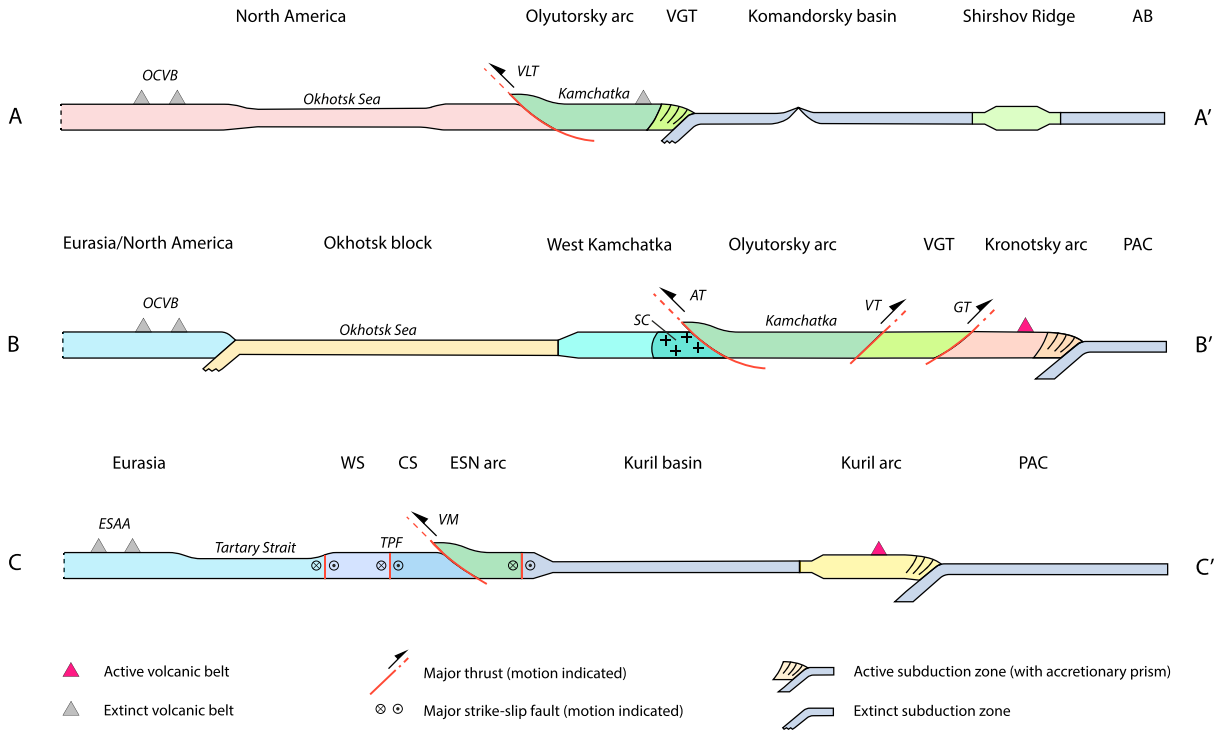

Figure 3. Schematic cross-sections of the geological structure of the northwest Pacific region. Locations are shown in Figure 2. See legend for an explanation of the different symbols. Abbreviations: AB = Aleutian Basin; AT = Andrianovka thrust; CS = Central Sakhalin; ESAA = East Sikhote-Alin arc; ESN arc = ast Sakhalin-Nemuro arc; GT = Grechishkin thrust; OCVB = Okhotsk-Chukotka volcanic belt; PAC = Pacific plate; SC = Sredinny Complex; TPF = Tym-Poronaysk fault; VGT = Vetlovsky-Govena terrane; VLT = Vatyn-Lesnaya thrust; VM = Vavai mélange zone; VT = Vetlovsky thrust; WS = West Sakhalin.

was floored by the major Izanagi, Farallon, and Pacific plates, which were separated by mid-ocean ridges (Engebretson, 1985; Wright et al., 2016; see Figure S1). Magnetic anomalies preserved on the Pacific plate suggest that at or before ~83 Ma a new oceanic plate, the Kula plate, formed out of lithosphere that previously belonged to the Pacific, Izanagi, and Farallon plates (Wright et al., 2016). Magnetic anomalies indicate that spreading between the Kula and Pacific plates continued until ~40 Ma (Wright et al., 2016). The Izanagi, Farallon, and Kula plates have now been almost completely lost to subduction.

The present-day trenches of the northwest Pacific region are separated from the stable Eurasian or North American plates by zones of intense deformation including marginal, partly oceanic basins, accretionary orogens, and ophiolite belts, as well as active and inactive volcanic arcs. Figure 3 shows schematic cross-sections of the geological structure of the northwest Pacific region, from the stable continent toward the oceanic basins. The region includes three major marginal basins: the Japan Sea, Okhotsk Sea, and Bering Sea (Figure 1). The Japanese islands, located between the Japan Sea back-arc basin and the Nankai and Japan Trenches (Figure 2), consist of the Japan accretionary prisms that hosts a discontinuous record of ocean-derived sedimentary and volcanic rocks as well as foreland basin sediments (Isozaki et al., 1990, 2010). On top of the accretionary prism is the active Japan volcanic arc, associated with the subduction below its two trenches. The northernmost large island of Japan, Hokkaido, consists mainly of accretionary prism units. Its geological structure includes Mesozoic accretionary prism units including ophiolites, HP-LT metamorphic rocks, and thick forearc basin deposits (Ueda, 2016). The N-S-trending subduction-related terranes that form the basement of central Hokkaido continue northward on the island of Sakhalin. The Cretaceous-Paleocene East Sikhote-Alin arc forms the volcanic arc associated with the subduction below Hokkaido and Sakhalin (Kemkin et al., 2016; Martynov et al., 2017; Nokleberg et al., 2000; Parfenov et al., 2009; Tang et al., 2016; Figures 2 and 4). Structurally above the units interpreted to belong to Eurasia, or on Hokkaido separated from Eurasia by a strike-slip fault, are the Late Cretaceous to early Paleogene East Sakhalin-Nemuro island-arc units found on east Hokkaido and east Sakhalin (e.g., Nokleberg et al., 1996, 2000; Ueda, 2016; Zharov, 2005; Figures 2–4). The Kuril volcanic arc, associated with the subduction of

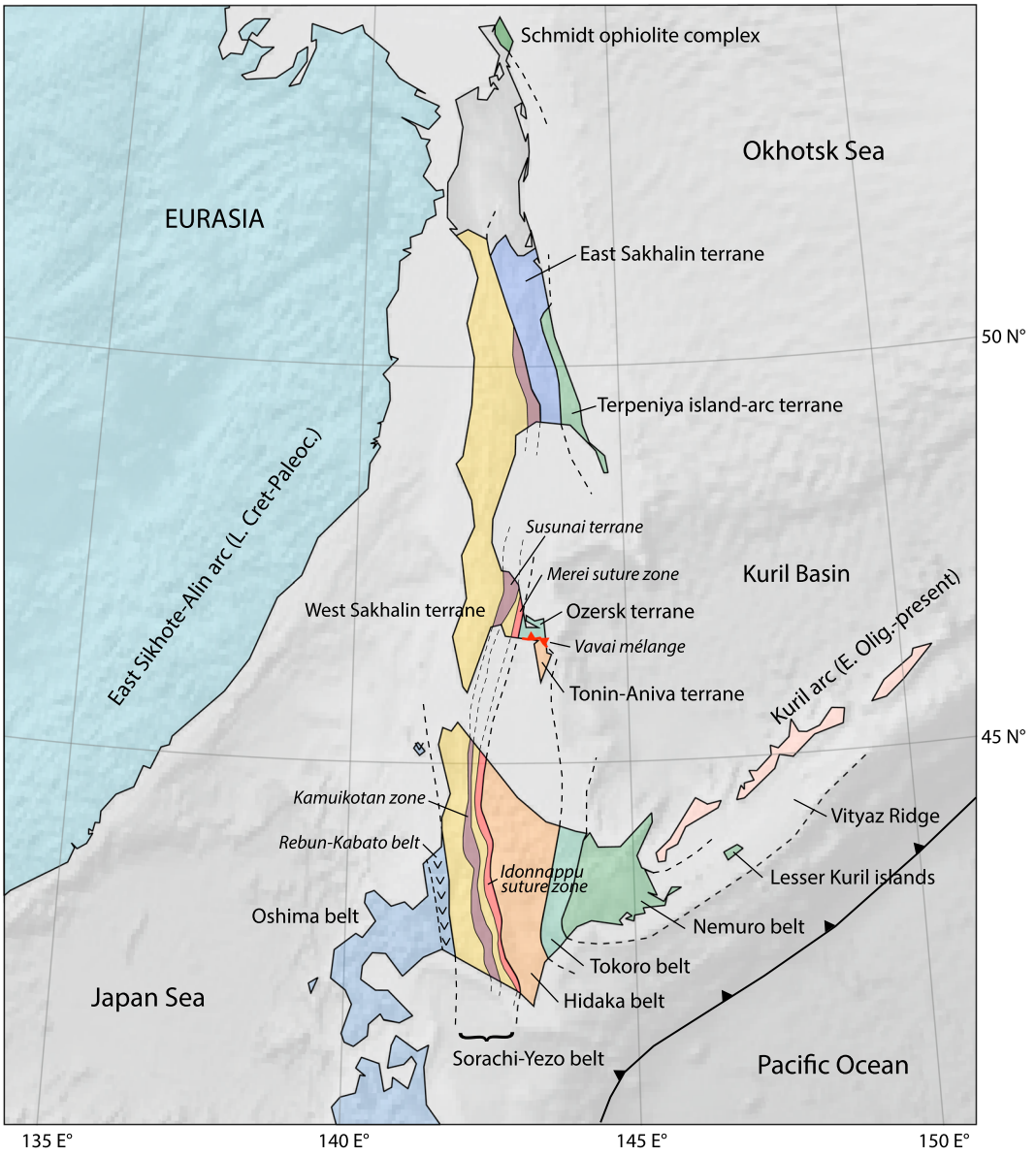

Figure 4. Schematic map of the basement terranes and belts of Hokkaido and Sakhalin. Sub-belts are denoted in italics. Dashed lines indicate the inferred location of the terrane/belt boundaries. Note that the (Mesozoic) terranes of the east Asian continent are not shown. Based on figures by, for example, Zharov (2005), Ueda (2016), and Liao et al. (2018).

the Pacific plate below the Kuril Trench, extends from eastern Hokkaido to the Kamchatka peninsula (Figures 1 and 2), with the oldest magmatic rocks dated as Early Oligocene (De Grave et al., 2016). Behind the Kuril arc is the wedge-shaped oceanic Kuril Basin (Figure 2). North of the Kuril Basin is the extensional Okhotsk Basin, underlying the marginal Okhotsk Sea. The Okhotsk Sea is separated from the East Sakhalin-Nemuro island-arc units on top of the eastern part of Sakhalin Island by a major dextral strike-slip system (Fournier et al., 1994; Schellart et al., 2003; Worrall et al., 1996; Figure 3). To the east, the Kamchatka peninsula consists of an accretionary prism and an active volcanic arc, associated with the subduction of the Pacific plate below the Kamchatka Trench. The basement of Kamchatka largely consists of Cretaceous ophiolites and Upper Cretaceous-lower Paleogene island-arc rocks of the Olyutorsky arc that are structurally above the basement rocks of NE Siberia to the west (e.g., Konstantinovskaya, 2011; Shapiro & Solov'ev, 2009). To the east, the Olyutorsky arc terrane structurally overlies the Paleogene accretionary prism units of the Vetlovsky-Govena terrane (Figure 3). Remnants of a second intraoceanic island-arc, the Late Cretaceous-Eocene Kronotsky arc, are found structurally below the Vetlovsky-Govena terrane on the

eastern peninsulas of Kamchatka (e.g., Alexeiev et al., 2006; Konstantinovskaya, 2011). East of Kamchatka lies the Bering Sea region, which is separated from the Pacific Ocean Basin by the Aleutian arc (Figure 1). The Aleutian arc extends from the Kamchatka Strait in the west—approximately 200 km east of the Kamchatka Mys Peninsula—to Alaska in the east. The Bering Sea comprises three oceanic basins: the Neogene Komandorsky Basin, and the Aleutian and Bowers Basins (Figure 2). Importantly, the precise age of the oceanic crust below the Aleutian and Bowers Basins is still unknown. The basins are bounded in the (north)east by the submarine Bowers and Shirshov Ridges. In the following, we review the geological records summarized above in detail, focused on kinematic constraints that allow reconstructing the Late Cretaceous to present tectonic history of this region, from south to north (east).

4.2. Japan Sea Region

4.2.1. Japan Fold-Thrust Belt

Japan lies in an overriding plate position relative to both the subducting Philippine Sea plate at the Nankai Trench and the Pacific plate at the Japan Trench (Figure 2). These trenches meet in the Boso trench-trench-trench triple junction, just southeast of Central Honshu, together with the intraoceanic Izu-Bonin-Marianas Trench where the Pacific plate subducts below the Philippine Sea plate (Figure 2). Japan is characterized by an accretionary fold-thrust belt composed of rocks derived from subducted oceanic lithosphere as well as trench-fill deposits derived from the overriding plate (e.g., Isozaki et al., 1990). The Japan fold-thrust belt is generally subdivided into a southwestern (including western Honshu, Shikoku, and Kyushu) and a northeastern (including northern Honshu and Hokkaido) segment. The boundary region between these is the structurally complex Fossa Magna region (Figure 2).

The Japan fold-thrust belt consists of an overall eastward and structurally downward younging series of accretionary complexes intruded by arc-related intrusives and was constructed over a ca. 600 Myr subduction history (Isozaki et al., 2010). During this period of successive accretion of crustal units from subducting oceanic lithosphere, the fold-thrust belt has grown for several hundreds of kilometers in the direction of the present-day Pacific Ocean.

In the southwestern segment, a large Mesozoic ENE-WSW-trending dextral strike-slip fault known as the Median Tectonic Line separates an older Inner Zone with lower Paleozoic granites and gneisses to the north from a younger Outer Zone with anchimetamorphic Upper Cretaceous to Paleogene trench-fill sediments to the south (Isozaki et al., 2010; Van Horne et al., 2017; Figure 2). No such distinction in the pre-Neogene bedrock was made in NE Japan, where the Median Tectonic Line and the Inner and Outer Zones are absent. In NE Japan, the bedrock is mainly composed of Paleozoic shallow marine sediments, unmetamorphosed Mesozoic accretionary sediments, and Mesozoic granitic intrusive rocks (Van Horne et al., 2017; and references therein).

The tectonic boundary between the NE and SW Japan is the Fossa Magna region (Martin, 2011): a diffuse zone of deformation bounded by the NNW-SSW-trending Itoigawa-Shizuoka Tectonic Line in the west and the NW-SE-trending Kashiwazaki-Choshi Tectonic Line in the east (Kato, 1992; Martin, 2011; Figure 2). The Fossa Magna region underwent Early to Middle Miocene subsidence and extension (Kato, 1992; Martin, 2011; Takeuchi, 2004). Extensional structures strike perpendicular to the fold-thrust belt and trench, and accommodated trench-parallel stretching (Martin, 2011; H. Sato et al., 2004; Takeuchi, 2004) of at least 25 km and perhaps up to 60 km of extension in the north and at least 40 km and perhaps up to 200 km in the south (Elouai et al., 2004; Martin, 2011; H. Sato et al., 2004), opening basins with 5–10 km of sediments (Kato, 1992).

After the early Middle Miocene, inversion led to the separation of north and south Fossa Magna (Kato, 1992; H. Sato et al., 2004; Takeuchi, 2004). The amount of shortening in the northern Fossa Magna Basin since the late Neogene varies from 11 km since the Late Miocene in the north to 23 km since the Middle Miocene in the south (Elouai et al., 2004; H. Sato et al., 2004). This along-strike diachroneity may relate to the (north) eastward migration of the Bono triple junction and the subducting Izu-Bonin arc relative to the Japan fold-thrust belt (Kato, 1992; Martin, 2011).

4.2.2. Japan Sea

The Japan fold-thrust belt and overlying arc became separated from the continental crust of the Eurasian plate in Late Oligocene to Middle Miocene times by the opening of the Sea of Japan back-arc basin (e.g.,

Jolivet et al., 1994; Jolivet & Tamaki, 1992; Martin, 2011; Otofuji et al., 1985; Sato, 1994; Van Horne et al., 2017). The Japan Sea consists of three main basins: the Japan Basin, the Yamato Basin, and the Tsushima or Ulleung Basin (Figure 2). Only the Japan Basin is underlain by typical oceanic crust, based on its structure and crustal thickness of ~8 km (Hirata et al., 1992; T. Sato et al., 2014). The Yamato and Tsushima/Ulleung Basins are underlain by crust with a thickness of 12–16 km (Hirata et al., 1989; Kim et al., 1998, 2003; Nakahigashi et al., 2013; Nishisaka et al., 2001; Sato et al., 2006, 2014; T. Sato et al., 2014; Yoon et al., 2014), interpreted as either thickened oceanic crust (Cho et al., 2004; Kim et al., 1998, 2003; T. Sato et al., 2014; Van Horne et al., 2017) or strongly attenuated island-arc crust (Jolivet & Tamaki, 1992; Nakahigashi et al., 2013; Sato et al., 2006; Tamaki et al., 1992; Yoon et al., 2014). The deep major basins are separated by basement highs with a continental (or arc) crustal thickness of about 18–22 km (Martin, 2011; Sato et al., 2006). Stretched continental crust also borders the eastern Russian margin and northeastern Honshu (Nakahigashi et al., 2013; Nishisaka et al., 2001), where it forms a transition zone between the Japan Sea Basin and the ~35 km thick crust of the Japan fold-thrust belt and arc (Iwasaki et al., 2013). A narrow, 50-km-wide zone of ~10 km thick (excluding sediments), thinned continental crust separates the Tsushima/Ulleung Basin from the Korean peninsula, which has a ~30 km crustal thickness (Kim et al., 1998, 2003; Sato et al., 2006).

The oceanic crust of the Japan Sea Basin has been dated by ^{40}Ar-^{39}Ar dating of basalts recovered by the Oceanic Drilling Program Leg 127/128 at Site 795 (Figure 2), providing an age range of 23.7 $\pm$ 1.2 to 17.1 $\pm$ 0.6 Ma (Kaneoka, 1992), although the reliability of these plateau ages has been questioned (Nohda, 2009). Basalt samples from Sites 794 and 797 (Figure 2) in the Yamato Basin showed ages from 21.2 $\pm$ 0.8 to 17.7 $\pm$ 0.5 Ma (Kaneoka, 1992) and tuffs overlying the basalts at Site 794 (east Yamato Basin) are dated as 14.9 $\pm$ 0.2 Ma (Barnes, 1992), suggesting that mafic magmatism ceased between 17.7 and 14.9 Ma (Nohda, 2009). Sediments directly overlying the basaltic basement at the different ODP sites were biostratigraphically dated at 13 to 18.5 Ma (Tamaki et al., 1992).

Estimates for the age of onset of extension between the Asian mainland and NE Japan prior to the ~20 Ma onset of oceanic crust formation in the Japan and Yamato Basins (Kaneoka, 1992; Nohda, 2009) range from the Oligocene to the earliest Miocene (e.g., Jolivet & Tamaki, 1992; Martin, 2011; Van Horne et al., 2017). Kano et al. (2007) argued that slow initial extension and subsidence may have occurred as early as 35 Ma, indicated by thin deposits of shallow marine sediments, but most authors assume that major extension started around 23 Ma (Ingle, 1992; Jolivet & Tamaki, 1992; Nakajima, 2013; Sato, 1994; van der Werff, 2000; Van Horne et al., 2017; Yoshida et al., 2014). Detailed seismic reflection studies between Korea and Japan (e.g., Cukur et al., 2015; Kim et al., 1998, 2007, 2015; Lee & Kim, 2002; Yoon et al., 2014) also suggested that the separation of SW Japan from the Korean peninsula started around 23 Ma (G-B Kim et al., 2011; Kim et al., 2007, 2015; Lee & Kim, 2002).

Van Horne et al. (2017) estimated that a total of ~500 km of extension occurred in the northeastern Japan Sea. Structural and seismic investigations suggest that the eastern Japan Sea margin experienced ESE-directed, that is, trench-perpendicular, extension from ~17 to 18 Ma, following the main phase of spreading in the Japan Sea (Sato, 1994; van der Werff, 2000). Rifting affected a ~100- to 150-km-wide zone of the western margin of present-day NE Honshu, leading to extensional basin formation and rapid subsidence (Martin, 2011; Nakajima, 2013; Yoshida et al., 2014). Hisada et al. (2008) and S. Kojima et al. (2008) suggested that prior to rifting, southwest Japan was located adjacent to the Korean peninsula based on geological correlation. Sillitoe (1977) suggested that SE Korea and SW Japan shared a single metallogenic belt that appears to have been of offset by 200–250 km after its pre-42 Ma formation and inferred that the belt was displaced along two major dextral strike-slip faults, the Yangsan and Tsushima-Goto faults (Figure 2). A recent study by Cheon et al. (2019) shows that the Yangsan fault did not accommodate any significant dextral motion during the opening of the Japan Sea, but earlier. Structural and stratigraphic data from the Korea Strait islands suggest 22–16 Ma dextral displacement on the Tsushima-Goto fault system (Fabbri et al., 1996), followed by a minor sinistral reactivation upon Middle Miocene basin inversion (Fabbri et al., 1996; Son et al., 2015). The amount of displacement along this fault remains poorly constrained, however.

The cessation of back-arc opening of the Japan Sea is considered to be at ~15 Ma (e.g., Jolivet et al., 1994; Martin, 2011; Van Horne et al., 2017). In the southwestern Japan Sea, this is marked by basin inversion at ~15.5 Mathat resulted from NW-SE compression, indicated by broad anticlines and thrust faults along the

southern margin of the Tsushima/Ulleung Basin (Kim et al., 2011; Lee et al., 2001, 2011; Lee & Kim, 2002). Tectonic inversion in the eastern part of the Japan Sea commenced in Pliocene times (~3.5 Ma), after a ~10 Myr transitional phase with a nearly neutral stress regime (Sato, 1994). The magnitude of shortening associated with inversion is limited, especially on the scale of the basin (Jolivet & Tamaki, 1992).

4.3. Okhotsk Sea Region

4.3.1. Hokkaido

Hokkaido, between Honshu, Sakhalin, and the Kuril island arc (Figure 1), is located at the triple junction between the subducting Pacific plate and the diffuse plate boundary between the Eurasian and the North American plate. The pre-Neogene basement of Hokkaido is divided into, from west to east, the N-S aligned Oshima, Sorachi-Yezo, Hidaka, Tokoro, and Nemuro tectonostratigraphic belts that are part of the Hokkaido-Sakhalin fold system (Nokleberg et al., 2000; Ueda, 2016; Ueda & Miyashita, 2005; Figure 4). The Oshima belt consists mainly of Jurassic accretionary complexes, with cherts and limestones dating back to the upper Carboniferous, which are intruded by Early Cretaceous granitoids and overlain by volcanic rocks of the Rebun-Kabato belt along its eastern margin (Ueda, 2016; and references therein; Figure 4). The belt is considered to be contiguous with the Japan fold-thrust belt and arc of NE Honshu (Ueda, 2016; Zharov, 2005). The Sorachi-Yezo belt consists of Middle Jurassic to Cretaceous accretionary complexes, ophiolites, and metamorphic rocks unconformably overlain by Cretaceous to Paleocene marine clastic sediments interpreted as forearc deposits (Ueda, 2016). HP-LT metamorphic rocks and serpentinites of the Kamuikotan Zone are locally exposed in the cores of anticlines within the forearc basin. These are thought to be the metamorphosed and exhumed equivalents of the ophiolites and arc-bearing accretionary complex of the Idonnappu suture zone that forms the eastern margin of the Sorachi-Yezo belt (Ueda, 2016; Figure 4).

The Hidaka belt lies structurally below the Sorachi-Yezo zone and is characterized by Paleocene-Eocene accretionary complexes containing mudstones and turbiditic sandstones (Nokleberg et al., 2000; Ueda, 2016). MORB-basalts and dolerites erupted and intruded into the unconsolidated trench-fill sediments, interpreted as seafloor spreading in the downgoing plate adjacent to the continental margin, that is, ridge subduction (Ueda, 2016; and references therein). The western boundary of the Hidaka Belt is formed by the Sakhalin-Hokkaido dextral shear zone, which was active from the Oligocene-Miocene (Fournier et al., 1994; Jolivet & Miyashita, 1985; Worrall et al., 1996; Figure 2). The westernmost fault branches of this shear zone continue south across the Tartary Strait along west Sakhalin and west Hokkaido (Fournier et al., 1994; Jolivet & Tamaki, 1992; Schellart et al., 2003; Figures 1 and 2).

The Hidaka belt is bounded to the east by the Tokoro belt that consists of Cretaceous to Paleogene accretionary complexes comprising Campanian to Lower Eocene volcanoclastic sediments, turbidites, and conglomerates, as well as Middle Jurassic to mid-Cretaceous oceanic rocks (Ueda, 2016; Zharov, 2005; Figure 4). The conglomerates contain clasts of alkali plutonic rocks that were interpreted to derive from the easternmost, Nemuro belt of Hokkaido (Ueda, 2016; Figures 2 and 4). In contrast with the characteristic north-south trend observed on Hokkaido, the Nemuro belt follows an approximately east-west structural trend (Maeda, 1990; Ueda, 2016) and continues in the forearc of the Lesser Kuril islands where it is exposed on several islands (Ueda, 2016), and may continue eastward to the submarine Vityaz Ridge (Lelikov & Emelyanova, 2011; Figures 1 and 4). The belt is composed of Campanian to Eocene volcanogenic sediments and volcanic rocks, mainly consisting of basalt and andesites (Ueda, 2016; Zharov, 2005). The oldest volcanic sequences are dated by K-Ar geochonology and radiolarians as Campanian-Maastrichtian (Nokleberg et al., 2000).

The zones of Hokkaido are interpreted to have formed in at least three different subduction zones. The Oshima, Sorachi-Yezo, Hidaka belts together with the East Sikhote-Alin arc are collectively interpreted to represent a foreland propagating accretionary prism, arc, and forearc system that formed on the Eurasian upper plate, equivalent to the Japan fold-thrust belt (Kemkin et al., 2016; Nokleberg et al., 2000; Ueda, 2016). Upper Jurassic-Lower Cretaceous island-arc rocks and andesite-chert sequences within the Idonnappu Zone are interpreted as remnants of a distant intraoceanic arc (the Oku-Niikappu arc) that went extinct tens of Myr prior to accretion in the accretionary prism below Eurasia in the mid-Cretaceous (Ueda & Miyashita, 2005; van der Meer et al., 2012). The rocks of the Nemuro belt are commonly interpreted as remnants of an intraoceanic island arc that formed above an east or southeast dipping intraoceanic subduction zone (Bazhenov & Burtman, 1994; Domeier et al., 2017; Konstantinovskaya, 2001; Maeda, 1990; Nokleberg

et al., 2000; Parfenov et al., 2011; Ueda & Miyashita, 2005). The Tokoro belt is suggested to have formed the forearc and accretionary wedge terrane associated with this intraoceanic subduction zone (Kanamatsu et al., 1992; Zharov, 2005). The Tokoro belt is thought to also thrust over the Hidaka belt (Kimura, 1994; Ueda, 2016), but how the juxtaposition of these belts may be influenced by the opening of the Sea of Okhotsk and Kuril Basins will be studied in the reconstruction part of this paper.

4.3.2. Sakhalin

The belts of central Hokkaido associated with subduction below the Asian margin continue northward on the 1,000 km-long, 25–170 km-wide island of Sakhalin (e.g., Nokleberg et al., 2000; Parfenov et al., 2009; Ueda, 2016; Zharov, 2005; Figures 1, 2, and 4), although different names are used for the Sakhalin terranes. Aptian-Paleocene turbidite units of the West Sakhalin terrane are correlated with the forearc deposits of the Sorachi-Yezo belt (Ando, 2003; Zharov, 2005; Figure 4). In southernmost Sakhalin, the metamorphic Susunai terrane lies to the east of this terrane, forming the continuation of the Kamuikotan zone with a similar Cretaceous age and structure (Kimura et al., 1992; Ueda, 2016; Zharov, 2005). The Merei suture zone is the northward continuation of the Idonnappu suture zone (Zharov, 2005). The Tonin-Aniva terrane, composed of Aptian-Cenomanian turbidites and olistostromes with lenses of Middle Triassic to Lower Cretaceous oceanic tholeiites and (sub)alkaline basalts, forms a subduction-related trench-fill terrane similar to the Hidaka belt (Nokleberg et al., 2000; Parfenov et al., 2009; Zharov, 2005). To the north, the East Sakhalin terrane forms a middle Cretaceous to Paleocene accretionary complex, hosting Upper Cretaceous-Paleocene metamorphic rocks and an ophiolitic mélange with tectonic slices of Permian-Late Cretaceous rocks (Khanchuk, 2006; Liao et al., 2018; Zhao et al., 2018; Zharov, 2005; Zyabrev, 2011; Figure 4).

Remnants of an Upper Cretaceous-Paleogene intraoceanic island arc and accretionary complex equivalent to the Nemuro and Tokoro belts are found on the eastern parts of the Tonin-Aniva and Terpeniya peninsulas and along east Sakhalin (Figures 1, 2, and 4; e.g., Grannik, 2012; Nokleberg et al., 2000; Parfenov et al., 2009; Zharov, 2005). Santonian-Campanian and Maastrichtian-Danian volcanic and volcanosedimentary rocks of the Terpeniya terrane are found on the Terpeniya peninsula, east of the East Sakhalin terrane (Khanchuk, 2006; Nokleberg et al., 2000; Terekhov et al., 2010; Zyabrev, 2011; Figure 4), and likely continue offshore (Terekhov et al., 2010). These sequences are straightforwardly correlated with the Nemuro belt of eastern Hokkaido, suggesting that they formed part of a contiguous intraoceanic island-arc now preserved in an area extending from eastern Sakhalin to eastern Hokkaido (Bazhenov et al., 2001; Grannik, 2012; Nokleberg et al., 2000; Parfenov et al., 2009; Ueda, 2016). Consequently, many authors infer that east Hokkaido was located next to southeastern Sakhalin prior to the Neogene opening of the Kuril back-arc basin (e.g., Kimura, 1994; Maeda, 1990; Ueda, 2016). The contrasting E-W trend of the Nemuro belt in the Kuril forearc (Figure 4) further suggests that the island-arc terrane was disrupted by post-accretion deformation of the Okhotsk Sea and Kuril Basin.

Ophiolite complexes that may be associated with the East Sakhalin arc are preserved on the Schmidt peninsula in northernmost Sakhalin (Nokleberg et al., 2000; Piip & Rodnikov, 2004; Raznitsin, 2012; Rodnikov et al., 2013; Figures 1 and 4), and are thought to continue offshore eastern Sakhalin based on gravity and magnetic anomalies (Raznitsin, 2012; Rodnikov et al., 2013), and deep seismic profiles (Piip & Rodnikov, 2004). The lowest structural unit of the Schmidt ophiolite complex consists of a serpentinite mélange with Upper Jurassic-Early Cretaceous radiolarian cherts (Nokleberg et al., 2000). Radiolarian cherts found within a pillow lava sequence structurally above the mélange have been dated as Albian-Cenomanian (Nokleberg et al., 2000; Raznitsin, 2012).

The accretionary prism below the East Sakhalin arc is preserved in the northern parts of the Tonin-Aniva peninsula and is known as the Ozersk terrane, correlated with the Tokoro belt on Hokkaido (Bazhenov et al., 2001; Zharov, 2005). The terrane was formed from the Campanian to Early Eocene based on tuffs, turbidites, flysch, and island arc basalts of that age. The Ozersk accretionary prism contains thrust slices of different ages and lithologies, the oldest being tholeiitic basalts and jaspers with late Permian to Middle Triassic ages (Bazhenov et al., 2001; Zharov, 2005). The Ozersk terrane is separated from the Tonin-Aniva terrane by the 5- to 8-km-wide, 70-km-long Vavai mélange zone including serpentinites, gabbroic lenses, fragments of Mesozoic oceanic crust, mid-Cretaceous accretionary units, and Campanian-Paleocene island-arc rocks (Zharov, 2005; Figure 4). It is interpreted as the suture zone between the Ozersk and Tonin-Aniva terranes that formed upon westward obduction of the East Sakhalin island arc (Bazhenov et al., 2001; Zharov, 2005).

On the Tonin-Aniva peninsula, the timing of obduction is marked by Early Eocene sediments and tuffs in the Ozersk terrane, the occurrence of mid-Eocene (44–38) Ma granitoid intrusions that cut the suture zone (Glorie et al., 2017; Liao et al., 2018; Zharov, 2005) and an unconformable cover of Upper Eocene-Lower Oligocene terrigenous sediments (Zharov, 2005; and references therein). These observations constrain the obduction in southern Sakhalin to the Middle Eocene (Bazhenov et al., 2001; Parfenov et al., 2011; Zharov, 2005). Zharov (2005) argued for early Paleogene obduction in east Sakhalin, most probably limited to the latest stages of the Paleocene. Recently, the collision of the East Sakhalin terrane and an exotic terrane, referred to by the authors as the Okhotsk Sea Plate, was constrained between 49 and 38 Ma, based on the maximum depositional age in the East Sakhalin accretionary complex and the Late Eocene age of both the undeformed sedimentary cover and the emplacement of granitic plutons (Zhao et al., 2018). Collectively, the constraints on the arc-continent collision in Sakhalin indicate that it occurred sometime between ~50 and 38 Ma.

4.3.3. Okhotsk Sea and Kuril Arc

The Okhotsk Sea forms an approximately 1,500-km-long and 800-km-wide marginal sea bounded by the Kamchatka peninsula to the east and separated from the Pacific Ocean to the south by the Kuril island arc and trench (Figure 1). The Okhotsk Sea is underlain by continental crust that varies in thickness from >25 km below the submarine rises to 20–25 km below the troughs (Gnibidenko & Khvedchuk, 1982; Piip & Rodnikov, 2004; Piskarev et al., 2012; Rodnikov et al., 2013; Savostin et al., 1983). Magmatic rocks recovered from the basement highs are dominated by Lower to Upper Cretaceous granitoids and felsic volcanics (Gnibidenko & Khvedchuk, 1982; Lelikov & Pugachev, 2016). Pre-Cretaceous rocks of Paleozoic age or even older have been suggested to occur in the Sea of Okhotsk basement (Gnibidenko & Khvedchuk, 1982; Piskarev et al., 2012; Worrall et al., 1996), but there are no reliable isotope ages to confirm these.

The intermediate crust beneath the Okhotsk Sea is generally considered to be a former microcontinental "Okhotsk" block (Parfenov & Natal'in, 1986; Worrall et al., 1996; Yang, 2013; Zhao et al., 2018; Zonenshain, 1990). Alternatively, Ueda and Miyashita (2005) suggested that the Sea of Okhotsk may instead be underlain by an amalgamation of far-traveled intra-Panthalassa island-arcs. The collision of the Okhotsk Block with the Siberian margin is correlated to cessation of continental arc magmatism in the 3,000-km-long Andean type Okhotsk-Chukotka volcanic belt in NE Siberia (Bindeman et al., 2002; Parfenov & Natal'in, 1986; Yang, 2013; Figure 2) around 81–77 Ma (Akinin & Miller, 2011; Hourigan & Akinin, 2004; Tikhomirov et al., 2012). In the easternmost part of the volcanic belt, ~2,000 km away from the Okhotsk Sea, subduction-related volcanism ended around the same time, at ~85 Ma (Pease et al., 2018).

The Okhotsk Sea accommodated major N-S-directed extension, first during the (mid-) Eocene to Early Miocene, as inferred from seismic subsurface data (Gnibidenko & Khvedchuk, 1982; Worrall et al., 1996). Progressively thinner crust toward the south suggests that the majority of extensional deformation took place in the central and southern parts of the Okhotsk Sea (Schellart et al., 2003). The southernmost part of the Okhotsk Sea is underlain by the oceanic Kuril Basin (Baranov et al., 2002; Gnibidenko & Khvedchuk, 1982; Savostin et al., 1983; Figures 2 and 4). This wedge-shaped oceanic basin is approximately 750 km long and has a maximum width of ~300 km (Figure 2). Although no distinct spreading ridge is observed, the geometry of the basin and orientation of faults implies a NW-SE opening (Maeda, 1990; Schellart et al., 2003; Takeuchi et al., 1999). The timing of opening remains poorly constrained due to the absence of marine magnetic anomalies or directly dated samples of the oceanic basement. Southward shifting volcanic activity from southern Sakhalin (23–21 Ma) to central and eastern Hokkaido (15–9 Ma) led Takeuchi et al. (1999) to constrain the opening of the basin from 23 to 9 Ma. This is consistent with the findings of Ikeda et al. (2000), who argued that spreading in the Kuril Basin continued to 7–9 Ma, based on the occurrence of basaltic rocks with back-arc affinity in northeast Hokkaido.

The N-S extension in both the Okhotsk Sea and the Kuril Basin is bounded in the west by the ~2,000-km-long, dextral, N-S-trending strike-slip faults of the eastern Sakhalin-Hokkaido dextral shear zone (Fournier et al., 1994; Schellart et al., 2003; Worrall et al., 1996). Formation of this shear zone followed upon the obduction of the East Sakhalin-Nemuro arc and started in the Late Eocene (Liao et al., 2016; Maeda, 1990; Schellart et al., 2003; Weaver et al., 2003; Worrall et al., 1996). Major faults include the Tym-Poronaysk fault, which runs from north to south through the central part of Sakhalin, the East Sakhalin fault, and offshore faults running through the Gulf of Tartary and the western Okhotsk Sea

(Figures 2 and 3). Movements along the strike-slip faults displaced the preexisting accretionary and subduction-related terranes of the basement of Hokkaido and Sakhalin. Most of the motion along the shear zone is suggested to have occurred since ~25 Ma, bounding the opening of the Okhotsk-Kuril Basins to the east (Fournier et al., 1994; Jolivet & Tamaki, 1992). Displacements are thought to be equal to the amount of extension in the Okhotsk-Kuril Basin. Schellart et al. (2003) estimate the amount of extension in the western Kuril Basin at ~300 km for the western part of the basin, that is, roughly equal to the width of the oceanic crust. Assuming a crustal thickness of 40 km prior to deformation, the total amount of extension in the western Okhotsk Sea would comprise an additional 500–700 km (Schellart et al., 2003). However, observed dextral displacements of the faults on Sakhalin show much lower values of displacement. Fournier et al. (1994) obtain a minimum of 50 km of dextral displacement since the Miocene along the strike-slip faults in the East Sakhalin Mountains, based on a summation of observed offsets of several en echelon faults. Fournier et al. (1994) and Schellart et al. (2003) suggested that the bulk of the motion must have been accommodated along offshore strike-slip faults.

The continuation of the Sakhalin-Hokkaido dextral shear zone through central Hokkaido is often named the Hidaka Shear Zone, which connects to the Japan Trench to the south (Jolivet & Miyashita, 1985; Jolivet & Tamaki, 1992; Figure 2). The displacement along the Hidaka Shear Zone is poorly constrained, but is expected to be somewhat higher than in Sakhalin as a result of extension in the Aniva Trough between Hokkaido and Sakhalin (Takeuchi et al., 1999; Figure 2). Existing models incorporate a total displacement of about 200 km (Itoh & Tsuru, 2006; Jolivet & Tamaki, 1992). This would place Sakhalin far to the north at ~23 Ma, very close to the Siberian margin, which implies high amounts of Neogene extension and crustal thinning north of Sakhalin that is not supported by observed crustal thicknesses (Bogdanov & Khain, 2000). Instead, we estimate 50 km of extension in the Aniva Trough between 23 and 9 Ma, based on the average crustal thickness of 25–27 km and assuming a preextensional thickness of 35 km (Bogdanov & Khain, 2000), giving a total of ~100 km of dextral displacement in the Hidaka Shear Zone between 23 and 9 Ma.

The Okhotsk Sea is separated from the Pacific Ocean by the >1,000-km-long Kuril island arc, forming a segment of the active Kuril-Kamchatka volcanic arc that formed above the subducting Pacific plate (Figures 1 and 2). The active part of the Kuril arc is thought to have developed in the Late Oligocene to Early Miocene (Avdeiko et al., 2007; Martynov et al., 2010). Recently, De Grave et al. (2016) obtained a U-Pb zircon age of 31.3 ± 1.1 Ma from a granodiorite intrusion derived from the basement of Kunashir Island, indicating that the Kuril arc started activity in or prior to the Early Oligocene. Dredged rocks of the submarine Vityaz Ridge similar to those of the onshore Nemuro belt (Lelikov & Emelyanova, 2011) imply that the modern Kuril arc was built upon crust of the East Sakhalin-Nemuro paleo-arc.

The most recent stage of deformation in Sakhalin and Hokkaido that followed upon dextral strike-slip-dominated tectonics was E-W compression compatible with the present-day motions. These led to shortening and uplift on both islands from the Middle-Late Miocene to present times (e.g., Fournier et al., 1994; Jolivet & Huchon, 1989). The amount of shortening and deformation is highest in the southern central parts of Hokkaido, estimated to be 60–100 km, where the Kuril and Japan arcs are actively converging since the Middle Miocene (~13 Ma), induced by westward motion of the Kuril forearc slive by oblique subduction (Ito, 2002; Iwasaki et al., 2004; Kato et al., 2004).

4.4. Kamchatka

The Kamchatka peninsula forms an assemblage of subduction-related terranes, including remnants of intraoceanic island arcs, accretionary wedges, and ophiolites, which progressively accreted from northwest to southeast since Cretaceous times (Geist et al., 1994; Harbert et al., 1998; Nokleberg et al., 2000; Zinkevich & Tsukanov, 1993; Zonenshain, 1990). The basement of Kamchatka can be divided into four terranes: the West Kamchatka terrane, the Olyutorsky (or Achaivayam-Valaginsky) arc terrane, the Vetlovsky-Govena terrane, and the Kronotsky arc terrane (Figures 2 and 3). The West Kamchatka terrane consists mainly of Upper Cretaceous to Eocene continental-derived turbiditic sandstones and shales (Harbert et al., 1998; Shapiro & Solov'ev, 2009), for which many different names are used depending on the location (e.g., the Ukelayat, Lesnaya, Khozgon Groups). The oldest rocks of the West Kamchatka terrane are formed by Upper Mesozoic high-grade metamorphic rocks of the Sredinny Complex consisting of granulites, amphibolites, migmatities, and granites. These are exposed in a north-south-oriented 200-km-long and 30- to 40km-

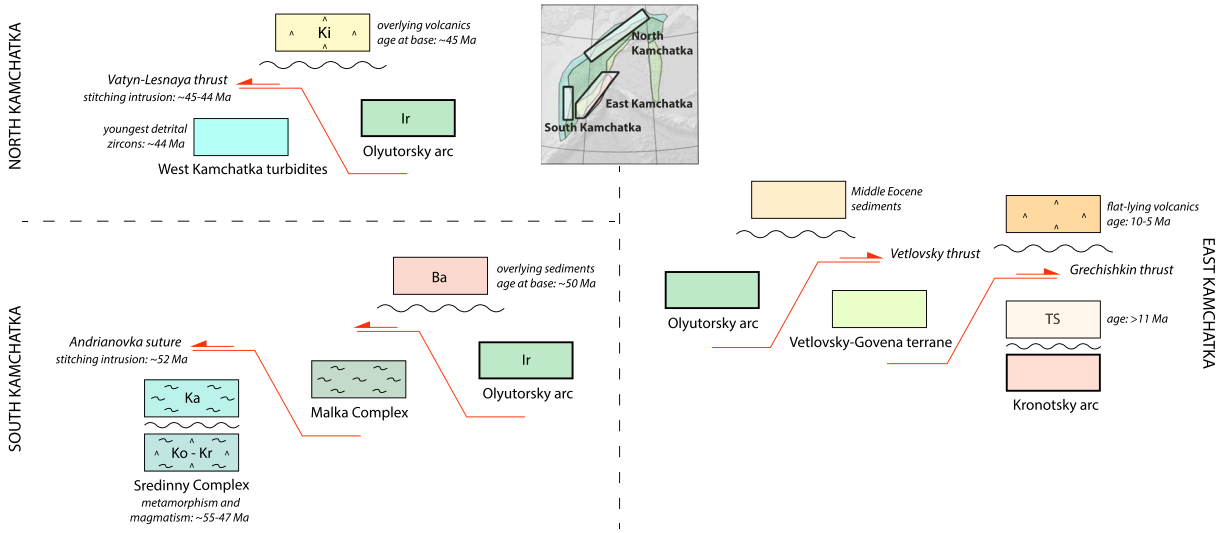

Figure 5. Schematic overview of the geological structure of Kamchatka. Each box represents a terrane/formation that is described in the text (section 4.4). Island-arc terranes are shown with thick boundaries. Key structural/spatial relationships and age constraints are indicated for north, east, and south Kamchatka (see inset map). See text for details. Major thrust faults are shown in red. Unconformities are shown by black wavy lines. Key to abbreviations: Ba = Baraba Formation; Ir = Iruney Formation; Ka = Kamchatka Group; Ki = Kinkil Group; Ko = Kolpakova Group; Kr = Krutogorov Complex; TS = Tyushev Series.

wide zone in the southern part of the Sredinny Range (Figure 1). The Sredinny Complex is either part of the Okhotsk block (e.g., Bindeman et al., 2002; Konstantinovskaya, 2011; Parfenov & Natal'in, 1986), or a separate West Kamchatka microcontinental block (Bogdanov & Chekhovich, 2002; Chekhovich et al., 2009; Filatova, 2014; Zonenshain, 1990), or represents the metamorphosed equivalent of the terrigenous sediments of the Asian continental margin (e.g., Hourigan et al., 2009; Kirmasov et al., 2004; Shapiro & Solov'ev, 2009). The structurally lowest and highest-grade unit, the Kolpakova Group, consists of Lower to Upper Cretaceous granulite- and amphibolite-facies gneisses and migmatites (Hourigan et al., 2009; Tararin, 2008; Vinogradov et al., 1988; Figure 5). These are cut by Campanian (78–80 Ma) gneissic granites (Krutogorov Complex; Hourigan et al., 2009; Luchitskaya et al., 2008), which are coeval with an inferred phase of regional metamorphism around 77 Ma (Bindeman et al., 2002). Both units are unconformably overlain by amphibolite- to greenschist-facies metasedimentary schists and gneisses of the Kamchatka Group (Rikhtyer, 1995; Figure 5), suggested to be of Paleocene age (~60 Ma; Hourigan et al., 2009). The youngest phase of metamorphism and felsic magmatism of the Sredinny Complex occurred during the Early Eocene (Bindeman et al., 2002; Hourigan et al., 2009; Luchitskaya & Soloviev, 2012). U-Pb (SHRIMP) zircon age data of metamorphic and magmatic rocks constrain peak metamorphism, migmatization, and granitic magmatism at 47–55 Ma (Bindeman et al., 2002; Hourigan et al., 2009; Luchitskaya et al., 2008; Luchitskaya & Soloviev, 2012). These events are correlated to the obduction of the Olyutorsky island-arc complex and underlying ophiolite onto the Sredinny complex (Bindeman et al., 2002; Hourigan et al., 2009; Luchitskaya & Soloviev, 2012).

The West Kamchatka terrane is overthrusted by the Olyutorsky island-arc terrane along a thrust front that extends along the entire length of Kamchatka (Figures 2, 3, and 5). The geological structure of the collision zone and the timing of collision/obduction are notably different in the southern part of Kamchatka (in the Sredinny Range) compared to the northern part (Kamchatka isthmus and Koryak Highlands; e.g., Shapiro et al., 2008). In the south, the Sredinny Complex is overthrusted by greenschist to amphibolite-facies metamorphic rocks of the Malka Complex along the Andrianovka thrust or suture (Figures 3 and 5), which is characterized by lenses of mafic and ultramafic rocks in a serpentinite mélange (Kirmasov et al., 2004; Rikhtyer, 1995). The Malka Complex consists of metamorphosed mafic volcanics, cherts, and siliceous sediments, interpreted to be derived from the Olyutorsky island-arc terrane (Hourigan et al., 2009; Kirmasov et al., 2004; Konstantinovskaya, 2011; Shapiro et al., 2008; Solov'ev & Palechek, 2004). The Malka Complex is structurally overlain by its nonmetamorphic equivalent, the Iruney Formation

(Figure 5), which consists of Santonian or Campanian to Maastrichtian volcanoclastics and cherts with locally occurring massive tuffs and pillow basalts (Hourigan et al., 2009; Konstantinovskaya, 2011; Luchitskaya et al., 2008).

The timing of arc-continent collision/obduction of the southern segment of the Olyutorsky arc over the West Kamchatka terrane in south Kamchatka is confined to a narrow time interval. The upper age limit is marked by continental conglomerates and sandstones that unconformably overlie both the Malka Complex and the Upper Cretaceous Olyutorsky island-arc rocks (Iruney Formation; Shapiro et al., 2008; Solov'ev, Hourigan, et al., 2004; Solov'ev et al., 2007; Figure 5). The sediments at the base of the succession, belonging to the Baraba Formation, contain pebbles from most of the basement rocks of the Sredinny Range, including the volcanics and Santonian-Campanian cherts from the Iruney Formation and the metamorphics of the Sredinny and Malka Complexes (Konstantinovskaya, 2011; Solov'ev, Hourigan, et al., 2004; Solov'ev et al., 2007; Zinkevich et al., 1994). A tuff layer from the lower part of the Baraba Formation provided an U-Pb (SHRIMP) zircon age of 50.5 ± 1.2 Ma (Solov'ev, Hourigan, et al., 2004). The lower age limit is provided by a detailed analysis of the age of detrital zircon grains that indicate that deposition of sediments between the margin and the Olyutorsky island-arc continued to ~55 Ma (Hourigan et al., 2009). In addition, granite intrusions cutting through the metamorphics of the Sredinny Complex yielded U-Pb (SHRIMP) ages of 50.1 ± 1.7 to 54.9 ± 0.5 Ma with one intrusion stitchingthe Andrianovka suture yielding an age of 51.5 ± 0.7 Ma (Hourigan et al., 2009; Luchitskaya et al., 2008), coeval with the timing of peak metamorphism of the Sredinny Complex at ~52 Ma (Hourigan et al., 2009; Konstantinovskaya, 2011). Collectively, obduction of the Olyutorsky arc over the southern part of Kamchatka is thus constrained to 55–50 Ma (Kirmasov et al., 2004; Shapiro et al., 2008).

The crystalline basement rocks of the Sredinny Massif that are structurally positioned below the remnants of the Olyutorsky arc are restricted to southern Kamchatka. In northern Kamchatka, in the Kamchatka isthmus and the Koryak Highlands, the Upper Cretaceous-Paleogene turbidite sediments of the West Kamchatka terrane directly underlie (unmetamorphosed) rocks of the Olyutorsky arc terrane, along the more than 800-km-long Vatyn-Lesnaya thrust fault (Filatova, 2013; Solov'ev et al., 2001, 2011; Figures 2, 3, and 5). The suture zone consists of a tectonic mélange of chert (dated by radiolarians as Santonian-Maastrichtian), tuff, pillow basalt, and volcanic sandstone blocks, with a matrix of highly deformed sediments derived from the West Kamchatka terrane (Solov'ev et al., 2001, 2011; Solov'ev, Shapiro, & Garver, 2002).

The timing of collision of the northern segment of the Olyutorsky island-arc can be tightly bracketed by the age of the youngest sediments below the suture and the age of the undeformed overlap sequence. Detrital zircon fission-track data from the upper part of the West Kamchatka sediments suggest that sedimentation continued up to the Middle Eocene, with the youngest dated detrital zircons yielding ages of ~44 Ma (Garver et al., 2000; Solov'ev, Shapiro, Garver, Shcherbinina, et al., 2002). In the Kamchatka isthmus, the Vatyn-Lesnaya Fault is uncomformably overlain by volcanics of the Kinkil Group (Figure 5), which contain Lutetian microfossils and from which basal rhyolites yielded U-Pb zircon, K-Ar biotite, and zircon and apatite fission-track ages between ~46 and 44 Ma (Solov'ev et al., 2011; Solov'ev, Shapiro, & Garver, 2002). These ages are consistent with a granodiorite massif that cuts through the fault zone and is dated at 45–44 Ma by a U-Pb and Rb-Sr geochronology (Solov'ev et al., 2011; Solov'ev, Shapiro, & Garver, 2002). The formation of the Vatyn-Lesnaya suture during obduction of the Olyutorsky arc in northern Kamchatka is thus tightly constrained at 45–44 Ma. The total displacement of the Olyutorsky arc over the continental margin is estimated to be at least 50–100 km (Solov'ev et al., 2011; Solov'ev, Shapiro, & Garver, 2002). From the above data, it follows that the obduction of the Olyutorsky arc onto NE Siberia occurred at different times in the north and south of Kamchatka: 55–50 Ma in the south and until ~45 Ma in the north (Kirmasov et al., 2004; Konstantinovskaya, 2001; Shapiro et al., 2008; Shapiro & Solov'ev, 2009; Solov'ev et al., 2011). Therefore, it was hypothesized that the arc may have been segmented by a transform fault, causing the northern segment to collide with the continental margin 5–10 Myr later (Shapiro et al., 2008; Shapiro & Solov'ev, 2009).

Apart from the Sredinny mountain range and the Koryak Highlands, the Olyutorsky arc rocks are also widely exposed in the Eastern Ranges and on Karaginsky Island (e.g., Hourigan et al., 2009; Konstantinovskaya, 2011; Figures 1 and 2). There, island-arc units mostly consist of basalts and andesites, as well as tuffs, volcaniclastic sandstones and siltstones, cherts, and jaspers (Konstantinovskaya, 2011). Radiolarians of the chert and mudstone layers in the Eastern Ranges have been dated as Campanian-Danian (Zinkevich et al., 1994). Ophiolites associated with the Olyutorsky arc are found in different localities in eastern Kamchatka. Upper Cretaceous peridotites, gabbros, and diabases belonging to a coherent

ophiolite complex are exposed within a serpentite mélange in the Kumroch Range (Tsukanov et al., 2009). A well-preserved ophiolite sequence from Karaginsky Island yielded U-Pb (SHRIMP) zircon ages of ~76–72 Ma (Campanian; Tararin et al., 2012). A Late Cretaceous age of formation of ~100–70 Ma was also obtained for the ophiolitic gabbros and peridotites in eastern Kamchatka (Tararin et al., 2012). Based on their geochemical signature, the ophiolites of the Kumroch Range and Karaginsky Island are interpreted to have formed in a suprasubduction zone setting (Kravchenko-Berezhnoy & Nazimova, 1991; Skolotnev et al., 2018; Tsukanov et al., 2009).

The Vetlovsky-Govena terrane comprises the highest structural unit of an accretionary prism that underlies the Olyutorsky arc to the east (Figures 2, 3, and 5), thought to have formed in a northwest-dipping subduction zone that existed from the Middle Eocene to the Pliocene to the east of the Olyutorsky arc (Bakhteev et al., 1994; Shapiro et al., 2004; Solov'ev, Shapiro, et al., 2004). The boundary between the Olyutorsky arc terranes and the Vetlovsky-Govena terrane is marked by the northwest-dipping Vetlovsky thrust zone that comprises a serpentinite-hosted tectonic mélange containing ultramafic rocks, gabbros, and sediments (Figures 3 and 5), running from the Shipunsky peninsula in the south through eastern Kamchatka and Karaginsky Island to the Govena peninsula in northern Kamchatka (Figures 1 and 2; Konstantinovskaya, 2011; Zinkevich & Tsukanov, 1993). The Vetlovsky thrust is unconformably overlain by a Middle Eocene mudstone and sandstone (Figure 5), limiting the age of the fault, and thereby the onset of westward subduction below the Olyutorsky arc terrane, to the latest Early Eocene (Bakhteev et al., 1994; Konstantinovskaya, 2011).

The oldest unit of the Vetlovsky-Govena terrane consists of Upper Paleocene to Lower Eocene volcaniclastic sediments, tuffs, cherts with lenses of basalts, jasper, and micritic limestone (Bakhteev et al., 1994; Gladenkov, 2016; Zinkevich & Tsukanov, 1993). Mafic volcanic rocks as well as pillow lavas and tuffs found in tectonic slices of the terrane, characterized by a tholeiitic MORB geochemical signature (Tsukanov et al., 2018; Zinkevich & Tsukanov, 1993). These MORB-like basalts are dated as Paleocene-Lower Eocene and may have formed by back-arc spreading behind the Olyutorsky arc (Bakhteev et al., 1994; Konstantinovskaya, 2001; Solov'ev, Shapiro, et al., 2004; Tsukanov et al., 2018). Middle-Upper Eocene terrigenous units of the East Kamchatka accretionary prism unconformably overlie this unit (Bakhteev et al., 1994; Gladenkov, 2016; Solov'ev, Shapiro, et al., 2004). The youngest sediments of the accretionary prism consist of Oligocene-Miocene flysch, which is separated from the Vetlovsky-Govena terrane by the steeply, top to the southeast, northwest-dipping, ophiolite-free Grechishkin thrust (Bakhteev et al., 1997; Solov'ev, Shapiro, et al., 2004; Figures 2, 3, and 5). To the east and in the footwall of this thrust lies the Kronotsky arc terrane, which incorporates accreted thrust units derived from the Kronotsky island-arc. Exotic Miocene pelagic cherts and the Early-Middle Miocene (24–11 Ma) age of the youngest deformed sandstones of the Tyushev Series below the Grechishkin thrust (Bakhteev et al., 1997; Solov'ev, Shapiro, et al., 2004). indicate that Kronotsky arc accretion probably occurred during the Late Miocene (Levashova et al., 2000; Solov'ev, Shapiro, et al., 2004). The upper age limit of the arc-continent collision is estimated from an angular unconformity between the deformed Lower to Middle Miocene marine sediments and flat-lying Upper Miocene-Pliocene (10–5 Ma) volcanics (Levashova et al., 2000; Shapiro et al., 1996; Figure 5).

The Kronotsky arc is interpreted as a second island-arc that accreted to the Asian margin of Kamchatka. Remnants of the arc are exposed on the Shipunsky, Kronotsky, and Kamchatka Mys peninsulas in eastern Kamchatka (e.g., Alexeiev et al., 2006; Bazhenov et al., 1992; Nokleberg et al., 2000; Zinkevich & Tsukanov, 1993; Figures 1 and 2). The intraoceanic volcanic arc was active from the Late Cretaceous (~85 Ma) to the Middle Eocene (e.g., Bazhenov et al., 1992; Levashova et al., 2000; Nokleberg et al., 2000; Shapiro & Solov'ev, 2009; Tsukanov et al., 2014). The youngest island-arc basalts are ~40 Ma (Beniamovsky et al., 1992; Gladenkov, 2016; Levashova et al., 2000). The Kronotsky arc was suggested to have formed above a northward dipping subduction zone (Alexeiev et al., 2006; Domeier et al., 2017; Konstantinovskaya, 2001; Shapiro & Solov'ev, 2009), evidenced by the relative position of the remnants of the volcanic belt, the fore-arc and the accretionary wedge, and the dip-direction of thrust planes in the accretionary wedge (Alexeiev et al., 2006). The Kronotsky arc overlies an ophiolite sequence exposed on the eastern peninsulas of Kamchatka. Three ophiolite complexes of the Kamchatka Mys peninsula are distinguished by Tsukanov et al. (2007): (i) an Aptian-Cenomanian complex of ancient oceanic crust, forming the basement of the Kronotsky arc, occurring mainly as thin tectonic slices in Campanian-Maastrichtian island-arc rocks on the Kamchatka Mys peninsula; (ii) an Upper Cretaceous ophiolite complex with

suprasubduction zone geochemistry; and (iii) a Paleocene-Lower Eocene complex of island-arc or back-arc origin, consisting of gabbros, diabase, and basalts.

Portnyagin et al. (2008) showed that enriched tholeiites from the Kamchatka Mys ophiolite, dated by microfauna as Albian-Cenomanian (~113–93 Ma; Khotin & Shapiro, 2006; and references therein), share similar geochemical characteristics with the northernmost, Detroit, and Meiji seamounts of the Hawaii-Emperor seamount chain. It was suggested that these Upper Cretaceous Hawaiian hotspot-related volcanics were accreted below the Kronotsky arc sometime during its intraoceanic activity (Khotin & Shapiro, 2006; Lander & Shapiro, 2007; Portnyagin et al., 2008). A subsequent geochemical study of ultradepleted melts in MORB-like basalts obtained from a serpentinite mélange in the Kamchatka Mys ophiolite complex suggested that the mid-ocean ridge at which the ophiolite formed may have had interaction with the Hawaiian hotspot during the middle-Cretaceous, that is, before subduction started below the Kronotsky arc (Batanova et al., 2014; Portnyagin et al., 2009). This suggests that the mid-Cretaceous oceanic crust on which Kronotsky arc formed, originated from a spreading center near the Hawaiian mantle plume. Following the arrest of intraoceanic subduction at ~40 Ma, the Kronotsky arc and its underlying accretionary prism welded to the Pacific plate and was transported toward Kamchatka where it arrived and accreted in the Late Miocene (Domeier et al., 2017; Konstantinovskaya, 2001; Shapiro & Solov'ev, 2009; van der Meer et al., 2018).

4.5. Bering Sea

The Bering Sea is the largest marginal sea basin of the Northern Pacific realm. It is separated from the Pacific Ocean by the Aleutian island arc, which extends over 2,000 km from the southwestern tip of Alaska to the southern Kamchatka peninsula (Figure 1). The Pacific plate is actively subducting below the North American plate at the Aleutian Trench, whereby the curved shape of the Aleutian Trench leads to an increasing subduction obliquity from east to west (e.g., Boyd & Creager, 1991). The oldest reliably dated rocks from the Aleutian Arc have $^{40}Ar/^{39}Ar$ isochron ages of 46.3 ± 0.9 Ma for an andesite of the deep submarine Murray Canyon west of Kiska Island and 46.2 ± 1.5 Ma for a tholeiitic basalt of Medny Island, in the western Aleutians (Jicha et al., 2006; Layer et al., 2007; Figure 1). The Bering and Medny islands (Figure 1), together referred to as the Komandorsky Islands, form the westernmost islands of the Aleutian arc, and were suggested to contain remnants of the Kronotsky island arc and fore-arc basin (Alexeiev et al., 2006; Bazhenov et al., 1992; Rostovtseva & Shapiro, 1998). Fore-arc deposits exposed on the Komandorsky Islands were dated as Late Paleocene to Early Eocene using bio-magnetostratigraphy (Bazhenov et al., 1992; Minyuk & Stone, 2009; Rostovtseva & Shapiro, 1998), although the interpretation of the biostratigraphy is debated (Scholl, 2007). The oldest radiometric ages from rocks interpreted to belong to the Aleutian arc of ~46 Ma are only a few million years younger than the youngest arc volcanics found on the Beringian margin (Figure 2), where K-Ar and U-Pb zircon ages from dredged arc volcanics are 54.4 to 50.2 Ma (Davis et al., 1989). Therefore, conventional tectonic models of the Bering Sea region suggest that subduction initiation below the Aleutian Trench was related to a jump of the subduction zone from the Beringian margin in the north toward the Aleutian Trench in the south around 50–46 Ma, likely related to the obduction of the Olyutorsky arc on Kamchatka (Scholl, 2007; Worrall, 1991).

The oceanic lithosphere of the Aleutian Basin underlies the largest deepwater basin of the Bering Sea. It has been suggested that the Aleutian Basin lithosphere was captured by the North American plate upon formation of the Aleutian subduction zone around 50 Ma (e.g., Cooper et al., 1976, 1992; Scholl et al., 1975). Since the age interpretation of observed marine magnetic anomalies remains uncertain (see section 3) and no dredge samples from the acoustic basement are available for direct age determination, the exact age and the origin of the Aleutian Basin is still unknown. Presently, any conceptual model of its formation must rely on indirect constraints. If the observed magnetic anomalies indeed represent magnetic reversals indicative of seafloor spreading (section 3), the orientation of the anomalies would provide an independent constraint for the orientation of the ridge at which the Aleutian Basin crust accreted. We use this constraint to test the predicted orientation of that ridge in our reconstruction.

Two major submarine highs are located below the Bering Sea: the Bowers and Shirshov Ridges (Figures 1 and 2). These separate the Aleutian Basin from the smaller Komandorsky and Bowers Basins. The Bowers Ridge forms an arcuate ridge extending from the Aleutian arc to the north. The ridge seems to be structurally connected to the Aleutian arc and has a asymmetric structure with a deep trench filled with about 8–10 km

of mainly Miocene sediments along its steep northern and eastern slopes (Cooper et al., 1981, 1987; Scholl, 2007). Recent new data on the composition and age of dredged rocks of the Bowers Ridge (Wanke et al., 2011, 2012) showed island-arc rocks on the northern slopes of the ridge (Figure 2) with a moderate adakitic chemical signature interpreted as indicator of the generation of melt above an obliquely subducting slab (Wanke et al., 2012). Those authors obtained ^{40}Ar-^{39}Ar ages ranging from 32.3 ± 2.0 to 26.0 ± 0.7 Ma for the volcanic rocks of the ridge. Two basement samples of trachybasalts from a seamount located on the western extension of the arcuate ridge were dated at 22.2 ± 2.7 and 24.4 ± 0.8 Ma. Two volcanic episodes were distinguished by Sato et al. (2016) based on ^{40}Ar-^{39}Ar dating of volcanic rocks collected at International Ocean Discovery Program Site U1342 (Expedition 323) from the northern part of the ridge (Figure 2): 34–32 and 28–26 Ma. All the above ages are considerably younger than the initiation of the Aleutian arc, suggesting that the Bowers Ridge formed within the Bering Sea during northward subduction at the Aleutian Trench. The age and origin of the back-arc basin west of the Bowers Ridge, the Bowers Basin, is still largely unknown (see section 3). The oldest sediments found on the basin floor of the Bowers Basin are Oligocene in age (Scholl, 2007). Cooper et al. (1992) and Chekhovich and Sukhov (2015) associated the formation of the Bowers Basin with relative motion of the Bowers Ridge and Trench to the NE relative to the Aleutian Trench.

The Shirshov Ridge forms an approximately 550 km-long N-S striking submarine ridge in the western part of the Bering Sea (Figure 2). The ridge is morphologically connected to the Asian mainland at Cape Olyutorsky in the north (Figure 1). No deformation structures indicative of a collisional contact between the Shirshov Ridge and the exposed rocks on Cape Olyutorsky are observed (Scholl, 2007; and references therein). The Shirshov Ridge is connected with the Bowers Ridge by a roughly E-W-trending fracture zone (Hoernle et al., 2016). According to Baranov et al. (1991), two different rock complexes form the main structure of the Shirshov Ridge: an oceanic complex consisting of amphibolites and gabbros, as well as deep-sea cherts and massive basaltic lavas. Microfauna obtained from the cherts constrain its age at Late Cretaceous (Campanian-Maastrichtian) to Early Paleogene (Baranov et al., 1991; and references therein), that is, contemporaneous with the Olyutorsky arc. Recent $^{40}Ar/^{39}Ar$ dating of dredged island-arc rocks from the central Shirshov Ridge gave ages of 65–69 Ma (Hauff et al., 2016). Island-arc rocks from the southern end of the ridge consisting of andesites and volcanoclastics provided a much younger age of 27.8 ± 1.1 Ma (Cooper et al., 1987). This young material may represent a fragment of the Aleutian Arc (Scholl, 2007), or the Bowers Ridge that rifted away in the Neogene, based on the occurrence of the rocks in a NW-SE-oriented sector of the ridge, which is parallel to the fracture zones in the Komandorsky Basin to the west of the Shirshov Ridge, and strike-slip faults in the western part of the Aleutian Arc. Amphiboles within the amphibolites from the oceanic complex were K-Ar dated as 47 ± 5 Ma and zircons gave a 72 ± 1.4 Ma age (Sukhov et al., 2011). The amphibolites, metagabbro, and Upper Cretaceous to Paleocene volcanic and sedimentary rocks all underwent intense deformation (Chekhovich et al., 2012).

The Komandorsky Basin, located west of the Shirshov Ridge has an estimated age of 10 and 20 Ma, based on interpreted marine magnetic anomalies (see section 3; Valyashko et al., 1993; Figure 2). The only dated sample from the basin floor is a basaltic rock that was dated at 9.3 ± 0.8 Ma (Rubenstone, 1984). The Komandorsky Basin is bounded in the west by a sediment-filled trench along the eastern margin of North Kamchatka (Avdeiko et al., 2007; Baranov et al., 1991; Figure 3), west of which is a Miocene-Pliocene calc-alkaline volcanic arc in the Kamchatka isthmus (Hochstaedter et al., 1994; Shapiro & Solov'ev, 2011).

5. Paleomagnetic Constraints

5.1. Compilation of Paleomagnetic Data

We compiled published paleomagnetic data from the NW Pacific region based on 112 paleomagnetic sites from >50 studies. The database was built using the online paleomagnetic analysis tool www.paleomagnetism.org (Koymans et al., 2016). We included data derived from Upper Cretaceous and younger island-arc rocks of the Aleutians, Kamchatka, Sakhalin, and Hokkaido (see Table S1). For the Japanese Islands, only data from Oligocene and younger rocks were compiled to test opening scenarios for the Japan Basin. We used selection criteria formulated by Lippert et al. (2014) and Li et al. (2017) excluding sites that (1) were not used by the authors of the original publication if reason for exclusion was provided; (2) were not

analyzed using principle component analysis (Kirschvink, 1980); (3) were (most likely) remagnetized according to the original authors; (4) include less than four samples for sedimentary or igneous sites, or less than four lava sites for volcanic localities; (5) have k-values (precision parameter of Fisher, 1953) below 50 for volcanic sites, or an A95 value exceeding $A95_{max}$, or below $A95_{min}$ sensu (Deenen et al., 2011) for igneous or sedimentary sites. We excluded paleomagnetic localities that were based on an average of multiple sedimentary site averages if statistical details on a per-site level were not reported.

The paleomagnetic analyses on paleomagnetism.org uses individual paleomagnetic directions as basis, facilitating compiling site averages weighed by the number of observations within such sites. For sediment-derived sites, the paleomagnetic direction of each sample can be approximated as a spot reading of the paleomagnetic field (Deenen et al., 2011). We therefore included paleomagnetic directions that together defined sedimentary sites where reported by the original authors. Unfortunately, original individual sample directions are rarely published in the paleomagnetic literature, and only statistical descriptions of the data sets are provided on a per site level. In such cases, we parametrically sampled sites (see Koymans et al., 2016). For lava sites, site averages do represent spot readings of the paleomagnetic field (provided $k < 50$ as reliability cut-off, following, e.g., Johnson et al., 2008, and Biggin et al., 2008) and these are normally published on a per-lava site level. In such cases, we compiled sites by including multiple nearby lava site directions in a locality (provided $n > 3$) without parametric sampling. The resulting paleomagnetic database (see supporting information) is used to test our reconstruction based on the kinematic constraints outlined in the previous section.

5.2. Paleomagnetic Constraints on the Opening of the Japan Sea

Paleomagnetic data from Japan show opposite rotations of southwest and northeast Japan during the Neogene (e.g., Kawai et al., 1961; Martin, 2011; Otofuji, 1996; Otofuji et al., 1985; Figure 4). Across southwest Honshu, that is, west of the Itoigawa-Shizuoka Tectonic Line, and northern Kyushu, paleomagnetic declinations consistently show a ~50° clockwise rotation between ~18 and 15 Ma (Figure 6c). Paleomagnetic data from northeast Honshu indicate ~30–40° counterclockwise rotations of northeast Japan between ~20 and 15 Ma (Figure 6b). A similar counterclockwise rotation history was recorded from West Hokkaido (Fujiwara & Sugiyama, 1986; Otofuji et al., 1994; Tanaka et al., 1991).

Declinations of Upper Oligocene to Lower Miocene sediments of Central Hokkaido indicate a ~30–35° clockwise rotation since the Early Miocene and 20° since Middle Miocene, ascribed to right-lateral displacements along the Sakhalin-Hokkaido Shear Zone (Kodama et al., 1993; Tamaki et al., 2010). Clockwise rotations similar to Central Hokkaido were found on Sakhalin, thought to be associated with deformation along the Sakhalin-Hokkaido Shear Zone (Takeuchi et al., 1999; Weaver et al., 2003). Following these authors, we do not consider these declinations as representative for regional block rotations, but interpret them as local, strike-slip-related rotations. These data do suggest, however, that East and West Hokkaido were not juxtaposed until after the Middle Miocene opening of the Japan Sea.

5.3. Paleomagnetic Constraints From Accreted Intraoceanic Island Arcs

The paleolatitudes obtained from paleomagnetic inclination data provide an independent means of constraining the plate motion history of the intraoceanic island arc terranes in the NW Pacific region since the Late Cretaceous. We compiled 32 paleomagnetic sites from 19 studies of island arc rocks from the East Sakhalin-Nemuro, Olyutorsky, and Kronotsky arcs (Figure 7). Most paleomagnetic sites consist of tuffs and volcanogenic sediments and were dated by radiolarians. Paleolatitudes for the Olyutorsky-East Sakhalin-Nemuro arc show a 25–30° northward paleolatitude shift between ~80 and ~50 Ma, after which time the inclination data generally correspond with the expected inclination of the North American plate (Figure 7b). When compared to the paleolatitude evolution of the reference location of 60°N/165°E tied to the Pacific plate, the data indicate that the Olyutorsky-East Sakhalin-Nemuro arc migrated faster northward between ~80 and 50 Ma than the Pacific plate, after which there was paleolatitudinal convergence between the two until today. In addition, the plot suggests that the Olyutorski-East Sakhalin-Nemuro arc was initially not far, that is, within ~5°, of the lithosphere that currently subducts below Kamchatka, which is estimated to be ~100 Ma (Müller et al., 2016; Wright et al., 2016). The majority of paleomagnetic declinations indicate that the Olyutorsky arc underwent a counterclockwise rotation of about 40–50° since the Late Cretaceous (Figure 7a). Data from upper Paleogene rocks also indicate counterclockwise

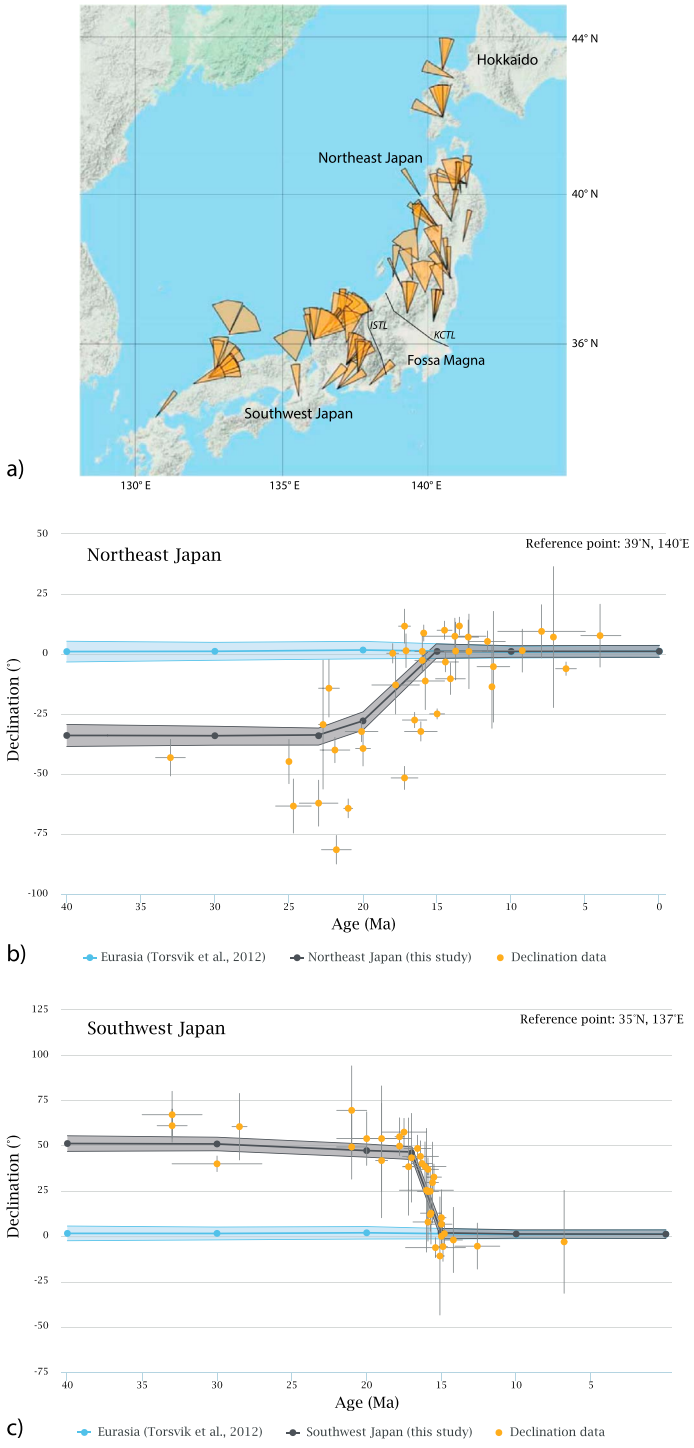

Figure 6. (a) Map showing the locations and declinations (and their uncertainties) of the paleomagnetic sites compiled for the Japanese islands. Black lines indicate the tectonic boundaries of southwest and northeast Japan: the Itoigawa-Shizuoka Tectonic Line (ISTL) and Kashiwazaki-Choshi Tectonic Line (KCTL). Data files and references are provided in the supporting information (Data Set S2). (b) Paleomagnetic declination curves predicted for a reference point on northeast Honshu (39°N, 140°E) using the Global Apparent Polar Wander Path of Torsvik et al. (2012), in the case that the reference point was rigidly attached to Eurasia (blue), and as reconstructed in this study (black). See section 2 for more details. The colored envelopes indicate the uncertainty range. Yellow dots (with errors) represent the compiled paleomagnetic declinations for northeast Japan (northeast Honshu and west Hokkaido). (c) Same as (b), but now for a reference point (35°N, 137°E) on southwest Honshu. The black curve shows the predicted declination through time for southwest Japan as reconstructed in this study. Yellow dots show the declinations for southwest Japan (southwest Honshu, Kyushu and the Oki islands).

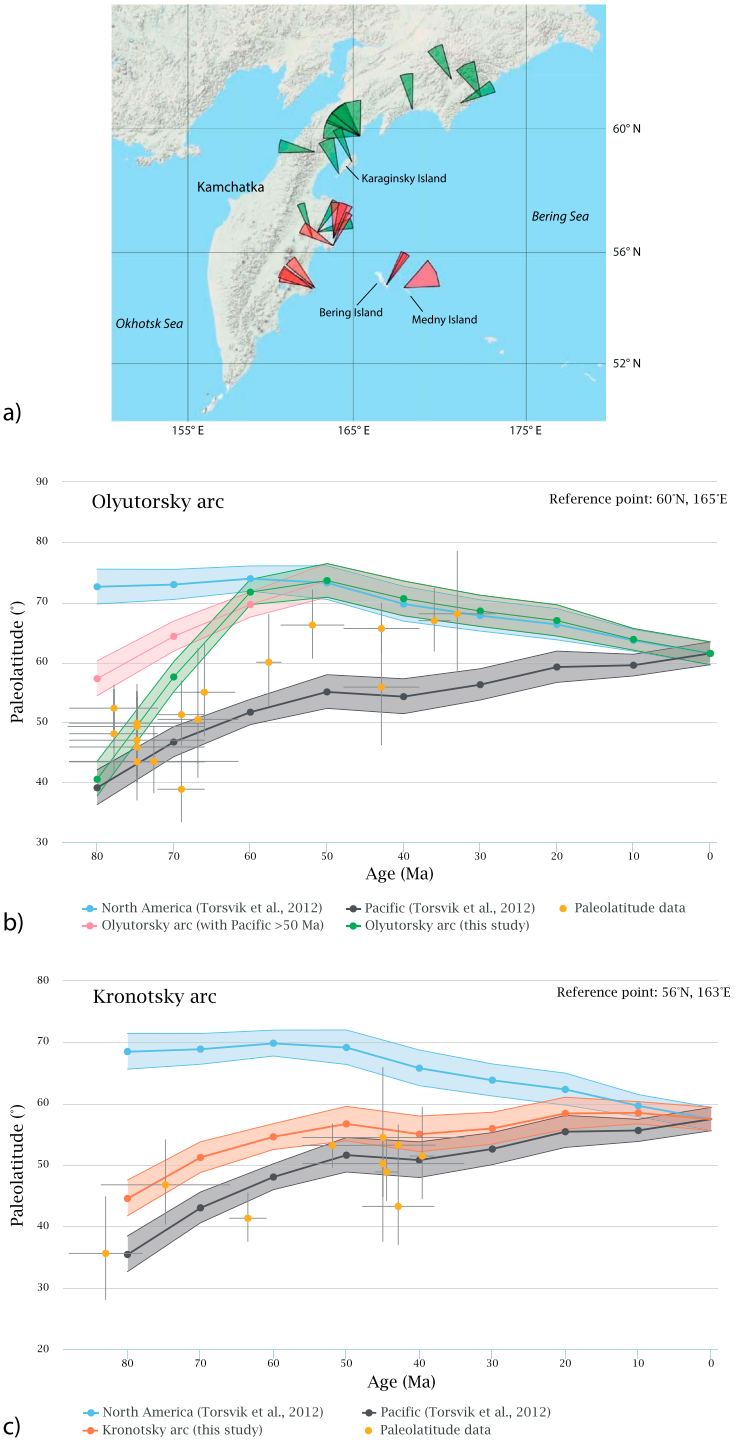

Figure 7. (a) Map showing the locations and declinations (and their uncertainties) of the paleomagnetic sites compiled for the Olyutorsky (green) and Kronotsky (red) island-arc terranes. Data files and references are provided in the supporting information (Data Set S2). (b) Paleolatitude paths predicted for a reference point (60°N, 165°E) on the Olyutorsky arc terrane using the Global Apparent Polar Wander Path of Torsvik et al. (2012), in the case that the reference point was rigidly attached to North America (blue), to the Pacific plate (black), to the Pacific plate prior to 50 Ma and North America <50 Ma (pink), and as reconstructed in this study (green). Yellow dots (with errors) represent the (uncorrected) paleomagnetic data for the Olyutorsky arc terrane. (c) Paleolatitude paths predicted for a reference point (56°N, 163°E) on the Kronotsky arc terrane using the Global Apparent Polar Wander Path of Torsvik et al. (2012), in the case that the reference point was rigidly attached to North America (blue), to the Pacific plate (black), and as reconstructed in this study (orange). Yellow dots (with errors) represent the (uncorrected) paleomagnetic data for the Kronotsky arc terrane.

rotations, possibly related to extension in the Okhotsk Sea west of Kamchatka. Taking into account the present-day NNE-SSW orientation of the Olyutorsky arc terrane, the paleomagnetic declination data suggests that the Olyutorsky arc-trench system was probably oriented ENE-WSW during the Late Cretaceous-early Paleogene.

Data published for the East Sakhalin-Nemuro arc that is thought to be equivalent to the Olyutorsky arc (Domeier et al., 2017; Grannik, 2012; Konstantinovskaya, 2001; Nokleberg et al., 2000) come from the Nemuro and Tokoro belts of Hokkaido and the Ozersk terrane of southeasternmost Sakhalin (see Figure S2). These show much shallower inclinations, indicating much lower paleolatitudes than expected if these terranes were part of the Eurasian continent, suggesting an allochthonous, intra-Panthalassa origin. The declinations from the Nemuro belt show that it experienced a ~15–25° counterclockwise rotation since the Late Cretaceous (Bazhenov & Burtman, 1994; Fujiwara & Ohtake, 1974; Figure S2). The site from the NNE-SSW-trending Tokoro belt shows a ~130° clockwise rotation (Kanamatsu et al., 1992). The above data suggests that paleo-strike of the East Sakhalin-Nemuro arc was approximately ENE-WSW-trending, similar to the Olyutorsky paleo-arc.

The data set of the Kronotsky arc of Kamchatka was mainly derived from Eocene tuffs and (volcanogenic) siltstones and sandstones. Inclinations from sediments are somewhat lower than expected for the Pacific APWP, whereas inclinations from lava localities of the Kronotsky peninsula provided a similar paleolatitude to the Pacific reference, suggesting that the Kronotsky arc moved together with the Pacific plate since the Eocene (Figure 7c).

6. Seismic Tomographic Constraints

The geological record predicts that several intraoceanic and continental margin subduction zones have been active in the North Pacific region since the Late Cretaceous, remnants of which are found in the upper and lower mantle below the North Pacific region. A comprehensive overview of slab-like anomalies in the mantle was recently provided on www.atlas-of-the-underworld.org (van der Meer et al., 2018), and two of these anomalies were recently used by Domeier et al. (2017) as a constraint on their kinematic model for NW Pacific evolution.

Below, we summarize the mantle anomalies from the global compilation of slabs of van der Meer et al. (2018) that are relevant for our reconstruction (Figure 8), as well as the correlations between anomalies and geological records of the NW Pacific region as proposed by van der Meer et al. (2018). We test our reconstruction against the presence of slabs in the mantle at locations predicted, although we may in places provide different interpretations than van der Meer et al. (2018), in the light of our new reconstruction. We assume that, after breakoff from surface plates, slabs sink vertically (Domeier et al., 2016; van der Meer et al., 2010), but that during their subduction they may roll back, or be dragged forward or sideways through the mantle (e.g., Chertova et al., 2014; Funiciello et al., 2008; Schellart et al., 2008; Spakman et al., 2018; van de Lagemaat et al., 2018). We therefore test whether slabs are present in the mantle at locations where our model predicts their break-off, at depths consistent with globally determined sinking rates of ~1–2 cm/year (Butterworth et al., 2014; van der Meer et al., 2010, 2018). When comparing our model to mantle structure, we place our reconstruction in the global moving hotspot reference frame of Doubrovine et al. (2012).

Active subduction zones in the northern Pacific region are associated with well-imaged slabs in the upper mantle, and in places also the top of the lower mantle. The Aleutian subduction zone is associated with the north-dipping Aleutian slab that is located in the upper mantle and transition zone (Gorbatov et al., 2000; Koulakov et al., 2011; Martin-Short et al., 2016; Qi et al., 2007; van der Meer et al., 2018; Figures 8a and 8b). At the Kuril-Kamchatka subduction zone, a northwest-dipping slab appears to penetrate into the lower mantle, where it connects to a subhorizontal slab segment at 800–1,000 km depth (Gorbatov et al., 2000; Jiang et al., 2009; Koulakov et al., 2011; Spakman et al., 1989; van der Hilst et al., 1991; van der Meer et al., 2018; Figures 8a and 8b). Van der Meer et al. (2018) interpreted this whole body as a single slab that subducted along the Kuril-Kamchatka Trench after polarity reversal upon Olyutorsky-Kamchatka collision, following (Shapiro & Solov'ev, 2009). Below Japan, the peculiar west-dipping Manchuria slab is over 2,500 km long, flat-lying and almost entirely contained in the upper mantle, disconnected from deeper anomalies in the lower mantle (Figures 8a and 8b). Van der Meer et al. (2018) followed the interpretation

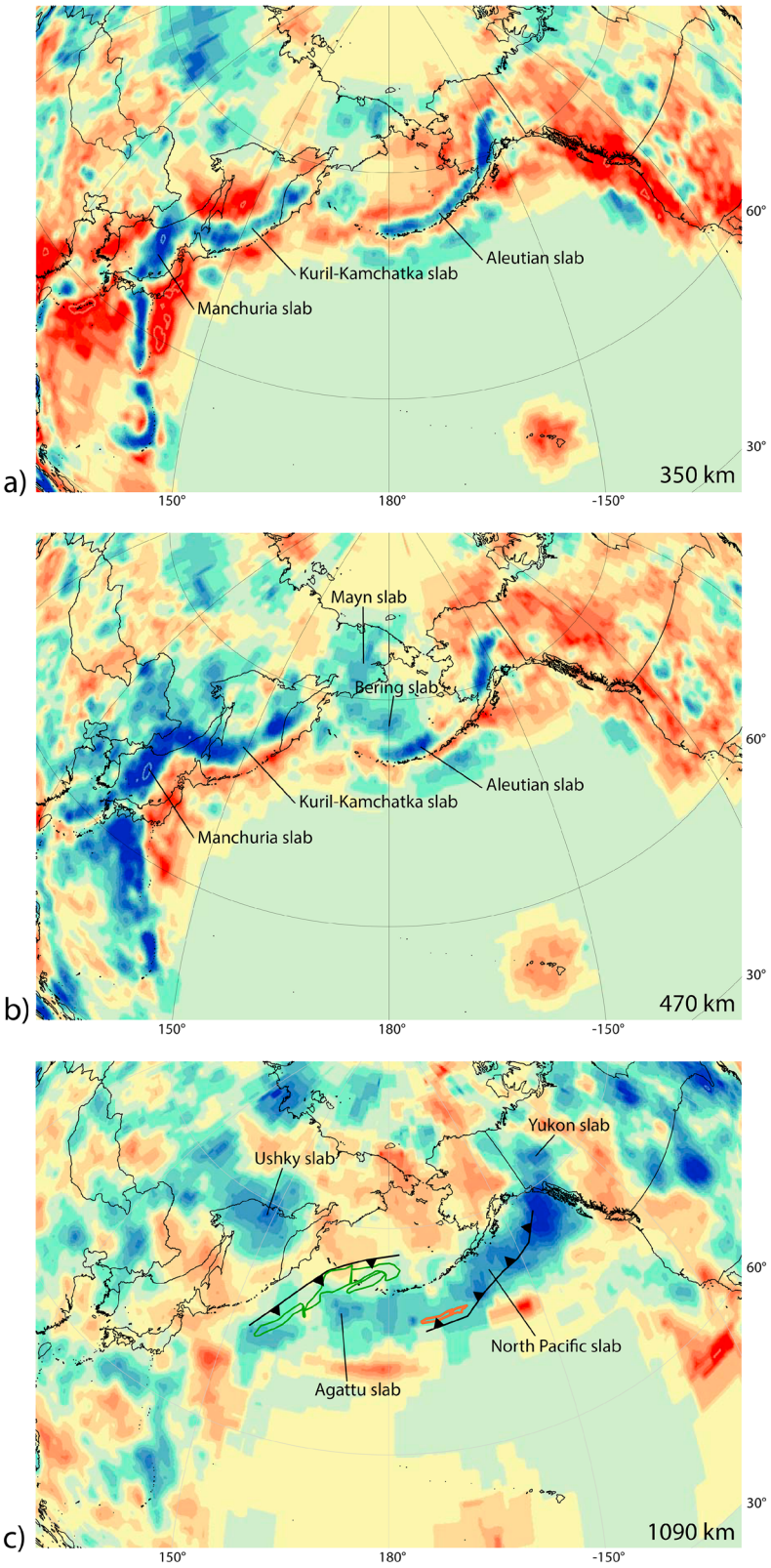

Figure 8. Horizontal depth slices through the UU-P07 P-wave velocity model (Amaru, 2007) of the present-day mantle structure at depths of (a) 350, (b) 470, and (c) 1090 km. Reconstructed positions of the Olyutorsky arc (green) and Kronotsky arc (orange) and the associated intraoceanic subduction zones (black with closed triangles) relative to the mantle at 60 Ma (using the mantle reference frame of Doubrovine et al., 2012) are shown in (c).

of Seton et al. (2015) that this slab represents Pacific plate lithosphere that subducted after the ~60–50 Ma arrival of the Izanagi-Pacific ridge at the Japan Trench.

In addition to these actively subducting slabs, a series of detached anomalies were identified (e.g., Domeier et al., 2017; van der Meer et al., 2018). In the upper-lower mantle transition zone below the central Bering Sea lies the Bering slab (Figure 8b), which was correlated by van der Meer et al. (2018) to Oligocene subduction at the Bowers Ridge. Also in the transition zone, but below Kamchatka, lies the Mayn slab (Figure 8b). Van der Meer et al. (2018) followed the interpretation of Chekhovich et al. (2012) that there was ~30–15 Ma subduction below the Shirshov Ridge, and proposed that this would have produced the Mayn slab. To the west, between ~1,600 and 800 km depth in the lower mantle below the northern Sea of Okhotsk lies the Ushky slab (Figure 8c). This slab was correlated by van der Meer et al. (2018) to Cretaceous subduction along the NE Asian margin producing the Okhotsk-Chukotka arc that ended around 80 Ma upon collision with the Okhotsk block (Akinin & Miller, 2011; Hourigan & Akinin, 2004; Pease et al., 2018; Tikhomirov et al., 2012; Yang, 2013). The Sakhalin slab toward the southwest, between ~1,000 and 700 km depth was interpreted by van der Meer et al. (2018) to be closely related to the Ushky slab, reflecting Cretaceous subduction prior to Okhotsk Block accretion below the Sakhalin margin producing the East Sikhote-Alin arc. South of the Komandorsky Islands, between 1,400 and 600 km depth lies the Agattu slab (Figure 8c). This slab is clearly south to southerly dipping, and even flat-lying around 1,200–1,400 km depth and was correlated by van der Meer et al. (2018) as well as Domeier et al. (2017) to the Olyutorsky arc. Toward the east, from southern Alaska toward the southwest, at a depth of 1,400–800 km, lies the North Pacific anomaly, which was correlated by (Domeier et al., 2017) and van der Meer et al. (2018) to intraoceanic subduction below the Kronotsky arc (Figure 8c). Finally, to the north of the North Pacific slab, between 1,100 and 800 km depth below Alaska lies the Yukon slab (Figure 8c), correlated by van der Meer et al. (2018) to the Late Cretaceous Kluane arc that is contained in the complex Alaskan orogen.

7. Reconstruction of NW Pacific Active Margins

We used the global plate circuit and the geological, kinematic, and paleomagnetic data reviewed above for a plate kinematic restoration of the NW Pacific region as illustrated in Figures 9 and 10. We present this history from today's configuration back in time to the Late Cretaceous (to 85 Ma) and explain below which interpretations are used in this reconstruction.

7.1. 25 to 0 Ma: Opening of Japan Sea, Kuril, and Komandorsky Basins

The Neogene history of the NW Pacific region includes the opening of the Japan Sea, Kuril, and Komandorsky back-arc basins, the main phase of dextral strike-slip motion along the Sakhalin-Hokkaido Shear Zone and the accretion of the extinct Kronotsky island-arc. To reconstruct these, we have divided the Japanese islands and Sakhalin into rigid blocks (see Figure 2) based on their Eocene-present (~40–0 Ma) tectonic history. A detailed reconstruction of the Late Cretaceous to Early Paleogene history of the (mostly Mesozoic) subduction-related terranes of the Asian margin, preserved on the Japanese Islands and Sakhalin (see Figure 4), is beyond the scope of this paper. In our reconstruction, we infer that also the undated Bowers Basin, between the Bowers Ridge and the Aleutian Trench, is of Miocene age, but because this follows from the Paleogene reconstruction of the Bowers Ridge subduction, we will explain this line of reasoning in section 7.2.2.

7.1.1. Opening of the Japan Sea Basin

The opening mechanism of the Japan Sea and its underlying basins is debated and two opposing models have been proposed. One model explains the Japan Sea as a pull-apart basin that formed as a releasing bend between two major dextral strike-slip zones: the Tsushima-Goto and the east Japan Sea fault zones (e.g., Fournier et al., 1994; Jolivet et al., 1994; Jolivet & Tamaki, 1992). If true, this model would require restoring northeast Japan toward the Sea of Okhotsk region, which would then strongly influence the reconstruction of Sakhalin and the East Sakhalin-Nemuro arc. A second model invokes trench-perpendicular extension leading to opposing rotations of the NE and SW Japan blocks (e.g., Martin, 2011; Otofuji et al., 1985). If correct, this model suggests that the Japan Sea and arc have moved mainly relative to Eurasia and restoring these motions does not influence the Okhotsk Sea region much. The second model, with opening of the Japan Sea through opposite rotations of NE and SW Japan, is clearly favored by paleomagnetic constraints (Figure 6), and is therefore included in our reconstruction.

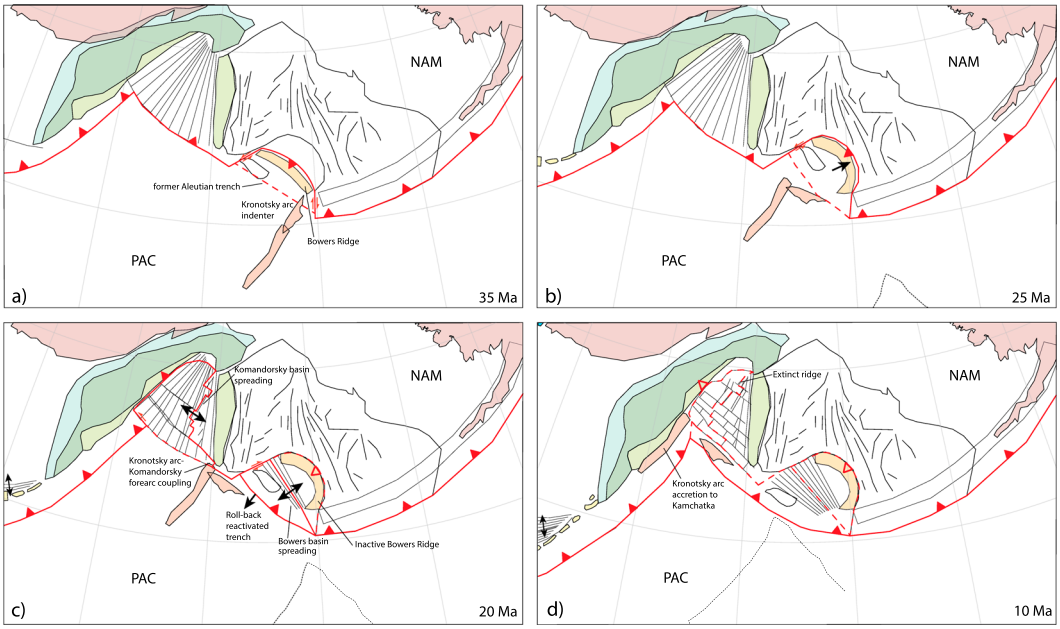

Figure 9. Snapshots of the plate-kinematic reconstruction of the Bering Sea region at (a) 35, (b) 25, (c) 20, and (d) 10 Ma, relative to a fixed North American plate. The dashed black line represents the reconstructed location of the edge of Pacific plate lithosphere that is presently subducting below the Kuril-Kamchatka and Aleutian Trenches southeast of Kamchatka. Dashed red lines indicate extinct plate boundaries. Red filled/open triangles indicate active/extinct subduction zones. Abbreviations: NAM = North American plate; PAC = Pacific plate.

We model NE and SW Japan as rigid blocks that rotated independently (following, e.g., Kim et al., 2007, 2015; Martin, 2011; Otofuji et al., 1985; Sato, 1994). We reconstruct the onset of rifting between SW Japan and the Korean peninsula at 23 to 18 Ma and follow Kim et al. (2011, 2015) in reconstructing 70 km SE-directed motion of SW Japan relative to the Korean peninsula during this stage, involving 60–70 km of extension at the southeastern margin of Korea to ~100 km between present-day North Korea and the Noto peninsula. For the northeast Japan Sea, we restore up to 100 km of 23–20 Ma extension between NE Honshu and stable Eurasia to represent the southeast-directed motion of NE Japan as a result of initial intra-arc rifting (Van Horne et al., 2017). We model this extension perpendicular to the Japan Trench, consistent with the opening direction of (half-) grabens in the northern Japan Sea (Sato, 1994; van der Werff, 2000).

The remaining extension is reconstructed during the main rifting phase between ~18 and 15 Ma for the southwest and ~20–15 ma for the northeastern Japan Basin (Kaneoka, 1992; Kim et al., 2015; Martin, 2011; Nohda, 2009; Sato, 1994; Van Horne et al., 2017), complying with the rapid rotations that follow from paleomagnetic data (Figure 6). We restore up to a maximum of 400 km of extension for both SW and NE Japan (Figures 10e and 10f), consistent with extension predicted by the crustal thicknesses in the Japan Sea Basin, assuming an initial thickness of 35 km. This results in a total amount of extension close to the 400–500 km of extension in the Japan Sea Basin as estimated by Martin (2011) and Van Horne et al. (2017). The resulting two-step opening of the Japan Sea by the oppositely rotating SW and NE Japan blocks is consistent with paleomagnetic declination data for southwest and northeast Japan (Figure 6). However, our reconstruction predicts a dextral displacement along the Tsushima-Goto fault zone west of southwestern Honshu of about 30 km between 23 and ~18 Ma, much lower than the maximum estimated 200 km by Jolivet and Tamaki (1992). Our new model shows that a reconstruction of the Japan Sea opening that is consistent with crustal thicknesses and paleomagnetic data does not require large-scale dextral along the strike-slip faults bounding the Japan Sea. In contrast, our model predicts a phase of sinistral transpression in southwesternmost Honshu and the Tsushima and Goto islands from ~17 to 15 Ma, consistent with observed Middle Miocene deformation along the Tsushima-Goto fault system (Fabbri et al., 1996; Son et al., 2015).

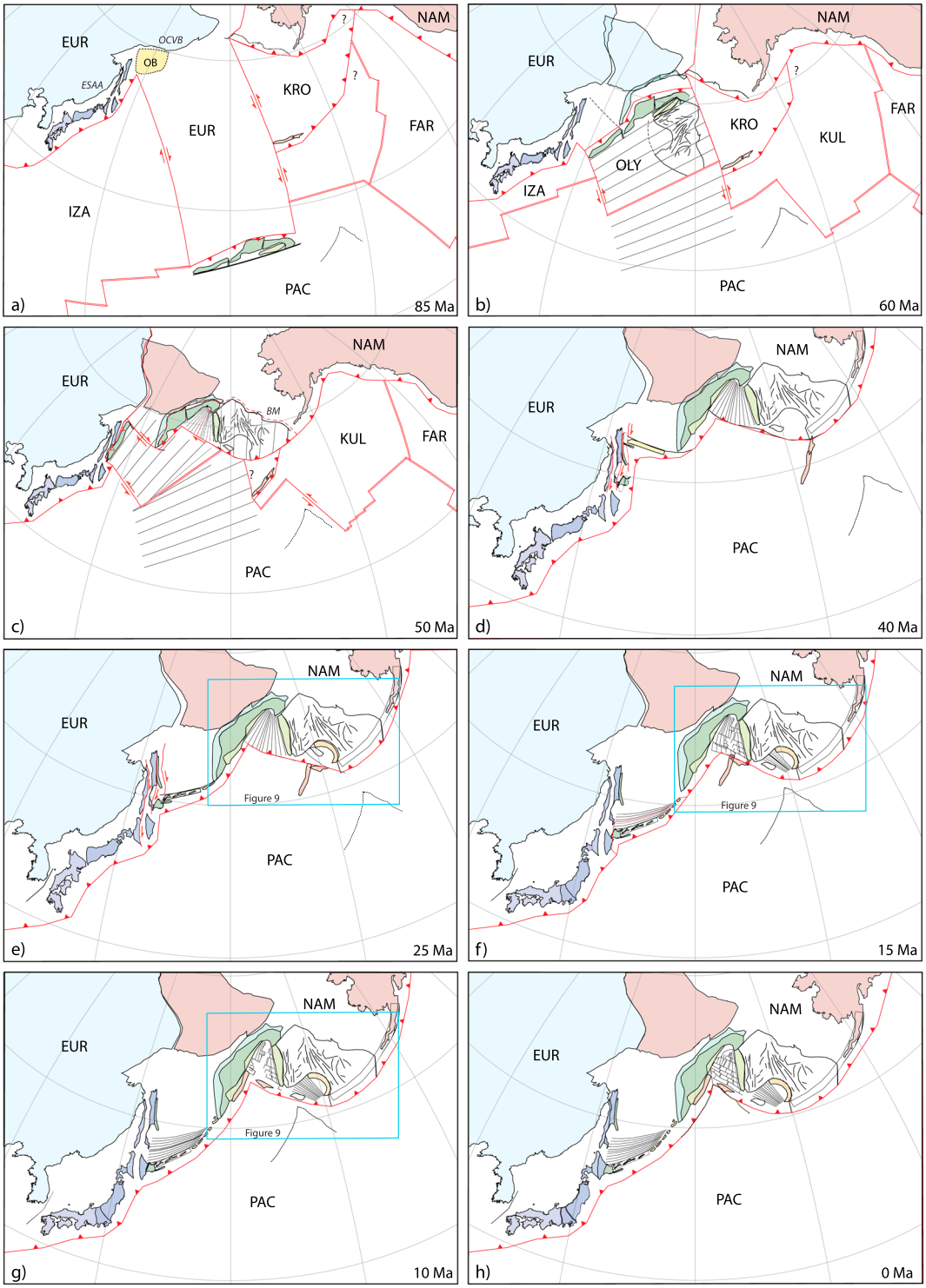

Figure 10. Plate boundary configurations of the northwest Pacific region between 85 Ma and present, shown at (a) 85, (b) 60, (c) 50, (d) 40, (e) 25, (f) 15, (g) 10, and (h) 0 Ma, relative to a fixed Eurasian plate. Plate boundaries are shown in red, with filled triangles, arrows and double lines indicating subduction zones, transforms, and spreading ridges, respectively. Straight, black lines indicate oceanic crust formed at the Olyutorsky-Pacific spreading ridge and the approximate orientation of associated magnetic anomalies. The dashed black line represents the reconstructed location of the edge of Pacific plate lithosphere that is presently subducting below the Kuril-Kamchatka and Aleutian Trenches southeast of Kamchatka. Abbreviations: EUR = Eurasian plate; FAR = Farallon plate; BM = Beringian margin; ESAA = East Sikhote-Alin arc; IZA = Izanagi plate; KRO = Kronotsky plate; KUL = Kula plate; NAM = North American plate; OCVB = Okhotsk-Chukotka volcanic belt; PAC = Pacific plate.

A two-step evolution of the Fossa Magna area between 23 and 15 Ma follows from the above reconstruction of NE and SW Japan. We infer a large fault zone between the oppositely rotating rigid blocks that accommodated dextral strike-slip motion during the first part of the opening of the Sea of Japan, similar to the model of Sato (1994). We model up to ~150 km of right-lateral displacement between 23 and 15 Ma, with most of the motion between 20 and 15 Ma, corresponding to the peak of spreading activity in the Japan and Yamato Basins. The inferred dextral fault zone is not clearly observed in the geological record, probably because it was overprinted by the formation of the Fossa Magna depression and associated basins. The opposite rotation of NE and SW Japan based on extensional records of the Sea of Japan predicts trench-parallel extension in the Fossa Magna region between 17 and 15 Ma. This involves about 30 km of extension in the northernmost part of Fossa Magna, corresponding well with estimated values of ~30–40 km from balanced cross-sections for the northern Fossa Magna Basin (Elouai et al., 2004; H. Sato et al., 2004). Our models predict up to ~200 km of extension in the southernmost part of Fossa Magna, which is equal to the estimate from Martin (2011).

Since ~15 Ma, the southwestern part of the Japanese islands are dominated by inversion tectonics, which may relate to the collision of the Philippine Sea plate due to a change in plate motion associated with a regional plate reorganization (e.g., Kimura et al., 2014; Sibuet et al., 2002; Son et al., 2015). Estimates of the shortening associated with the recent tectonics are in the order of tens of kilometers and are not taken into account in this reconstructed.

7.1.2. Opening of the Kuril Basin

Following from our reconstruction of NE Japan as outlined above, we restored ~170 km of dextral strike slip between the Central Hokkaido and West Sakhalin terranes and Eurasia during the opening of the Japan Sea between 23 and 15 Ma accommodated along offshore faults running through the Tartary Strait (Fournier et al., 1994; Figures 10e and 10f). We reconstructed 50 km of dextral N-S motion between the island-arc units of eastern Sakhalin and Central Sakhalin, following the estimate of Fournier et al. (1994). We model a similar dextral offset of ~50 km along the Tym-Poronaysk fault between 23 and 9 Ma, synchronous with the opening of the Kuril Basin (Schellart et al., 2003; Takeuchi et al., 1999). In addition, we restore 50 km of extension in the Aniva Trough, which results in ~100 km of dextral motion along the Hidaka Shear Zone.

We then reconstructed the Kuril Basin extension by restoring the Kuril Trench up to ~400 km toward the northeast between 23 and 9 Ma (Figures 10e–10g). This corresponds to the full width of the bathymetric depression of the Kuril Basin and is ~100 km more than the estimate of Schellart et al. (2003). The geometry of the back-arc basin (Figures 1 and 2) suggests that this basin opening was associated with a counterclockwise rotation of the Kuril forearc relative to the Okhotsk block north of the Kuril Basin. The Nemuro and Lesser Kuril islands Cretaceous to Paleogene arc fragments as well as the Tokoro belt restore with the Kuril forearc bringing the Tokoro belt adjacent to southeast Sakhalin, consistent with geological observations (Kimura, 1994; Maeda, 1990; Ueda, 2016; Zharov, 2005). After opening of the Kuril Basin, between ~9 Ma and the present, we modeled the eastern parts of Sakhalin and Hokkaido as part of the North American plate. This predicts ~70 km of NE-SW convergence in central Sakhalin to 100 km in southern Hokkaido, consistent with geological shortening estimates (e.g., Iwasaki et al., 2004).

7.1.3. Kronotsky Arc Collision and Opening of the Komandorsky Basin

Magnetic anomalies in the Komandorsky Basin suggest that between ~20 and ~10 Ma, up to ~450 km of NW-SE extension was accommodated by ocean spreading in the SW of the basin. Toward the north, extension amounts abruptly decrease across two transform faults, and we modeled the 20–10 Ma evolution of the basin by three transform-ridge bounded microplates (SW, Central, and NW Komandorsky microplates) that moved northwest relative to the Shirshov Ridge, subducting below NE Kamchatka (Baranov et al., 1991; Nokleberg et al., 2000; Scholl, 2007; Valyashko et al., 1993; Figures 9c and 9d). As argued by Scholl (2007), there is no evidence for relative motion between Kamchatka and the Shirshov Ridge during the Neogene. We therefore reconstruct the subduction below northern Kamchatka of oceanic crust that prior to the Neogene floored a proto-Komandorsky Basin. This episode of subduction is consistent with Miocene-Pliocene calc-alkaline volcanism in the Kamchatka isthmus (Hochstaedter et al., 1994; Shapiro & Solov'ev, 2011), as well as the sediment-filled trench on the eastern margin of northern Kamchatka (Avdeiko et al., 2007; Baranov et al., 1991). We modify the interpretation of van der Meer et al. (2018) and correlate the Mayn slab to subduction of the proto-Komandorsky Basin between 20 and 10 Ma, instead of

Cenozoic subduction below the Shirshov Ridge, for which there is no compelling evidence (see also section 7.2).

Spreading is inferred to have been accommodated around a pole to the north of the Komandorsky Basin. Stretched arc and an arc-ocean crustal transition was interpreted from geophysical data, but no relics of arc crust that accreted during Miocene subduction are found along eastern Kamchatka. There is thus no positive evidence that prior to the early Miocene the Shirshov Ridge was wider than today, and we model the subducted, proto-Komandorsky Basin as oceanic, with crust whose age is not directly constrained by observations. Restoring the reported marine magnetic anomalies (Baranov et al., 1991) suggests, however, that relict crust of such a proto-Komandorsky Basin may still be present in the northwestern part of the basin (Figure 9d).

Scholl (2007) suggested that the Komandorsky Basin opened as a forearc sliver, equivalent to, for example, the Andaman Sea. This interpretation is elegant in the light of the observation from the plate circuit that between 20 and 10 Ma, the Pacific-North America motion vector is parallel to the spreading direction of the Komandorsky Basin, and the amount of motion equals the amount of reconstructed spreading, in other words, the southwestern Komandorsky microplate appears to have coupled to the Pacific plate, generating Komandorsky Basin extension (Figure 9c). We infer that a likely reason for this coupling was the highly oblique collision of the Kronotsky arc: when the collision age of Kronotsky with Kamchatka is modeled as 10 Ma (within the geologically constrained collision age range of 5–10 Ma), the Kronotsky arc couples with the Komandorsky crust around 20 Ma, moves in tandem with the SW Komandorsky microplate and generates proto-Komandorsky Basin subduction below NE Kamchatka (see Figure 9). Upon Kronotsky-Kamchatka collision, Komandorsky spreading and subduction ceased. The direct interaction of the Kronotsky arc with the Komandorsky crust is consistent with the interpretation that the Komandorsky Islands consist of Kronotsky arc rather than Aleutian arc crust (Alexeiev et al., 2006; Bazhenov et al., 1992; Rostovtseva & Shapiro, 1998; Figure 9). We model the Komandorsky Islands as a part of the Kronotsky arc that broke off and were left in their current position at ~13 Ma.

7.2. 40 to 25 Ma: Opening of Okhotsk Sea Basin; Subduction at Bowers Ridge

The 40 to 25 Ma period covers the time interval following upon the final accretion of the Greater Olyutorsky arc and the final extinction of the Kronotsky arc. The period was characterized by the opening of the Okhotsk Sea and the enigmatic subduction history forming the Bowers Ridge.

7.2.1. Opening of the Okhotsk Sea Basin

We restore the Late Eocene to Early Miocene opening of the Sea of Okhotsk back-arc basin as a counterclockwise rotation of the Kuril Trench and arc around a pole relative to NE Asia located in south Kamchatka. We model up to 800 km of N-S extension along the transform boundary with Sakhalin (Figure 10), following Schellart et al. (2003). This requires that the Kuril Trench must have existed and rolled back since at least 40 Ma, and subduction thus starting prior to the oldest dated island-arc rocks from the Kuril volcanic arc that have an Early Oligocene age (De Grave et al., 2016). Our reconstructions suggest that up to 3,000 km of subduction occurred along the Kuril-Kamchatka Trench, consistent with the long slab in the upper and top of the lower mantle, whereby the flat portion of the Kuril-Kamchatka slab (Figure 8) is similar in length to the amount of extension modeled in the Sea of Okhotsk and Kuril Basin.

Restoring the Okhotsk Sea back-arc basin shows that in Middle Eocene time, just after their obduction onto NE Asia, the East Sakhalin, Nemuro, and Olyutorsky arc segments were oriented at high angles to each other (Figure 10d). The East Sakhalin arc was oriented ~N-S relative to a fixed Asia. The Nemuro-Kuril forearc segment restores to a NW-SE orientation connecting the northern part of Sakhalin with south Kamchatka, and defined the restored southern margin of the Okhotsk block. The Olyutorsky arc was oriented NE-SW, parallel to Kamchatka (Figure 10d).

7.2.2. Subduction and Spreading in the Bering Sea Region

The isolated Bowers Ridge intraoceanic arc within the Aleutian back-arc is one of the most enigmatic features of the northern Pacific tectonic history, but may be understood in terms of arc-arc collision between the Kronotsky and Aleutian arcs. As shown above, modeling the Kronotsky arc as a contiguous part of the Pacific plate after its 40 Ma cessation generates a straightforward Miocene tectonic history of the

Komandorsky Basin, and restores the Kronotsky arc southwest of the Bowers Ridge at about 25 Ma, in the center of the Bowers Basin (Figure 9b). The northern part of the Kronotsky arc, however, overlaps with the modern Aleutian arc by ~150 km. This overlap is generated between ~34 and 26 Ma (Figures 9a and 9b), that is, in the time period during which the Bowers intraoceanic arc was active (Sato et al., 2016; Wanke et al., 2012). This suggests that subduction below the western Aleutian Trench was temporarily interrupted around 34 Ma due to indentation of the extinct Kronotsky arc, and was instead accommodated by southwestward subduction north of the indenter at the Bowers Ridge. As shown by van der Meer et al. (2018), 34–26 Ma subduction below the Bowers Ridge is fully consistent with the location of the Bering Sea slab.

Our reconstruction of the Bowers Ridge contains similarities with the New Hebrides subduction zone in the SW Pacific. There, a subduction polarity reversal occurred behind the Melanesian arc due to collision of a buoyant indenter formed by the Ontong-Java Plateau (Hall, 2002; Knesel et al., 2008). Our reconstruction of the Bowers Ridge as a result of arc-arc collision predicts that the Bowers Basin, whose age is poorly constrained through direct geological or geophysical observation, was not formed by Eocene-Oligocene back-arc spreading behind the Bowers Ridge as previously suggested (Cooper et al., 1992), but as a result of Miocene southwestward roll-back of the western Aleutian Trench to its modern orientation (Figure 9c). Figure 9d shows synthetic marine magnetic anomalies based on a southwestward direction of trench roll-back. The resulting NW-SE to NNW-SSE orientation of these anomalies is not fully consistent with the marine magnetic anomalies in the eastern part of the Bowers Basin as interpreted by Cooper et al. (1976, 1992), which have a N-S orientation instead. If these anomalies represent isochrons, then the roll-back of the Aleutian Trench and the associated back-arc extension may have been more westward, oblique to the modern Aleutian Trench, then modeled here.

Several authors suggested that subduction also occurred below the Shirshov Ridge during the Eocene-Oligocene (e.g., Scholl, 2007; van der Meer et al., 2018; Yogodzinski et al., 1993). There is, however, no convergence between Kamchatka and the Aleutian Basin between 40 and 25 Ma: the Olyutorsky arc did not move relative to Kamchatka after 45 Ma (Solov'ev et al., 2011; Solov'ev, Shapiro, & Garver, 2002) and relative motion between the Aleutian Basin and Alaska at the Beringian margin ceased around 50 Ma (e.g., Scholl, 2007; Worrall, 1991). There is no evidence for arc volcanism of the Shirshov ridge in this time period, and there is no record of Eocene-Oligocene E-W spreading orthogonal to the ridge to the east or west. We therefore model the Shirshov Ridge at its current relative position to Kamchatka between 40 and 25 Ma, contiguous with the lithosphere underlying the Aleutian Basin.

7.3. 60 to 40 Ma: Aligning the East Sakhalin-Nemuro, Olyutorsky, and Shirshov Arcs; Initiation of Aleutian Subduction

Around 60–55 Ma, the distal passive margin of southern Kamchatka started to become involved in subduction below the Olyutorsky arc (Konstantinovskaya, 2001, 2011; Shapiro et al., 2008; Shapiro & Solov'ev, 2009), culminating in final, diachronous obduction at ~50 Ma in south Kamchatka, ~45 Ma in north Kamchatka, and ~45 Ma in East Sakhalin, the arrest of subduction at the Beringian margin around 50 Ma, and the presumed initiation of subduction at the Aleutian trench. In this section, we provide a restoration of the obduction and segmentation of the Olyutorsky-east Sakhalin-Nemuro arc and propose a new scheme to explain the separation of the Shirshov Ridge from the Olyutorsky arc, leading to the opening of a proto-Komandorsky basin and a subduction jump from the Beringian margin to the Aleutian trench. Only few constraints are available on the pre-40 Ma position of the Kronotsky arc, and we will describe its restoration between 40 Ma and the initiation of subduction around 85 Ma in section 7.4.2.

Because of the strong similarities in the composition and age range of arc volcanism, the Olyutorsky-east Sakhalin-Nemuro arc is widely assumed to have been a single, coherent arc (Domeier et al., 2017; Konstantinovskaya, 2001; Nokleberg et al., 2000; Shapiro & Solov'ev, 2009). To arrive at a contiguous belt, we reconstruct a breakup of the Olyutorsky arc into two segments that are separated by a transform fault (Figures 10b and 10c), following Shapiro et al. (2008). We restore ~80 km of relative sinistral motion between a northern and southern segment between 50 and 45 Ma, that is, the period between the cessation of

obduction of both segments. Between 50 and 45 Ma, we restore ~50 km of convergence between the northern segment of the arc and the West Kamchatka zone, accommodated by thrusting along the Vatyn-Lesnaya fault (Solov'ev et al., 2011; Solov'ev, Shapiro, & Garver, 2002).

The Shirshov Ridge appears to be a Cretaceous volcanic arc that is contiguous with the lithosphere underlying the Aleutian basin (Scholl, 2007). Because of its location close to the Olyutorsky arc and the fact that it is physiogeographically connected to the Olyutorsky arc terrane at Cape Olyutorsky (Figures 1 and 2), we suggest that the Shirshov Ridge was originally part of the Olyutorsky arc. The modern distance between the Olyutorsky arc and Shirshov Ridge is >500 km, which is unrealistically wide for a volcanic arc, suggesting that an extensional basin—the proto-Komandorsky basin—split the Shirshov Ridge off the Olyutorsky arc leading to the extinction of the Shirshov Ridge. Such a scenario of "arc splitting" may be analogous to the history of the modern Lau basin that split the Tonga arc in two, whereby the trenchward segment remained active (Malahoff et al., 1994). The youngest volcanic rocks dredged from the Shirshov Ridge suggest that this arc splitting occurred after ~65–60 Ma. The proto-Komandorsky basin is a triangular basin, suggesting that its opening was associated with a ~40° counterclockwise rotation of the Shirshov Ridge—and consequently also the Aleutian basin lithosphere—relative to the Olyutorsky arc (Figures 10b and 10c) around a pole at the position of the Bering Strait. This requires convergence between the Aleutian basin and North America, which was accommodated by northeastward subduction at the Beringian margin until ~50 Ma (Davis et al., 1989; Miller et al., 2018; Scholl, 2007; Worrall, 1991). We therefore model the opening of the proto-Komandorsky basin largely between 60 and 50 Ma. This restoration aligns the marine magnetic anomalies recovered from the Aleutian basin lithosphere with the restored strike of the Olyutorsky arc at and before 60 Ma (Figure 10b).

Aligning a single Greater Olyutorsky arc at 60 Ma also requires reconstructing a counterclockwise rotation of ~40° of the East Sakhalin-Nemuro arc and now-subducted oceanic crust to its east, between 60 and ~45 Ma, but here around a pole close to Hokkaido. This rotation was guided in the north by a transform fault with a ~800 km dextral displacement along the southwestern margin of the Okhotsk Block. We infer that the E-W-trending part of the Nemuro belt and its eastward continuation into the Lesser Kuril forearc and Vityaz Ridge are segments that were left behind in this transform fault.

It is interesting to note that the shape of the modern Aleutian trench approximates a small circle around the Euler pole that defines the relative Aleutian basin-Olyutorsky arc rotation during the opening of the proto-Komandorsky basin. This may suggest that the Aleutian trench formed initially as a transform fault during the ~60–50 Ma rotation. This transform fault, as well as the one that developed along the southern Okhotsk Block margin, had a strike approximately orthogonal to the trench along the Greater Olyutorsky arc, and may thus have reactivated transform faults or fracture zones in the Greater Olyutorsky back-arc region (Figure 10b). Convergence between the Aleutian basin lithosphere and North America ceased around 50 Ma upon Olyutorsky arc-Kamchatka collision, which hampered ongoing Aleutian basin-Alaska convergence, and led to the arrest of subduction at the Beringian margin and inception of subduction along the Aleutian trench, inverting the preexisting transform fault.

The onset of rotation of the Aleutian basin and the East Sakhalin-Nemuro arc split the Olyutorsky arc and underlying lithosphere into two plates separated by a transform. We model the lithosphere south (west) of the Aleutian transform/trench (i.e., the remnant Olyutorsky plate, see section 7.4.1) as contiguous with the East Sakhalin arc, which would suggest that subduction polarity reversal behind the southern Olyutorsky arc occurred immediately upon obduction of the arc onto Kamchatka, ~55–50 Ma. This slab was connected to the East Sakhalin-Nemuro arc lithosphere as it rotated and moved toward Sakhalin, dipping below the south Okhotsk block transform, such that upon arc-continent collision at Sakhalin, a Kuril slab was already present that started retreating southward shortly after at ~40 Ma (Figure 10d), associated with the large-scale extension in the Okhotsk Sea (section 7.2.1).

The Olyutorsky arc restores above the location of the top of the Agattu slab around the 60–55 Ma inception of obduction and its likely moment of break-off (Figure 8c). A separate slab segment was not identified by van der Meer et al. (2018) that may have broken off during obduction of the East Sakhalin segment, but we tentatively interpret this slab to form part of the Sakhalin slab, and perhaps the lower part of the horizontal segment of the Kuril-Kamchatka slab. Because the Alaskan orogenic

belt underwent major Cretaceous to Eocene translations parallel to North America, and oroclinal buckling (e.g., Johnston, 2001), reconstructing the Beringian margin prior to arrest of subduction around 50 Ma is challenging and not contained in our current reconstruction. If the oroclinal buckling proposed by Johnston (2001) is correct, then the Beringian margin restores >500 km to the east in Late Cretaceous time, making the Yukon slab and the Kluane arc (Nokleberg et al., 2000) possible relics of Beringian subduction.

7.4. 85 to 60 Ma: Intraoceanic Subduction Initiation and Evolution of the Greater Olyutorsky and Kronotsky Arcs

The most challenging part of the reconstruction is the intraoceanic subduction history, between ~85–60 Ma for the Greater Olyutorsky arc and ~85–40 Ma for the Kronotsky arc. Absolute positions of the arc may be inferred from paleomagnetic data and seismic tomographic constraints on modern slab positions that may correspond to these arcs. Relative positions versus the Pacific plate may be inferred from the age of ophiolites and accreted oceanic rocks associated with the arcs in combination with restorations of the Izanagi plate reconstructed from its conjugate anomalies on the Pacific plate.

7.4.1. Greater Olyutorsky Arc and Back-Arc

Our ~60 Ma reconstruction reveals a contiguous, 2,500 km-long Greater Olyutorsky arc above a southeasterly dipping intraoceanic subduction zone with the Aleutian Basin, including 13 marine magnetic anomalies interpreted as magnetic polarity reversals (Cooper et al., 1976), oriented roughly parallel to the restored arc and trench, in its overriding plate. The southeastward polarity of subduction below the Greater Olyutorsky arc requires that it converged with Eurasia, but there are different approaches to estimate how much.

Because many of the paleomagnetic sites from the Olyutorsky arc are derived from sedimentary rocks and tuffs, Domeier et al. (2017) suspected that the inclinations provided by these sites may have shallowed due to compaction. They therefore corrected these data with a widely used average flattening factor of 0.6 (e.g., Torsvik et al., 2012), which would suggest that the paleolatitude of the Greater Olyutorsky arc throughout the Late Cretaceous was ~55°N. They use these corrected data as a basis to reconstruct the paleo-location of the Olyutorsky arc. When placed in a mantle reference frame (Doubrovine et al., 2012), this places the Greater Olyutorsky arc above the southern, deepest imaged portions of the Agattu slab, which they therefore inferred to be the absolute position of the arc at subduction initiation. If correct, the amount of 85–55 Ma convergence between the Pacific plate and NE Asia, and between the Greater Olyutorsky arc and Eurasia, are similar, that is, the Olyutorsky arc would be part of the Pacific plate. Domeier et al. (2017) inferred that subduction initiation may have started at the Izanagi-Pacific ridge or along oceanic detachment faults adjacent to that ridge, a scenario shown by Maffione et al. (2015) and Maffione and van Hinsbergen (2018) for ophiolites in the Mediterranean region. Such a setting of subduction initiation at a ridge is consistent with the similar ages between the ophiolitic basement and the arc (see section 4.4).

We consider this reconstruction of Domeier et al. (2017) problematic for two reasons. First, the global plate circuit in the mantle reference frame of Doubrovine et al. (2012) shows that the inferred location of the youngest marine magnetic anomaly contained in the modern Pacific plate lithosphere (M0, ~120–126 Ma depending on the time scale used; Cande & Kent, 1995; Gradstein et al., 2012) is located >4,000 km to the south of the Olyutorsky Trench position at subduction initiation predicted by Domeier et al. (2017). This would therefore require full Izanagi-Pacific spreading rates of >20 cm/year for ~35–40 Myr between M0 and the time of subduction initiation, ~85 Ma, much faster than the highest spreading rates reconstructed from the modern ocean floor. Such rates are extremely high, much more than pre-120 Ma spreading rates of ~8 cm/year (Seton et al., 2012), and must have peaked at even higher rates since prior to ridge inversion and subduction initiation, spreading rates must first decrease toward zero. Second, marine geophysical studies of the upper plate behind the Olyutorsky arc, preserved below the Aleutian Basin, interpreted the north-south-trending marine magnetic anomalies in the Aleutian Basin as being formed by seafloor spreading (Cooper et al., 1976, 1992; Scheirer et al., 2016; Steinberger & Gaina, 2007), which if correct, falsifies the scenario of Domeier et al. (2017), in which the upper plate would have entirely formed during the Cretaceous Normal Superchron (Table 1).

We therefore take a different approach, which may be considered an opposite end-member of the Domeier et al. (2017) reconstruction. We follow the suggestion of Domeier et al. (2017) that subduction

Table 1
Model Predictions for the Bering Sea Region

a)	Name	Predicted age (Ma)	Age (west), Ma	Age (east), Ma	Age (IODP), Ma	Paleolatitude	Model
	Aleutian Basin	~85–60	~85	~60	~78	<60°, decreasing toward west	This study
		~100–85	~85	~100	~90	<60°, decreasing toward east	Domeier et al. (2017)
		<50	<50	<50	<50	~60–70°	In situ formation

b)	Name	Published ages	Age (this study), Ma	Sources
	Aleutian arc	~46–0 Ma	50–0	Jicha et al. (2006), Layer et al. (2007)
	Bowers Basin	Eocene-Oligocene	**~25–10**	Cooper et al. (1992)
	Bowers Ridge	34–26 Ma	34–26	Wanke et al. (2012), Sato et al. (2016)
	Komandorsky Basin	~20–10 Ma	20–10	Valyashko et al. (1993)
	Komandorsky Islands	Paleocen-Eocene[a]	**~85–40**[a]	Bazhenov et al. (1992), Rostovtseva and Shapiro (1998)
	Shirshov Ridge	L. Cret.-E. Paleog.	~85–60	Baranov et al. (1991), Hauff et al. (2016)

Note. a) Predicted age and paleolatitude during formation for the Aleutian Basin basement based on three models. Note that our prediction is based on the assumption that the Aleutian Basin crust completely formed on the northern side of the spreading ridge. Predictions for the model of Domeier et al. (2017) are based on the assumption that the Aleutian Basin contains Pacific plate lithosphere formed by Izanagi-Pacific spreading prior to ridge inversion, after which it formed the overriding plate south of the Olyutorsky arc. West and east indicate the western and easternmost parts of the basin. Age (IODP) = predicted age at the proposed sites in the IODP Drilling Proposal 888-full. Estimated paleolatitude for in situ formation is based on a Paleogene age of formation (between 50 and 23 Ma). b) Ages of the main tectonic features of the Bering Sea region, as published in literature and as adopted in or predicted by this study. Predicted ages are indicated in bold.
[a]The age of the Komandorsky Islands refers to its basement, interpreted to be derived from the Kronotsky (fore)arc.

started at the Izanagi-Pacific ridge, but instead infer the position of that ridge by extrapolating the ~8 cm/year full spreading rates from the Early Cretaceous (Figure 10a). The southwestward continuation of the trench along the Greater Olyutorsky arc is uncertain. Because subduction below the Japanese islands and Sakhalin continued throughout the Late Cretaceous, we model a right-lateral transform fault between northern Sakhalin and the southwestern termination of the Olyutorsky Trench. As there is no evidence for arc accretion south of Hokkaido during the Cenozoic, we infer that the Izanagi-Pacific ridge remained active between the Pacific plate and the Japan active margin (Figures 10a and 10b). Further extrapolation of the Early Cretaceous full spreading rates would lead to the widely inferred subduction of the Izanagi-Pacific ridge below Japan around ~60–50 Ma (e.g., Liu et al., 2017; Seton et al., 2012; Seton et al., 2015; Whittaker et al., 2007; Figures 10b and 10c), consistent with geological and seismic tomographical observations such as the presence of MORB basalts intruding wet Paleocene-Lower Eocene foreland basin sediments (Ueda, 2016) and the length of the modern Manchuria slab below Japan (e.g., van der Meer et al., 2018).

Assuming 8 cm/year full Izanagi-Pacific spreading during the Cretaceous Normal Superchron brings the initial location of the Olyutorsky arc at ~85 Ma about 2,000–2,500 km farther south than proposed by Domeier et al. (2017). Such a position is consistent with the Late Cretaceous paleolatitudes suggested by paleomagnetic data (Figure 7b). This reconstruction would require that the Greater Olyutorsky arc underwent faster absolute northward motion than the Pacific plate between ~85 and 60–50 Ma, creating ~2,500–3,000 km of Pacific-Olyutorsky divergence that must have been accommodated by a spreading ridge between an Olyutorsky plate and the Pacific plate. Following the scenarios of Maffione et al. (2015) and van Hinsbergen et al. (2015), we model that the original Izanagi-Pacific ridge, preserved in the forearc above the nascent southward intraoceanic subduction zone, was reactivated and became the Pacific-Olyutorsky plate boundary. The geochemical signatures predicted by such a scenario are found in the suprasubduction zone signature of Upper Cretaceous ophiolites associated with the Olyutorsky arc (Geist et al., 1994; Kravchenko-Berezhnoy & Nazimova, 1991; Tsukanov et al., 2009) and the presence of Paleocene-Upper Eocene MORB-lavas of the Vetlovsky-Govena terrane in the accretionary prism below the Olyutorsky arc nappes in Kamchatka (Bakhteev et al., 1994; Gladenkov, 2016; Zinkevich & Tsukanov, 1993) is straightforwardly explained by a spreading center between the Olyutorsky arc and the Pacific plate. In this scenario, the Olyutorsky-Pacific ridge likely became active shortly after subduction initiation at ~85 Ma, and we therefore estimate that seafloor spreading south (east) of the Olyutorsky arc occurred between ~85 and 60–50 Ma. The magnetic anomalies predicted by this reconstruction are more or less parallel to the magnetic anomalies of

the Aleutian Basin in our restoration at 60 Ma (Figure 10b). At 60 Ma, the modern easternmost part of the Aleutian Basin lithosphere restores adjacent to the reconstructed Olyutorsky-Pacific ridge, which would be a logical structure bounding the rotating microplate that contained the Aleutian Basin lithosphere during opening of the proto-Komandorsky Basin. Our reconstruction therefore predicts that the Aleutian Basin lithosphere was formed between 85 and 60 Ma by back-arc spreading at the Olyutorsky-Pacific ridge (Table 1). Between 83 and 60 Ma, there are about 15 magnetic polarity reversals, which allows a scenario in which the anomalies interpreted from the Aleutian Basin crust were formed at the northern flank of the spreading ridge. Spreading at the Olyutorsky-Pacific ridge may have continued until the collision of the East Sakhalin-Nemuro arc with Sakhalin, or even longer until it subducted below the fast-retreating Kuril trench.

As far as we can see, this reconstruction explains all key observations and provides a straightforward plate kinematic scenario. It would require, however, that the Agattu slab underwent ~2,000 km of roll-back from its location of subduction initiation to its modern mantle position. Roll-back of such magnitude may well be possible, but dragging a slab over such a distance through the mantle may be unrealistic—although we note that >1,200 km of slab dragging was recently shown for the Tonga slab (van de Lagemaat et al., 2018). Also, the implied rate of roll-back in our model of ~10 cm/year is very high. In addition, while our reconstruction is consistent with reported paleomagnetic paleolatitudes, the (unknown) effects of inclination shallowing are not corrected for in the Olyutorsky arc data and more northerly paleolatitudes are thus permitted. We therefore consider our model an end-member, and we consider a more northerly position of subduction initiation possible. We note, however, that a more northerly position of Olyutorsky subduction initiation requires that the fossil Olyutorsky-Pacific ridge is contained in the Aleutian Basin, which may be tested in future geophysical expeditions. Alternatively, if subduction initiated significantly north of the Izanagi-Pacific ridge, the Izanagi-Pacific ridge may have continued activity for several 10 Myr and may have been responsible for the faster northward motion of the Olyutorsky arc relative to the Pacific plate. However, this scenario is problematic as the preserved magnetic anomalies indicate that the Aleutian Basin crust was formed after the Cretaceous Normal Superchron. Since there is no compelling evidence for major convergence between the Shirshov Ridge and the Aleutian Basin crust, this requires that seafloor spreading occurred at a short distance behind the Shirshov Ridge, that is, the Greater Olyutorsky arc. In any case, if the magnetic anomalies in the Aleutian Basin represent magnetic polarity reversals, this would be consistent with our reconstruction in which the Aleutian Basin was formed by post-83 Ma spreading between the Olyutorsky arc and the Pacific plate (Table 1). We note that we have not been able to develop a kinematically feasible scenario that would allow the anomalies in the Aleutian Basin to be the Upper Jurassic-Lower Cretaceous M-series as tentatively suggested by Cooper et al. (1976). The above shows that any pre-50 Ma reconstruction of the Bering Sea region, including the one presented here, is strongly dependent on the age of the Aleutian Basin crust. We therefore argue that future studies on the age of the basin crust, through marine geophysics or drillings as recently proposed in Drilling Proposal 888 submitted to the International Ocean Discovery Program, are required to test the validity of our reconstruction, or that of Domeier et al. (2017), of the northwest Pacific region between 85 and 50 Ma.

7.4.2. Evolution of the Kronotsky Arc

Between ~85 and 40 Ma, the Kronotsky arc was active at a location within the northern Panthalassa Ocean. Our approach of assuming that the arc moved as part of the Pacific plate after its ~40 Ma arrest places it to the east of the Olyutorsky arc (Figure 10d). This suggests that the two formed adjacent to each other as previously also inferred by Shapiro and Solov'ev (2009), Domeier et al. (2017), and van der Meer et al. (2018), rather than in-sequence as portrayed by Konstantinovskaya (2001).

Like for the Greater Olyutorsky arc, data sets available for determining the absolute location of the Kronotsky arc are paleomagnetism, seismic tomography, and the age of Kronotsky basement and accretionary prism rocks. In particular, the Kamchatka Mys ophiolite and prism of the Kronotsky arc assemblage shows that the arc was either built on ~113–93 Ma ocean crust that spread at a ridge that interacted with the Hawaii-Emperor plume, or that a hotspot seamount of that age accreted below the arc (see section 4.4). In addition, during subduction below the Kronotsky arc, a second subduction zone was active to its north, first at the Beringian margin and after the presumed ~50 Ma switch at the Aleutian Trench. Our new reconstruction of the Kronotsky arc and the Olyutorsky arc and back-arc indeed generates simultaneous convergence across these trenches as well as at the Kronotsky Trench.

Pre-40 Ma paleomagnetic data are sparse, and most predict paleolatitudes for the Kronotsky arc that are lower than for the Pacific reference curve (Figure 7c). This would require that the Kronotsky arc was located within the current Pacific plate, which is impossible, and it is thus likely that the paleomagnetic data—derived from sedimentary rocks—experienced inclination shallowing. Domeier et al. (2017) therefore suggested that the Kronotsky arc was in a mantle-stationary position above the North Pacific slab, at a location immediately east of a transform fault bounding the Greater Olyutorsky arc. When we place the Kronotsky arc at its inferred 85 Ma inception above the North Pacific slab in the position suggested by Domeier et al. (2017; see Figure 10a) and construct the marine magnetic anomalies of the Izanagi plate using their conjugate set preserved on the Pacific plate, it follows that the arc was built on ~110-Ma-old Izanagi crust, which is what we adopt in our reconstruction. This is consistent with the age of the Kamchatka Mys ophiolite, but suggests that subduction initiation either did not occur at the Izanagi-Pacific ridge as previously inferred by Domeier et al. (2017), or, if it did, that subduction initiation below the Kronotsky arc occurred much earlier than the inferred ~85 Ma, around 110 Ma.

Domeier et al. (2017) suggested that the Kronotsky Trench accommodated subduction of the Kula plate that broke off Pacific, Izanagi, and Farallon lithosphere around 83 Ma. Anomalies conjugate to the Kula plate are preserved on the Pacific plate to the east of the inferred position of the Kronotsky arc. Domeier et al. (2017) therefore inferred that the Kula-Pacific ridge was located >2,000 km north of the northernmost preserved Pacific lithosphere at 83 Ma, ~1,000 km south of the restored Kronotsky arc position at 40 Ma, and ended at a transform fault with the Olyutorsky plate. The amount of Kula-Pacific spreading between 83 and 40 Ma restored from preserved anomalies on the Pacific plate (Wright et al., 2016) is ~2,000 km. From this it follows that if Domeier et al. (2017) are correct, the Pacific-Kula ridge would have arrived in the Kronotsky subduction zone around 40 Ma, thereby providing an elegant explanation for the arrest of Kronotsky arc volcanism. We include this in our reconstruction (Figures 10c and 10d).

North American absolute plate motion north of the Kronotsky arc was ~500 km southward between 85 and 60 Ma (Doubrovine et al., 2012). This would generate sufficient convergence between a presumed mantle-fixed Kronotsky arc and North America to drive convergence across the Beringian margin. Between 60 and 40 Ma, northern North America did not move significantly relative to the mantle. In addition, the distance between its inferred position above the North Pacific slab and its 40 Ma position as part of the Pacific plate after its extinction requires that the Kronotsky arc moved ~850 km to the northwest, while rotating ~30° counterclockwise. A similar rotation was constructed for the Kula plate (Wright et al., 2016), although its absolute northwestward motion was higher (~2,000 km). We therefore model trench advance for the Kronotsky arc between 60 and 40 Ma (Figures 10b and 10c), driving subduction at the late Beringian, and early Aleutian Trenches, and rotate the arc counterclockwise, simultaneously with the Kula plate.

8. Discussion

In the time window of our reconstruction, two major plate reorganizations occurred within the Pacific realm. The ~85 Ma onset of intraoceanic subduction inferred from the geological records of the Olyutorsky and Kronotsky arcs is not an isolated event. Around the same time, the Kula plate broke off the Pacific, Farallon, and Izanagi plates (Woods & Davies, 1982; Wright et al., 2016). In the south, the Hikurangi plateau collided with the Gondwana margin, merging the Pacific plate with Zealandia, which subsequently broke off Gondwana, effectively merging the Pacific plate for the first time with the global plate circuit (Matthews et al., 2015). A likely driver of subduction initiation at the Olyutorsky arc is the collision of the Okhotsk block with Eurasia (Konstantinovskaya, 2001; Shapiro & Solov'ev, 2009) that led to the ~80 Ma arrest of the Okhotsk-Chukotka arc (Akinin & Miller, 2011; Hourigan & Akinin, 2004; Pease et al., 2018; Tikhomirov et al., 2012; Yang, 2013) and the break-off of the Ushky slab (van der Meer et al., 2018). There is no record of subduction below NE Siberia between ~80 Ma and the onset of the Kuril-Kamchatka arc around 55–45 Ma, and it is thus likely that the segment of original Izanagi lithosphere between the Okhotsk block and the Olyutorsky arc, in our model bounded to the NE and SW by transforms, became part of the Eurasian plate (Figure 10a). The blocking of subduction at the Eurasian margin then required the formation of a new, Olyutorsky subduction zone. Whether this event also caused the formation of the Kula

plate and the Kronotsky subduction zone at ~85 Ma is difficult to assess. The temporal relationship is striking, but at this stage, we do not see a straightforward dynamic link.

The main aim of our research was to assess whether the tectonic evolution of the NW Pacific region may form a straightforward trigger for the ~50–45 Ma plate reorganization, driving the absolute Pacific plate motion from northwest to west. Previous models infer that inception of subduction of Pacific plate lithosphere in the west is a likely driver of this absolute plate motion change (Domeier et al., 2017; Faccenna et al., 2012; Seton et al., 2015; Whittaker et al., 2007), but how and where this Pacific plate started subducting varied between models.

Our reconstruction strongly suggests that the collision of the Greater Olyutorsky arc with NE Asia, resulting in the formation of the Aleutian and Kuril-Kamchatka Trenches, is not a straightforward candidate driver for the ~50 Ma Pacific plate reorganization. This is mainly because the plates that started to subduct below the Aleutian and Kuril-Kamchatka Trenches are not likely to be the Pacific plate as concluded by Domeier et al. (2017), but plates separated from the Pacific plate by ridges and/or trenches. Subduction at the Aleutian Trench at ~50 Ma consumed the Kronotsky plate, separated from the Pacific by the Kronotsky Trench as well as the Kula plate and the Kula-Pacific ridge. Subduction at the Kuril-Kamchatka Trench consumed the Olyutorsky plate, separated by a ridge from the Pacific plate. The subduction jump and the polarity reversal around 50 Ma in the north Pacific thus did not directly involve the Pacific plate (Figure 10c). If it is possible that dynamic changes affecting neighboring plates propagated across plate boundaries to affect the Pacific plate, which we consider well possible, then there are many other candidates to have driven the Pacific plate motion change. These may include the ~50 Ma onset or acceleration of westward absolute motion of South America forming the Andes (Faccenna et al., 2017; Schellart, 2017; Schepers et al., 2017) or the change in North American plate motion from SW to W driving breaking of the Caribbean plate (Boschman et al., 2014), both affecting the Farallon plate adjacent to the Pacific plate. Whittaker et al. (2007) noted that the Australian plate started accelerating northward around 50 Ma, and even the major India-Asia slowdown around 50 Ma (Copley et al., 2010; van Hinsbergen et al., 2011) may have propagated regionally. If absolute plate motion changes of one plate may propagate across the plate circuit, then these changes may have been dominant over the relatively small-scale collisions and reorganizations of the NW Pacific region.

Other candidates to have accommodated inception of Pacific subduction around 50 Ma is subduction initiation at the Izu-Bonin-Marianas Trench (Faccenna et al., 2012; Ishizuka et al., 2011; Seton et al., 2015) and the Tonga-Kermadec Trench (e.g., Sutherland et al., 2017). However, as there was only very minor Pacific-Australia convergence before 45 Ma, and most if not all such convergence was accommodated at the New Caledonia-Northland subduction zone between the modern Tonga Trench and Australia until 30 Ma Tonga-Kermadec subduction initiation is kinematically quite unlikely to have happened long before 30 Ma (van de Lagemaat et al., 2018). Subduction initiation at the Izu-Bonin-Marianas Trench is widely considered to have started simultaneously with the inception of forearc spreading at 51 Ma (Ishizuka et al., 2011), but this critically hinges on the assumption that subduction initiation was a spontaneous event (Arculus et al., 2015; Stern, 2004; Stern et al., 2012). This assumption is based on a conceptual model that explains how typical suprasubduction zone-type ophiolitic assemblages may result from such spontaneous subduction initiation (Stern & Bloomer, 1992), but Guilmette et al. (2018) recently showed that very similar geological records of the Oman ophiolite must have formed ~10 Myr after the inception of subduction below that ophiolite. Consequently, while the onset of spreading above the Izu-Bonin-Marianas subduction zone may well be related to the events driving the Hawaii-Emperor bend, it may well be the result instead of the cause of the plate reorganization. Moreover, there is considerable debate on the initial orientation of this trench during subduction initiation, which may have been E-W rather than N-S striking during subduction zone infancy, gradually rotating during spreading into its modern orientation (Hall, 2002; Sdrolias et al., 2004; Zahirovic et al., 2014).

If the Pacific plate reorganization occurred as a result of the plate's initial westward subduction, we consider Izanagi-Pacific ridge subduction below Japan the best candidate. Aside from the arguments already provided by Seton et al. (2015), including the arrival of the ridge assuming constant 8 cm/year Izanagi-Pacific spreading rates, and the lull in arc volcanism, we note that the finding of MORB-basalts intruding unconsolidated Paleocene-Lower Eocene foreland basin sediments on west Hokkaido (Ueda, 2016; and references therein) is an elegant geological display of ridge subduction. Our reconstruction, however, demonstrates that the

segment over which the Pacific plate may have started to subduct westward is much shorter than previously incorporated in numerical models (Faccenna et al., 2012; Seton et al., 2015), and the Pacific lithosphere that started subducting after ridge subduction was extremely young and hence buoyant, so whether that would provide sufficient slab pull to drive the major 50–45 Ma plate reorganization remains to be tested in future modeling efforts.

9. Conclusions

In this paper, we present a new kinematic reconstruction of the NW Pacific region since the Late Cretaceous based on quantitative geological and marine geophysical data constraints, combined with paleomagnetic data and seismic tomographic images of the mantle. Based on our final model, we conclude the following:

1. The contiguous NE-SW-trending Greater Olyutorsky intraoceanic island-arc was active from ~85 to 60–50 Ma above a southeasterly dipping subduction zone that consumed oceanic lithosphere of the Eurasian plate, which previously belonged to the Izanagi plate. The subduction culminated in the obduction of the arc and associated ophiolites onto NE Asia at ~55–50 Ma in south Kamchatka, and ~45 Ma in north Kamchatka and east Sakhalin. Obduction of the Olyutorsky arc in south Kamchatka was followed by a subduction polarity reversal at ~55–50 Ma. In the Okhotsk Sea, slab retreat of a northward-dipping slab started upon collision of the East Sakhalin arc segment with Sakhalin, leading to up to ~800 km of N-S extension of the Okhotsk block and the formation of the present-day geometry of the Kuril-Kamchatka subduction zone.
2. Olyutorsky subduction likely initiated at a weakness zone at or close to the Izanagi-Pacific ridge, possibly induced by the collision of the Okhotsk Block with NE Siberia. We postulate that the ridge was reactivated, accommodating ~2,500–3,000 km of divergence between the Pacific plate and the Olyutorsky arc from ~85 to 60–50 Ma. We predict that part of this crust is preserved in the present-day Aleutian Basin. At ~60 Ma, the break-up of the Greater Olyutorsky arc led to the opening of the triangular proto-Komandorsky Basin and the formation of the Shirshov Ridge. The rotation of Olyutorsky plate lithosphere behind the Shirshov Ridge between ~60 and 50 Ma was accommodated by oblique subduction below the Beringian margin until around 50 Ma, when the Olyutorsky arc collided with Kamchatka and subduction jumped south to the Aleutian Trench, capturing the ~85–60 Ma oceanic lithosphere that currently underlies the Aleutian Basin. We emphasize that future direct age determination of the Aleutian Basin crust is required to test whether this scenario is correct.
3. The Kronotsky intraoceanic island-arc formed above a northward-dipping subduction zone northeast of the Greater Olyutorsky arc at ~85 Ma. The Kronotsky subduction zone consumed oceanic lithosphere of the Kula plate until its cessation at around 40 Ma, possibly induced by the arrival of the Kula-Pacific ridge. After 40 Ma, the arc moved passively with the Pacific plate toward the northwest. Oblique collision of the Kronotsky arc with the Aleutian arc induced the formation of the Bowers Ridge between ~34 and 26 Ma. Coupling of the Kronotsky arc with oceanic crust of the proto-Komandorsky Basin generated NW-SE-directed seafloor spreading in the Komandorsky Basin between and subduction of the old proto-Komandorsky Basin crust below north Kamchatka, between ~20 and 10 Ma, until the Kronotsky arc collided with eastern Kamchatka at around 10 Ma.
4. The polarity reversal following the collision of the Greater Olyutorsky arc with NE Asia is not a straightforward driver for the 50–45 Ma Pacific plate reorganization, as the Pacific plate was still separated from this subduction zone by a ridge. We argue that Izanagi-Pacific ridge subduction below East Asia, limited to the margin south of Sakhalin, is the best candidate driver for the reorganization. Future numerical modeling is required to test whether this subduction would be sufficient to cause a change in the absolute plate motion of the Pacific plate.

Acknowledgments
D. J. J. v. H. was supported by NWO Vidi grant 864.11.004. L. M. B. acknowledges NWO grant 824.01.004. We thank Maren Wanke (ETH Zürich) for sharing her unpublished MSc thesis with isotopic ages from the Shirshov Ridge dredge samples. We thank Wim Spakman for discussion. Mathew Domeier and David Scholl are thanked for their helpful reviews. The supporting information provides two additional figures, the compilation of paleomagnetic data (Table S1), and the data files of our GPlates reconstruction (Data Set S1) and the paleomagnetic data for paleomagnetism.org (Data Set S2). See the text for a description of these data files. The additional figures include the plate configuration at 90 Ma (Figure S1) and paleomagnetic data of the East Sakhalin-Nemuro arc (Figure S2). The paleomagnetic data set is compiled from sources provided in the References From the Supporting Information section of this paper.

References

Akinin, V. V., & Miller, E. L. (2011). Evolution of calc-alkaline magmas of the Okhotsk-Chukotka volcanic belt. *Petrology*, *19*(3), 237–277. https://doi.org/10.1134/S0869591111020020

Alexeiev, D. V., Gaedicke, C., Tsukanov, N. V., & Freitag, R. (2006). Collision of the Kronotskiy arc at the NE Eurasia margin and structural evolution of the Kamchatka–Aleutian junction. *International Journal of Earth Sciences*, *95*(6), 977–993. https://doi.org/10.1007/s00531-006-0080-z

Amaru, M. (2007). *Global travel time tomography with 3-D reference models*. Utrecht University.

Ando, H. (2003). Stratigraphic correlation of Upper Cretaceous to Paleocene forearc basin sediments in Northeast Japan: cyclic sedimentation and basin evolution. *Journal of Asian Earth Sciences*, *21*(8), 921–935. https://doi.org/10.1016/S1367-9120(02)00111-6

Arculus, R. J., Ishizuka, O., Bogus, K. A., Gurnis, M., Hickey-Vargas, R., Aljahdali, M. H., et al. (2015). A record of spontaneous subduction initiation in the Izu–Bonin–Mariana arc. *Nature Geoscience*, *8*(9), 728–733. https://doi.org/10.1038/ngeo2515

Avdeiko, G., Savelyev, D., Palueva, A., & Popruzhenko, S. (2007). *Evolution of the Kurile-Kamchatkan volcanic arcs and dynamics of the Kamchatka-Aleutian Junction*, (pp. 37–55). The Kamchatka Region: Volcanism and Subduction.

Bakhteev, M., Ben'yamovskii, V., Bragin NYu, V. D., Morozov, O., Sinel'nikova, V., Tikhomirova, S., & Shatser, A. (1994). New data on Mesozoic-Cenozoic stratigraphy of the Eastern Kamchatka (Valaginsky Range). *Stratigr Geol Correlation*, *2*, 555–562.

Bakhteev, M., Morozov, O., & Tikhomirova, S. (1997). Structure of the eastern Kamchatka ophiolite-free collisional suture–Grechishkin thrust. *Geotectonics*, *31*, 236–246.

Baranov, B., Seliverstov, N., Murav'ev, A., & Muzurov, E. (1991). The Komandorsky Basin as a product of spreading behind a transform plate boundary. *Tectonophysics*, *199*, 237–269.

Baranov, B., Wong, H. K., Dozorova, K., Karp, B., Lüdmann, T., & Karnaukh, V. (2002). Opening geometry of the Kurile Basin (Okhotsk Sea) as inferred from structural data. *Island Arc*, *11*(3), 206–219. https://doi.org/10.1046/j.1440-1738.2002.00366.x

Barnes, D. (1992). Sedimentology, phenocryst chemistry, and age-Miocene "Blue Tuff": Sites 794 and 796, Japan Sea, Proc. ODP Scientific Results, pp. 115–130.

Batanova, V. G., Lyaskovskaya, Z. E., Savelieva, G. N., & Sobolev, A. V. (2014). Peridotites from the Kamchatsky Mys: Evidence of oceanic mantle melting near a hotspot. *Russian Geology and Geophysics*, *55*(12), 1395–1403. https://doi.org/10.1016/j.rgg.2014.11.004

Bazhenov, M. L., & Burtman, V. S. (1994). Upper Cretaceous paleomagnetic data from Shikotan Island, Kuril Arc: Implications for plate kinematics. *Earth and Planetary Science Letters*, *122*(1–2), 19–28. https://doi.org/10.1016/0012-821X(94)90048-5

Bazhenov, M. L., Burtman, V. S., Krezhovskikh, O. A., & Shapiro, M. N. (1992). Paleomagnetism of Paleogene rocks of the Central—East Kamchatka and Komanorsky Islands: Tectonic implications. *Tectonophysics*, *201*(1–2), 157–173. https://doi.org/10.1016/0040-1951(92)90181-5

Bazhenov, M. L., Zharov, A. E., Levashova, N. M., Kodama, K., Bragin, N. Y., Fedorov, P. I., et al. (2001). Paleomagnetism of a Late Cretaceous island arc complex from South Sakhalin, East Asia: Convergent boundaries far away from the Asian continental margin? *Journal of Geophysical Research*, *106*(B9), 19,193–19,205. https://doi.org/10.1029/2000JB900458

Beniamovsky, V. N., Fregatova, N., Spirina, L., Boyarinova, M., Volobueva, V., & Gladenkov, Y. B. (1992). Zonation of planktonic and benthic foraminifera in Paleogene deposits of East Kamchatka. *Izvestiya Akademii Nauk SSSR Seriya Geologicheskaya*, *1*, 100–113.

Bernard, A., Munschy, M., Rotstein, Y., & Sauter, D. (2005). Refined spreading history at the Southwest Indian Ridge for the last 96 Ma, with the aid of satellite gravity data. *Geophysical Journal International*, *162*(3), 765–778. https://doi.org/10.1111/j.1365-246X.2005.02672.x

Biggin, A. J., Strik, G. H. M. A., & Langereis, C. G. (2008). Evidence for a very-long-term trend in geomagnetic secular variation. *Nature Geoscience*, *1*(6), 395–398. https://doi.org/10.1038/ngeo181

Bindeman, I. N., Vinogradov, V. I., Valley, J. W., Wooden, J. L., & Natal'in, B. A. (2002). Archean protolith and accretion of crust in Kamchatka: SHRIMP dating of zircons from Sredinny and Ganal Massifs. *The Journal of Geology*, *110*(3), 271–289. https://doi.org/10.1086/339532

Bogdanov, N. A., & Chekhovich, V. D. (2002). On the collision between the West Kamchatka and Sea of Okhotsk plates. *Geotectonics*, *36*(1), 63–75.

Bogdanov, N., & Khain, V. (2000). The Tectonic Map of the Sea of Okhotsk Region, Scale 1: 2500000. Moscow: Institute of the Lithosphere of Marginal Seas of RAS 1.

Boschman, L. M., van Hinsbergen, D. J. J., Torsvik, T. H., Spakman, W., & Pindell, J. L. (2014). Kinematic reconstruction of the Caribbean region since the Early Jurassic. *Earth-Science Reviews*, *138*, 102–136. https://doi.org/10.1016/j.earscirev.2014.08.007

Boyd, T. M., & Creager, K. C. (1991). The geometry of Aleutian subduction: Three-dimensional seismic imaging. *Journal of Geophysical Research*, *96*(B2), 2267–2291. https://doi.org/10.1029/90JB01919

Boyden, J. A., Müller, R. D., Gurnis, M., Torsvik, T. H., Clark, J. A., Turner, M., et al. (2011). Next-generation plate-tectonic reconstructions using GPlates.

Butterworth, N., Talsma, A., Müller, R., Seton, M., Bunge, H.-P., Schuberth, B., et al. (2014). Geological, tomographic, kinematic and geodynamic constraints on the dynamics of sinking slabs. *Journal of Geodynamics*, *73*, 1–13.

Cande, S. C., & Kent, D. V. (1995). Revised calibration of the geomagnetic polarity timescale for the Late Cretaceous and Cenozoic. *Journal of Geophysical Research*, *100*(B4), 6093–6095. https://doi.org/10.1029/94JB03098

Cande, S. C., Patriat, P., & Dyment, J. (2010). Motion between the Indian, Antarctic and African plates in the early Cenozoic. *Geophysical Journal International*, *183*(1), 127–149. https://doi.org/10.1111/j.1365-246X.2010.04737.x

Chekhovich, V. D., & Sukhov, A. N. (2015). Geodynamics of the formation of the Paleogenic island arc of the Bauers submarine ridge (Bering Sea). *Doklady Earth Sciences*, *461*(1), 221–225. https://doi.org/10.1134/S1028334X15030101

Chekhovich, V. D., Sukhov, A. N., Kononov, M. V., & Palandzhyan, S. A. (2009). Geodynamics of the northwestern sector of the Pacific mobile belt in the Late Cretaceous-Early Paleogene. *Geotectonics*, *43*(4), 283–304.

Chekhovich, V. D., Sukhov, A. N., Sheremet, O. G., & Kononov, M. V. (2012). Cenozoic geodynamics of the Bering Sea region. *Geotectonics*, *46*(3), 212–231. https://doi.org/10.1134/S001685211203003X

Cheon, Y., Cho, H., Ha, S., Kang, H.-C., Kim, J.-S., & Son, M. (2019). Tectonically controlled multiple stages of deformation along the Yangsan Fault Zone, SE Korea, since Late Cretaceous. *Journal of Asian Earth Sciences*, *170*, 188–207. https://doi.org/10.1016/j.jseaes.2018.11.003

Chertova, M. V., Spakman, W., Geenen, T., van den Berg, A. P., & van Hinsbergen, D. J. J. (2014). Underpinning tectonic reconstructions of the western Mediterranean region with dynamic slab evolution from 3-D numerical modeling. *Journal of Geophysical Research: Solid Earth*, *119*, 5876–5902. https://doi.org/10.1002/2014JB011150

Cho, H. M., Kim, H. J., Jou, H. T., Hong, J. K., & Baag, C. E. (2004). Transition from rifted continental to oceanic crust at the southeastern Korean margin in the East Sea (Japan Sea). *Geophysical Research Letters*, *31*, L07606. https://doi.org/10.1029/2003GL019107

Christeson, G. L., & Barth, G. A. (2015). Aleutian basin oceanic crust. *Earth and Planetary Science Letters*, *426*, 167–175. https://doi.org/10.1016/j.epsl.2015.06.040

Cooper, A. K., Marlow, M. S., & Ben-Avraham, Z. (1981). Multichannel seismic evidence bearing on the origin of Bowers Ridge, Bering Sea. *Geological Society of America Bulletin*, *92*(7), 474–484. https://doi.org/10.1130/0016-7606(1981)92<474:MSEBOT>2.0.CO;2

Cooper, A. K., Marlow, M. S., & Scholl, D. W. (1976). Mesozoic magnetic lineations in the Bering Sea Marginal Basin. *Journal of Geophysical Research*, *81*(11), 1916–1934. https://doi.org/10.1029/JB081i011p01916
Cooper, A., Marlow, M., & Scholl, D. (1987). Geologic framework of the Bering Sea crust.
Cooper, A. K., Marlow, M. S., Scholl, D. W., & Stevenson, A. J. (1992). Evidence for Cenozoic crustal extension in the Bering Sea region. *Tectonics*, *11*(4), 719–731. https://doi.org/10.1029/92TC00214
Copley, A., Avouac, J. P., & Royer, J. Y. (2010). India-Asia collision and the Cenozoic slowdown of the Indian plate: Implications for the forces driving plate motions. *Journal of Geophysical Research*, *115*, B03410. https://doi.org/10.1029/2009JB006634
Cox, A., & Hart, R. B. (2009). *Plate tectonics: How it works*. John Wiley & Sons.
Croon, M. B., Cande, S. C., & Stock, J. M. (2008). Revised Pacific-Antarctic plate motions and geophysics of the Menard Fracture Zone. *Geochemistry, Geophysics, Geosystems*, *9*, Q07001. https://doi.org/10.1029/2008GC002019
Cukur, D., Kim, S.-P., Horozal, S., Ryu, B.-J., Kim, G.-Y., & Kong, G.-S. (2015). Seismic stratigraphy and structural analysis of the western South Korea Plateau (WSKP), East Sea. *Quaternary International*, *384*, 145–159. https://doi.org/10.1016/j.quaint.2015.05.023
Davis, A. S., Pickthorn, L.-B. G., Valuer, T. L., & Marlow, M. S. (1989). Petrology and age of volcanic-arc rocks from the continental margin of the Bering Sea: Implications for Early Eocene relocation of plate boundaries. *Canadian Journal of Earth Sciences*, *26*(7), 1474–1490. https://doi.org/10.1139/e89-125
De Grave, J., Zhimulev, F. I., Glorie, S., Kuznetsov, G. V., Evans, N., Vanhaecke, F., & McInnes, B. (2016). Late Palaeogene emplacement and late Neogene–Quaternary exhumation of the Kuril island-arc root (Kunashir island) constrained by multi-method thermochronometry. *Geoscience Frontiers*, *7*(2), 211–220. https://doi.org/10.1016/j.gsf.2015.05.002
Deenen, M. H. L., Langereis, C. G., van Hinsbergen, D. J. J., & Biggin, A. J. (2011). Geomagnetic secular variation and the statistics of palaeomagnetic directions. *Geophysical Journal International*, *186*(2), 509–520. https://doi.org/10.1111/j.1365-246X.2011.05050.x
DeMets, C., Iaffaldano, G., & Merkouriev, S. (2015). High-resolution Neogene and quaternary estimates of Nubia-Eurasia-North America plate motion. *Geophysical Journal International*, *203*(1), 416–427. https://doi.org/10.1093/gji/ggv277
Domeier, M., Doubrovine, P. V., Torsvik, T. H., Spakman, W., & Bull, A. L. (2016). Global correlation of lower mantle structure and past subduction. *Geophysical Research Letters*, *43*, 4945–4953. https://doi.org/10.1002/2016GL068827
Domeier, M., Shephard, G. E., Jakob, J., Gaina, C., Doubrovine, P. V., & Torsvik, T. H. (2017). Intraoceanic subduction spanned the Pacific in the Late Cretaceous-Paleocene. *Sciences Advances*, *3*. eaao2303
Doubrovine, P. V., Steinberger, B., & Torsvik, T. H. (2012). Absolute plate motions in a reference frame defined by moving hot spots in the Pacific, Atlantic, and Indian oceans. *Journal of Geophysical Research*, *117*, L17203. https://doi.org/10.1029/2011JB009072
Elouai, D., Sato, H., Hirata, N., Kawasaki, S., Takeshita, T., Kato, N., & Takeda, T. (2004). Deep seismic reflection profiling across the Northern Fossa Magna: The ERI 1997 and the JNOC 1996 seismic lines, active faults and geological structures. *Earth, Planets and Space*, *56*(12), 1331–1338. https://doi.org/10.1186/BF03353358
Engebretson, D. C. (1985). Relative motions between oceanic and continental plates in the Pacific basin. *Geological Society of America*, *206*. https://doi.org/10.1130/SPE206-p1
Fabbri, O., Charvet, J., & Fournier, M. (1996). Alternate senses of displacement along the Tsushima fault system during the Neogene based on fracture analyses near the western margin of the Japan Sea. *Tectonophysics*, *257*(2–4), 275–295. https://doi.org/10.1016/0040-1951(95)00151-4
Faccenna, C., Becker, T. W., Lallemand, S., & Steinberger, B. (2012). On the role of slab pull in the Cenozoic motion of the Pacific plate. *Geophysical Research Letters*, *39*, L03305. https://doi.org/10.1029/2011GL050155
Faccenna, C., Oncken, O., Holt, A. F., & Becker, T. W. (2017). Initiation of the Andean orogeny by lower mantle subduction. *Earth and Planetary Science Letters*, *463*, 189–201. https://doi.org/10.1016/j.epsl.2017.01.041
Filatova, N. I. (2013). New data on the structure and history of formation of the conjunction zone between the Middle Cretaceous Okhotsk-Koryak and Cenozoic Olyutor-Kamchatka Orogen belts (Vatyn-Ukelayat Suture Zone). *Doklady Earth Sciences*, *448*(1), 7–11. https://doi.org/10.1134/S1028334X13010108
Filatova, N. I. (2014). New data on the tectonic position of Mesozoic rocks in western Kamchatka structures of the middle Cretaceous orogenic belt in Eastern Asia. *Doklady Earth Sciences*, *455*(2), 389–394.
Fisher, R. (1953). Dispersion on a sphere. Proceedings of the Royal Society of London. Series A. *Mathematical and Physical Sciences*, *217*(1130), 295–305. https://doi.org/10.1098/rspa.1953.0064
Fournier, M., Jolivet, L., Huchon, P., Sergeyev, K. F., & Oscorbin, L. S. (1994). Neogene strike-slip faulting in Sakhalin and the Japan Sea opening. *Journal of Geophysical Research*, *99*(B2), 2701–2725. https://doi.org/10.1029/93JB02026
Fujiwara, Y., & Ohtake, T. (1974). Paleomagnetism of late Cretaceous alkaline rocks in the Nemuro peninsula, Hokkaido, NE Japan. *Journal of Geomagnetism and Geoelectricity*, *26*(6), 549–558. https://doi.org/10.5636/jgg.26.549
Fujiwara, Y., & Sugiyama, R. (1986). Post-Oligocene tectonic rotation of southeast Hokkaido. *Rock Magnetism and Paleogeophysics*, *15*.
Fukuma, K., Shinjoe, H., & Hamano, Y. (1998). Origin of the absence of magnetic lineations in the Yamato Basin of the Japan Sea: Magnetic properties of mafic rocks from Ocean Drilling Program Hole 794 D. *Journal of Geophysical Research*, *103*(B8), 17,791–17,805. https://doi.org/10.1029/98JB01486
Funiciello, F., Faccenna, C., Heuret, A., Lallemand, S., Di Giuseppe, E., & Becker, T. W. (2008). Trench migration, net rotation and slab–mantle coupling. *Earth and Planetary Science Letters*, *271*(1–4), 233–240. https://doi.org/10.1016/j.epsl.2008.04.006
Gaina, C., Roest, W. R., & Müller, R. D. (2002). Late Cretaceous–Cenozoic deformation of northeast Asia. *Earth and Planetary Science Letters*, *197*(3–4), 273–286. https://doi.org/10.1016/S0012-821X(02)00499-5
Garver, J. I., Soloviev, A. V., Bullen, M. E., & Brandon, M. T. (2000). Towards a more complete record of magmatism and exhumation in continental arcs, using detrital fission-track thermochrometry. *Physics and Chemistry of the Earth, Part A: Solid Earth and Geodesy*, *25*(6–7), 565–570. https://doi.org/10.1016/S1464-1895(00)00086-7
Geist, E. L., Vallier, T. L., & Scholl, D. W. (1994). Origin, transport, and emplacement of an exotic island-arc terrane exposed in eastern Kamchatka, Russia. *Geological Society of America Bulletin*, *106*(9), 1182–1194. https://doi.org/10.1130/0016-7606(1994)106<1182:OTAEOA>2.3.CO;2
Gladenkov, Y. B. (2016). Paleogene and Neogene reference sections of Eastern Kamchatka. *Stratigraphy and Geological Correlation*, *24*(1), 58–74. https://doi.org/10.1134/S0869593816010032
Glorie, S., Alexandrov, I., Nixon, A., Jepson, G., Gillespie, J., & Jahn, B.-M. (2017). Thermal and exhumation history of Sakhalin Island (Russia) constrained by apatite U-Pb and fission track thermochronology. *Journal of Asian Earth Sciences*, *143*, 326–342. https://doi.org/10.1016/j.jseaes.2017.05.011
Gnibidenko, H. S., & Khvedchuk, I. I. (1982). The tectonics of the Okhotsk Sea. *Marine Geology*, *50*(3), 155–197. https://doi.org/10.1016/0025-3227(82)90138-4

Gorbatov, A., Widiyantoro, S., Fukao, Y., & Gordeev, E. (2000). Signature of remnant slabs in the North Pacific from P-wave tomography. *Geophysical Journal International*, *142*(1), 27–36. https://doi.org/10.1046/j.1365-246x.2000.00122.x

Gradstein, F. M., Ogg, J. G., Schmitz, M., & Ogg, G. (2012). The geologic time scale. Elsevier.

Grannik, V. M. (2012). East Sakhalin island arc paleosystem of the Sea of Okhotsk region. *Doklady Earth Sciences*, *445*(2), 934–938. https://doi.org/10.1134/S1028334X12080041

Granot, R., Cande, S. C., Stock, J. M., & Damaske, D. (2013). Revised Eocene-Oligocene kinematics for the West Antarctic rift system. *Geophysical Research Letters*, *40*, 279–284. https://doi.org/10.1029/2012GL054181

Guilmette, C., Smit, M. A., van Hinsbergen, D. J. J., Gürer, D., Corfu, F., Charette, B., et al. (2018). Forced subduction initiation recorded in the sole and crust of the Semail Ophiolite of Oman. *Nature Geoscience*, *11*(9), 688–695. https://doi.org/10.1038/s41561-018-0209-2

Hall, R. (2002). Cenozoic geological and plate tectonic evolution of SE Asia and the SW Pacific: Computer-based reconstructions, model and animations. *Journal of Asian Earth Sciences*, *20*(4), 353–431. https://doi.org/10.1016/S1367-9120(01)00069-4

Harbert, W., Kepezhinskas, P., Krylov, K., Grigoriev, V., Sokolov, S., Aleksuitin, M., et al. (1998). Paleomagnetism and tectonics of the Kamchatka region, northeastern Russia: Implications for the development and evolution of the northwest Pacific basin. *Polarforschung*, *68*, 297–308.

Hassan, R., Müller, R. D., Gurnis, M., Williams, S. E., & Flament, N. (2016). A rapid burst in hotspot motion through the interaction of tectonics and deep mantle flow. *Nature*, *533*, 239.

Hauff, F., Werner, R., Portnyagin, M., Baranov, B., Yogodzinski, G., Botcharnikov, R., et al. (2016). Exploring the origin of the Bering Sea: Initial Results of Cruise SO249–2 (17th July-13th August 2016), AGU Fall Meeting Abstracts.

Hirata, N., Karp, B. Y., Yamaguchi, T., Kanazawa, T., Suyehiro, K., Kasahara, J., et al. (1992). Oceanic crust in the Japan Basin of the Japan Sea by the 1990 Japan-USSR Expedition. *Geophysical Research Letters*, *19*(20), 2027–2030. https://doi.org/10.1029/92GL02094

Hirata, N., Tokuyama, H., & Chung, T. W. (1989). An anomalously thick layering of the crust of the Yamato Basin, southeastern Sea of Japan: The final stage of back-arc spreading. *Tectonophysics*, *165*(1–4), 303–314. https://doi.org/10.1016/0040-1951(89)90055-3

Hisada, K.i., Takashima, S., Arai, S., & Lee, Y. I. (2008). Early Cretaceous paleogeography of Korea and Southwest Japan inferred from occurrence of detrital chromian spinels. *Island Arc*, *17*(4), 471–484. https://doi.org/10.1111/j.1440-1738.2008.00638.x

Hochstaedter, A. G., Kepezhinskas, P. K., Defant, M. J., Drummond, M. S., & Bellon, H. (1994). On the tectonic significance of arc volcanism in northern Kamchatka. *The Journal of Geology*, *102*(6), 639–654. https://doi.org/10.1086/629709

Hoernle, K., Werner, R., Portnyagin, M., Yogodzinski, G., Hauff, F., Baranov, B., & Silantyev, S. (2016). New insights into the origin of the Bering Sea from SO201 and SO249 cruises, AGU Fall Meeting Abstracts.

Horner-Johnson, B. C., Gordon, R. G., & Argus, D. F. (2007). Plate kinematic evidence for the existence of a distinct plate between the Nubian and Somalian plates along the Southwest Indian Ridge. *Journal of Geophysical Research*, *112*, B05418. https://doi.org/10.1029/2006JB004519

Hourigan, J. K., & Akinin, V. V. (2004). Tectonic and chronostratigraphic implications of new 40Ar/39Ar geochronology and geochemistry of the Arman and Maltan-Ola volcanic fields, Okhotsk-Chukotka volcanic belt, northeastern Russia. *Geological Society of America Bulletin*, *116*(5), 637–654. https://doi.org/10.1130/B25340.1

Hourigan, J. K., Brandon, M. T., Soloviev, A. V., Kirmasov, A. B., Garver, J. I., Stevenson, J., & Reiners, P. W. (2009). Eocene arc-continent collision and crustal consolidation in Kamchatka, Russian Far East. *American Journal of Science*, *309*(5), 333–396. https://doi.org/10.2475/05.2009.01

Ikeda, Y., Stern, R. J., Kagami, H., & Sun, C. H. (2000). Pb, Nd, and Sr isotopic constraints on the origin of Miocene basaltic rocks from northeast Hokkaido, Japan: Implications for opening of the Kurile back-arc basin. *Island Arc*, *9*(2), 161–172. https://doi.org/10.1046/j.1440-1738.2000.00269.x

Ingle, J. C. Jr. (1992). *Subsidence of the Japan Sea: Stratigraphic evidence from ODP sites and onshore sections*, (pp. 1197–1218). Proc. ODP Scientific Results.

Isezaki, N. (1986). A magnetic anomaly map of the Japan Sea. *Journal of Geomagnetism and Geoelectricity*, *38*(5), 403–410. https://doi.org/10.5636/jgg.38.403

Ishizuka, O., Tani, K., Reagan, M. K., Kanayama, K., Umino, S., Harigane, Y., et al. (2011). The timescales of subduction initiation and subsequent evolution of an oceanic island arc. *Earth and Planetary Science Letters*, *306*(3–4), 229–240. https://doi.org/10.1016/j.epsl.2011.04.006

Isozaki, Y., Aoki, K., Nakama, T., & Yanai, S. (2010). New insight into a subduction-related orogen: A reappraisal of the geotectonic framework and evolution of the Japanese Islands. *Gondwana Research*, *18*(1), 82–105. https://doi.org/10.1016/j.gr.2010.02.015

Isozaki, Y., Maruyama, S., & Furuoka, F. (1990). Accreted oceanic materials in Japan. *Tectonophysics*, *181*(1–4), 179–205. https://doi.org/10.1016/0040-1951(90)90016-2

Ito, T. (2002). Active faulting, lower crustal delamination and ongoing Hidaka arc-arc collision, Hokkaido, Japan. *Seismotectonics in Convergent Plate Bounbdary*, 219–224.

Itoh, Y., & Tsuru, T. (2006). A model of late Cenozoic transcurrent motion and deformation in the fore-arc of northeast Japan: Constraints from geophysical studies. *Physics of the Earth and Planetary Interiors*, *156*, 117–129.

Iwasaki, T., Adachi, K., Moriya, T., Miyamachi, H., Matsushima, T., Miyashita, K., et al. (2004). Upper and middle crustal deformation of an arc–arc collision across Hokkaido, Japan, inferred from seismic refraction/wide-angle reflection experiments. *Tectonophysics*, *388*(1–4), 59–73. https://doi.org/10.1016/j.tecto.2004.03.025

Iwasaki, T., Levin, V., Nikulin, A., & Iidaka, T. (2013). Constraints on the Moho in Japan and Kamchatka. *Tectonophysics*, *609*, 184–201. https://doi.org/10.1016/j.tecto.2012.11.023

Jiang, G., Zhao, D., & Zhang, G. (2009). Seismic tomography of the Pacific slab edge under Kamchatka. *Tectonophysics*, *465*(1–4), 190–203. https://doi.org/10.1016/j.tecto.2008.11.019

Jicha, B. R., Scholl, D. W., Singer, B. S., Yogodzinski, G. M., & Kay, S. M. (2006). Revised age of Aleutian Island Arc formation implies high rate of magma production. *Geology*, *34*(8), 661. https://doi.org/10.1130/G22433.1

Johnson, C. L., Constable, C. G., Tauxe, L., Barendregt, R., Brown, L. L., Coe, R. S., et al. (2008). Recent investigations of the 0–5 Ma geomagnetic field recorded by lava flows. *Geochemistry, Geophysics, Geosystems*, *9*, Q04032. https://doi.org/10.1029/2007GC001696

Johnston, S. T. (2001). The Great Alaskan Terrane Wreck: Reconciliation of paleomagnetic and geological data in the northern Cordillera. *Earth and Planetary Science Letters*, *193*, 259–272.

Jolivet, L., & Huchon, P. (1989). Crustal-scale strike-slip deformation in Hokkaido, northern Japan. *Journal of Structural Geology*, *11*, 509–522.

Jolivet, L., & Miyashita, S. (1985). The Hidaka Shear Zone (Hokkaido, Japan): Genesis during a right-lateral strike-slip movement. *Tectonics*, *4*(3), 289–302. https://doi.org/10.1029/TC004i003p00289

Jolivet, L., & Tamaki, K. (1992). Neogene kinematics in the Japan Sea region and volcanic activity of the Northeast Japan Arc, Proc. ODP Scientific Results, pp. 1311–1331.
Jolivet, L., Tamaki, K., & Fournier, M. (1994). Japan Sea, opening history and mechanism: A synthesis. *Journal of Geophysical Research*, *99*(B11), 22,237–22,259. https://doi.org/10.1029/93JB03463
Kanamatsu, T., Nanayama, F., Iwata, K., & Fujiwara, Y. (1992). Pre-Teriary Systems on the western side of the Abashiri Tectonic Line in the Shiranuka area, eastern Hokkaido, Japan: Implications to the tectonic relationship between the Nemuro and Tokoro Belts. *The Journal of the Geological Society of Japan*, *98*(12), 1113–1128_1. https://doi.org/10.5575/geosoc.98.1113
Kaneoka, I. (1992). ^{40}Ar-^{39}Ar analysis of volcanic rocks recovered from the Japan Sea floor: Constraints on the age of formation of the Japan Sea. Proceedings of the Ocean Drilling Program. *Scientific Results*, *127*, 819–836.
Kano, K., Uto, K., & Ohguchi, T. (2007). Stratigraphic review of Eocene to Oligocene successions along the eastern Japan Sea: Implication for early opening of the Japan Sea. *Journal of Asian Earth Sciences*, *30*(1), 20–32. https://doi.org/10.1016/j.jseaes.2006.07.003
Kato, H. (1992). Fossa Magna-A masked border region separating southwest and northeast Japan. *Bulletin of the Geological Survey of Japan*, *43*, 1–30.
Kato, N., Sato, H., Orito, M., Hirakawa, K., Ikeda, Y., & Ito, T. (2004). Has the plate boundary shifted from central Hokkaido to the eastern part of the Sea of Japan? *Tectonophysics*, *388*(1–4), 75–84. https://doi.org/10.1016/j.tecto.2004.04.030
Kawai, N., Ito, H., & Kume, S. (1961). Deformation of the Japanese Islands as inferred from rock magnetism. *Geophysical Journal International*, *6*, 124–130.
Kemkin, I., Khanchuk, A., & Kemkina, R. (2016). Accretionary prisms of the Sikhote-Alin Orogenic Belt: Composition, structure and significance for reconstruction of the geodynamic evolution of the eastern Asian margin. *Journal of Geodynamics*, *102*, 202–230.
Khanchuk, A. (2006). Geodynamics, magmatism and metallogeny of the eastern Russia. *Dal'nauka, Vladivostok*, *1*, 1–572.
Khotin, M. Y., & Shapiro, M. N. (2006). Ophiolites of the Kamchatsky Mys Peninsula, eastern Kamchatka: Structure, composition, and geodynamic setting. *Geotectonics*, *40*, 297–320.
Kim, H.-J., Han, S.-J., Lee, G. H., & Huh, S. (1998). Seismic study of the Ulleung Basin crust and its implications for the opening of the East Sea (Japan Sea). *Marine Geophysical Researches*, *20*, 219–237.
Kim, H.-J., Jou, H.-T., Cho, H.-M., Bijwaard, H., Sato, T., Hong, J.-K., et al. (2003). Crustal structure of the continental margin of Korea in the East Sea (Japan Sea) from deep seismic sounding data: Evidence for rifting affected by the hotter than normal mantle. *Tectonophysics*, *364*, 25–42.
Kim, H.-J., Lee, G. H., Choi, D.-L., Jou, H.-T., Li, Z., Zheng, Y., et al. (2015). Back-arc rifting in the Korea Plateau in the East Sea (Japan Sea) and the separation of the southwestern Japan Arc from the Korean margin. *Tectonophysics*, *638*, 147–157. https://doi.org/10.1016/j.tecto.2014.11.003
Kim, H.-J., Lee, G. H., Jou, H.-T., Cho, H.-M., Yoo, H.-S., Park, G.-T., & Kim, J.-S. (2007). Evolution of the eastern margin of Korea: Constraints on the opening of the East Sea (Japan Sea). *Tectonophysics*, *436*(1–4), 37–55. https://doi.org/10.1016/j.tecto.2007.02.014
Kim, G. B., Yoon, S. H., Chough, S. K., Kwon, Y. K., & Ryu, B. J. (2011). Seismic reflection study of acoustic basement in the South Korea Plateau, the Ulleung Interplain Gap, and the northern Ulleung Basin: Volcano-tectonic implications for Tertiary back-arc evolution in the southern East Sea. *Tectonophysics*, *504*, 43–56.
Kimura, G. (1994). The latest Cretaceous-Early Paleogene rapid growth of accretionary complex and exhumation of high pressure series metamorphic rocks in northwestern Pacific margin. *Journal of Geophysical Research*, *99*(B11), 22,147–22,164. https://doi.org/10.1029/94JB00959
Kimura, G., Hashimoto, Y., Kitamura, Y., Yamaguchi, A., & Koge, H. (2014). Middle Miocene swift migration of the TTT triple junction and rapid crustal growth in southwest Japan: A review. *Tectonics*, *33*, 1219–1238. https://doi.org/10.1002/2014TC003531
Kimura, G., Sakakibara, M., Ofuka, H., Ishizuka, H., Miyashita, S., Okamura, M., et al. (1992). A deep section of accretionary complex: Susunai complex in Sakhalin island, northwest Pacific margin. *Island Arc*, *1*(1), 166–175. https://doi.org/10.1111/j.1440-1738.1992.tb00067.x
Kirmasov, A., Solov'ev, A., & Hourigan, J. (2004). Collision and postcollision structural evolution of the Andrianovka Suture, Sredinny Range, Kamchatka. *Geotectonics*, *38*, 294–316.
Kirschvink, J. (1980). The least-squares line and plane and the analysis of palaeomagnetic data. *Geophysical Journal International*, *62*, 699–718.
Knesel, K. M., Cohen, B. E., Vasconcelos, P. M., & Thiede, D. S. (2008). Rapid change in drift of the Australian plate records collision with Ontong Java plateau. *Nature*, *454*, 754.
Kodama, K., Takeuchi, T., & Ozawa, T. (1993). Clockwise tectonic rotation of Tertiary sedimentary basins in central Hokkaido, northern Japan. *Geology*, *21*(5), 431–434. https://doi.org/10.1130/0091-7613(1993)021<0431:CTROTS>2.3.CO;2
Kojima, S., Tsukada, K., Otoh, S., Yamakita, S., Ehiro, M., Dia, C., et al. (2008). Geological relationship between Anyui metamorphic complex and Samarka terrane, Far East Russia. *Island Arc*, *17*, 502–516.
Konstantinovskaya, E. (2001). Arc–continent collision and subduction reversal in the Cenozoic evolution of the Northwest Pacific: An example from Kamchatka (NE Russia). *Tectonophysics*, *333*, 75–94.
Konstantinovskaya, E. (2011). *Early Eocene arc–continent collision in Kamchatka, Russia: Structural evolution and geodynamic model, Arc-Continent Collision*, (pp. 247–277). Springer.
Koulakov, I. Y., Dobretsov, N., Bushenkova, N., & Yakovlev, A. (2011). Slab shape in subduction zones beneath the Kurile–Kamchatka and Aleutian arcs based on regional tomography results. *Russian Geology and Geophysics*, *52*, 650–667.
Koymans, M. R., Langereis, C. G., Pastor-Galán, D., & van Hinsbergen, D. J. (2016). Paleomagnetism. org: An online multi-platform open source environment for paleomagnetic data analysis. *Computers & Geosciences*, *93*, 127–137.
Kravchenko-Berezhnoy, I., & Nazimova, Y. (1991). The Cretaceous Ophiolite of Karaginsky Island (the Western Bering Sea). *Ofioliti*, *16*, 79–110.
Lander, A. V., & Shapiro, M. N. (2007). *The origin of the modern Kamchatka subduction zone*, (pp. 57–64). The Kamchatka Region: Volcanism and Subduction.
Layer, P., Scholl, D., & Newberry, R. (2007). *Ages of igneous basement from the Komandorsky Islands*. AGU Fall Meeting Abstracts: Far Western Aleutian Ridge.
Lee, G. H., & Kim, B. (2002). Infill history of the Ulleung Basin, East Sea (Sea of Japan) and implications on source rocks and hydrocarbons. *Marine and Petroleum Geology*, *19*, 829–845.
Lee, G. H., Kim, H. J., Han, S. J., & Kim, D. C. (2001). Seismic stratigraphy of the deep Ulleung Basin in the East Sea (Japan Sea) back-arc basin. *Marine and Petroleum Geology*, *18*, 615–634.

Lee, G. H., Yoon, Y., Nam, B. H., Lim, H., Kim, Y.-S., Kim, H. J., & Lee, K. (2011). Structural evolution of the southwestern margin of the Ulleung Basin, East Sea (Japan Sea) and tectonic implications. *Tectonophysics*, *502*(3–4), 293–307. https://doi.org/10.1016/j.tecto.2011.01.015

Lelikov, E. P., & Emelyanova, T. A. (2011). Geology and volcanism of the underwater Vityaz Ridge (Pacific slope of the Kuril Island Arc). *Oceanology*, *51*(2), 315–328. https://doi.org/10.1134/S0001437011020081

Lelikov, E., & Pugachev, A. (2016). Granitoid magmatism of the Japan and Okhotsk seas. *Petrology*, *24*, 196–213.

Lemaux, J., Gordon, R. G., & Royer, J.-Y. (2002). Location of the Nubia-Somalia boundary along the Southwest Indian ridge. *Geology*, *30*(4), 339–342. https://doi.org/10.1130/0091-7613(2002)030<0339:LOTNSB>2.0.CO;2

Levashova, N. M., Shapiro, M. N., Beniamovsky, V. N., & Bazhenov, M. L. (2000). Paleomagnetism and geochronology of the Late Cretaceous-Paleogene island arc complex of the Kronotsky Peninsula, Kamchatka, Russia: Kinematic implications. *Tectonics*, *19*(5), 834–851. https://doi.org/10.1029/1998TC001087

Li, S., Advokaat, E. L., van Hinsbergen, D. J. J., Koymans, M., Deng, C., & Zhu, R. (2017). Paleomagnetic constraints on the Mesozoic-Cenozoic paleolatitudinal and rotational history of Indochina and South China: Review and updated kinematic reconstruction. *Earth-Science Reviews*, *171*, 58–77. https://doi.org/10.1016/j.earscirev.2017.05.007

Liao, J. P., Alexandrov, I., & Jahn, B.-M. (2016). Eocene Granitoids of the Okhotsk Complex in Sakhalin Island, Russian Far East: Petrogenesis and tectonic implications from zircon U-Pb ages, geochemical and Sr-Nd isotopic characteristics, EGU General Assembly Conference Abstracts, p. 6720.

Liao, J.-P., Jahn, B.-M., Alexandrov, I., Chung, S.-L., Zhao, P., Ivin, V., & Usuki, T. (2018). Petrogenesis of Mid-Eocene granites in South Sakhalin, Russian Far East: Juvenile crustal growth and comparison with granitic magmatism in Hokkaido and Sikhote-Alin. *Journal of Asian Earth Sciences*, *167*, 103–129. https://doi.org/10.1016/j.jseaes.2018.05.020

Lippert, P. C., Van Hinsbergen, D. J. J., & Dupont-Nivet, G. (2014). Early Cretaceous to present latitude of the central proto-Tibetan Plateau: A paleomagnetic synthesis with implications for Cenozoic tectonics, paleogeography, and climate of Asia. *Geological Society of America Special Papers*, *507*, 1–21. https://doi.org/10.1130/2014.2507(01)

Liu, X., Zhao, D., Li, S., & Wei, W. (2017). Age of the subducting Pacific slab beneath East Asia and its geodynamic implications. *Earth and Planetary Science Letters*, *464*, 166–174.

Luchitskaya, M. V., & Soloviev, A. V. (2012). Early Eocene magmatism in the Sredinnyi Range, Kamchatka: Composition and geodynamic aspects. *Petrology*, *20*, 147–187.

Luchitskaya, M. V., Solov'ev, A. V., & Hourigan, J. K. (2008). Two stages of granite formation in the Sredinny Range, Kamchatka: Tectonic and geodynamic setting of granitic rocks. *Geotectonics*, *42*, 286–304.

Maeda, J. I. (1990). Opening of the Kuril Basin deduced from the magmatic history of Central Hokkaido, North Japan. *Tectonophysics*, *174*, 235–255.

Maffione, M., Thieulot, C., Van Hinsbergen, D. J. J., Morris, A., Plümper, O., & Spakman, W. (2015). Dynamics of intraoceanic subduction initiation: 1. Oceanic detachment fault inversion and the formation of supra-subduction zone ophiolites. *Geochemistry, Geophysics, Geosystems*, *16*, 1753–1770. https://doi.org/10.1002/2015GC005746

Maffione, M., & van Hinsbergen, D. J. J. (2018). Reconstructing plate boundaries in the Jurassic neo-Tethys from the east and west Vardar ophiolites (Greece and Serbia). *Tectonics*, *37*(3), 858–887. https://doi.org/10.1002/2017TC004790

Malahoff, A., Kroenke, L. W., Cherkis, N., & Brozena, J. (1994). *Magnetic and tectonic fabric of the North Fiji Basin and Lau Basin, Basin formation, ridge crest processes, and metallogenesis in the North Fiji Basin*, (pp. 49–61). Springer.

Martin, A. K. (2011). Double saloon door tectonics in the Japan Sea, Fossa Magna, and the Japanese Island Arc. *Tectonophysics*, *498*(1–4), 45–65. https://doi.org/10.1016/j.tecto.2010.11.016

Martin-Short, R., Allen, R. M., & Bastow, I. D. (2016). Subduction geometry beneath south central Alaska and its relationship to volcanism. *Geophysical Research Letters*, *43*, 9509–9517. https://doi.org/10.1002/2016GL070580

Martynov, Y. A., Khanchuk, A. I., Grebennikov, A. V., Chashchin, A. A., & Popov, V. K. (2017). Late Mesozoic and Cenozoic volcanism of the East Sikhote-Alin area (Russian Far East): A new synthesis of geological and petrological data. *Gondwana Research*, *47*, 358–371. https://doi.org/10.1016/j.gr.2017.01.005

Martynov, A. Y., Kimura, J. I., Martynov, Y. A., & Rybin, A. V. (2010). Geochemistry of late Cenozoic lavas on Kunashir Island, Kurile arc. *Island Arc*, *19*, 86–104.

Matthews, K. J., Williams, S. E., Whittaker, J. M., Müller, R. D., Seton, M., & Clarke, G. L. (2015). Geologic and kinematic constraints on Late Cretaceous to mid Eocene plate boundaries in the southwest Pacific. *Earth-Science Reviews*, *140*, 72–107. https://doi.org/10.1016/j.earscirev.2014.10.008

Miller, E. L., Meisling, K. E., Akinin, V. V., Brumley, K., Coakley, B. J., Gottlieb, E. S., et al. (2018). Circum-Arctic Lithosphere Evolution (CALE) Transect C: Displacement of the Arctic Alaska–Chukotka microplate towards the Pacific during opening of the Amerasia Basin of the Arctic. *Geological Society, London, Special Publications*, *460*(1), 57–120. https://doi.org/10.1144/SP460.9

Minyuk, P. S., & Stone, D. B. (2009). Paleomagnetic determination of paleolatitude and rotation of Bering Island (Komandorsky Islands) Russia: Comparison with rotations in the Aleutian Islands and Kamchatka. *Stephan Mueller Special Publication Series*, *4*, 329–348. https://doi.org/10.5194/smsps-4-329-2009

Mortimer, N., van den Bogaard, P., Hoernle, K., Timm, C., Gans, P. B., Werner, R., & Riefstahl, F. (2019). Late Cretaceous oceanic plate reorganization and the breakup of Zealandia and Gondwana. *Gondwana Research*, *65*, 31–42. https://doi.org/10.1016/j.gr.2018.07.010

Müller, R. D., Royer, J.-Y., Cande, S. C., Roest, W. R., & Maschenkov, S. (1999). *New constraints on the Late Cretaceous/Tertiary plate tectonic evolution of the Caribbean, Sedimentary basins of the world*, (pp. 33–59). Elsevier.

Müller, R. D., Seton, M., Zahirovic, S., Williams, S. E., Matthews, K. J., Wright, N. M., et al. (2016). Ocean basin evolution and global-scale plate reorganization events since Pangea breakup. *Annual Review of Earth and Planetary Sciences*, *44*(1), 107–138. https://doi.org/10.1146/annurev-earth-060115-012211

Nakahigashi, K., Shinohara, M., Yamada, T., Uehira, K., Mochizuki, K., & Kanazawa, T. (2013). Seismic structure of the extended continental crust in the Yamato Basin, Japan Sea, from ocean bottom seismometer survey. *Journal of Asian Earth Sciences*, *67-68*, 199–206. https://doi.org/10.1016/j.jseaes.2013.02.028

Nakajima, T. (2013). Late Cenozoic tectonic events and Intra-arc Basin development in northeast Japan. Mechanism of Sedimentary Basin Formation-Multidisciplinary Approach on Active Plate Margins. InTech.

Nishisaka, H., Shinohara, M., Sato, T., Hino, R., Mochizuki, K., & Kasahara, J. (2001). Crustal structure of the Yamato basin and the margin of the northeastern Japan Sea using ocean bottom seismographs and controlled sources. *Journal of the Seismological Society of Japan*, *54*, 365–379.

Nohda, S. (2009). Formation of the Japan Sea basin: Reassessment from Ar–Ar ages and Nd–Sr isotopic data of basement basalts of the Japan Sea and adjacent regions. *Journal of Asian Earth Sciences*, *34*, 599–609.
Nokleberg, W. J., Parfenov, L. M., Monger, J. W., Baranov, B. V., Byalobzhesky, S. G., Bundtzen, T. K., et al. (1996). Summary Circum-North Pacific tectonostratigraphic terrane map. US Geological Survey.
Nokleberg, W. J., Parfenov, L. M., Monger, J. W., Norton, I. O., Khanchuk, A. I., Stone, D. B., et al. (2000). *Phanerozoic tectonic evolution of the Circum-North Pacific*.
O'Connor, J. M., Steinberger, B., Regelous, M., Koppers, A. A., Wijbrans, J. R., Haase, K. M., et al. (2013). Constraints on past plate and mantle motion from new ages for the Hawaiian-Emperor Seamount Chain. *Geochemistry, Geophysics, Geosystems*, *14*, 4564–4584. https://doi.org/10.1002/ggge.20267
Ogg, J. G., Ogg, G., & Gradstein, F. M. (2016). *A concise geologic time scale: 2016*. Elsevier.
Oncken, O., Hindle, D., Kley, J., Elger, K., Victor, P., & Schemmann, K. (2006). Deformation of the central Andean upper plate system—Facts, fiction, and constraints for plateau models, The Andes. Springer, pp. 3–27.
Otofuji, Y. I. (1996). Large tectonic movement of the Japan Arc in late Cenozoic times inferred from paleomagnetism: Review and synthesis. *Island Arc*, *5*(3), 229–249. https://doi.org/10.1111/j.1440-1738.1996.tb00029.x
Otofuji, Y.-I., Kambara, A., Matsuda, T., & Nohda, S. (1994). Counterclockwise rotation of Northeast Japan: Paleomagnetic evidence for regional extent and timing of rotation. *Earth and Planetary Science Letters*, *121*(3–4), 503–518. https://doi.org/10.1016/0012-821X(94)90087-6
Otofuji, Y.-I., Matsuda, T., & Nohda, S. (1985). Opening mode of the Japan Sea inferred from the palaeomagnetism of the Japan Arc. *Nature*, *317*(6038), 603–604. https://doi.org/10.1038/317603a0
Parfenov, L. M., Badarch, G., Berzin, N. A., Khanchuk, A. I., Kuzmin, M. I., Nokleberg, W. J., et al. (2009). Summary of Northeast Asia geodynamics and tectonics. *Stephan Mueller Special Publication Series*, *4*, 11–33. https://doi.org/10.5194/smsps-4-11-2009
Parfenov, L. M., & Natal'in, B. A. (1986). Mesozoic tectonic evolution of northeastern Asia. *Tectonophysics*, *127*(3–4), 291–304. https://doi.org/10.1016/0040-1951(86)90066-1
Parfenov, L. M., Nokleberg, W. J., Berzin, N. A., Badarch, G., Dril, S. I., Gerel, O., et al. (2011). *Tectonic and metallogenic model for northeast Asia*. US Geological Survey.
Pease, V., Miller, E., Wyld, S. J., Sokolov, S., Akinin, V., & Wright, J. E. (2018). U–Pb zircon geochronology of Cretaceous arc magmatism in eastern Chukotka, NE Russia, with implications for Pacific plate subduction and the opening of the Amerasia Basin. *Geological Society, London, Special Publications*, *460*(1), 159–182. https://doi.org/10.1144/SP460.14
Piip, V. B., & Rodnikov, A. G. (2004). The Sea of Okhotsk crust from deep seismic sounding data. *Russian Journal of Earth Sciences*, *6*(1), 35–48. https://doi.org/10.2205/2003ES000140
Piskarev, A. L., Butsenko, V. V., Poselov, V. A., & Savin, V. A. (2012). Deep structure of the crust beneath the Sea of Okhotsk inferred from 3D seismic density modeling. *Oceanology*, *52*(3), 411–421. https://doi.org/10.1134/S0001437012030095
Portnyagin, M., Hoernle, K., & Savelyev, D. (2009). Ultra-depleted melts from Kamchatkan ophiolites: Evidence for the interaction of the Hawaiian plume with an oceanic spreading center in the Cretaceous? *Earth and Planetary Science Letters*, *287*(1–2), 194–204. https://doi.org/10.1016/j.epsl.2009.07.042
Portnyagin, M., Savelyev, D., Hoernle, K., Hauff, F., & Garbe-Schönberg, D. (2008). Mid-Cretaceous Hawaiian tholeiites preserved in Kamchatka. *Geology*, *36*(11), 903. https://doi.org/10.1130/G25171A.1
Qi, C., Zhao, D., & Chen, Y. (2007). Search for deep slab segments under Alaska. *Physics of the Earth and Planetary Interiors*, *165*(1–2), 68–82. https://doi.org/10.1016/j.pepi.2007.08.004
Raznitsin, Y. N. (2012). Geodynamics of ophiolites and formation of hydrocarbon fields on the shelf of eastern Sakhalin. *Geotectonics*, *46*(1), 1–15. https://doi.org/10.1134/S0016852112010062
Rikhtyer, A. (1995). Structure of the metamorphic complex of the Central Kamchatka Massif. *Geotectonics*, *29*, 65–72.
Rodnikov, A. G., Sergeyeva, N. A., & Zabarinskaya, L. P. (2013). Ancient subduction zone in Sakhalin Island. *Tectonophysics*, *600*, 217–225. https://doi.org/10.1016/j.tecto.2012.12.014
Rostovtseva, Y. V., & Shapiro, M. (1998). Provenance of the Palaeocene-Eocene clastic rocks of the Komandorsky Islands. *Sedimentology*, *45*(1), 201–216. https://doi.org/10.1046/j.1365-3091.1998.00144.x
Royer, J. Y., & Chang, T. (1991). Evidence for relative motions between the Indian and Australian Plates during the last 20 m.y. from plate tectonic reconstructions: Implications for the deformation of the Indo-Australian Plate. *Journal of Geophysical Research*, *96*(B7), 11,779–11,802. https://doi.org/10.1029/91JB00897
Rubenstone, J. L. (1984). Geology and geochemistry of early Tertiary submarine volcanic rocks of the Aleutian Islands, and their bearing on the development of the Aleutian Island Arc.
Sato, H. (1994). The relationship between Late Cenozoic tectonic events and stress field and basin development in northeast Japan. *Journal of Geophysical Research*, *99*(B11), 22,261–22,274. https://doi.org/10.1029/94JB00854
Sato, H., Iwasaki, T., Ikeda, Y., Takeda, T., Matsuta, N., Imai, T., et al. (2004). Seismological and geological characterization of the crust in the southern part of northern Fossa Magna, central Japan. *Earth, Planets and Space*, *56*(12), 1253–1259. https://doi.org/10.1186/BF03353348
Sato, K., Kawabata, H. W., Scholl, D., Hyodo, H., Takahashi, K., Suzuki, K., & Kumagai, H. (2016). ^{40}Ar–^{39}Ar dating and tectonic implications of volcanic rocks recovered at IODP Hole U1342A and D on Bowers Ridge, Bering Sea. *Deep Sea Research Part II: Topical Studies in Oceanography*, *125-126*, 214–226. https://doi.org/10.1016/j.dsr2.2015.03.008
Sato, T., No, T., Kodaira, S., Takahashi, N., & Kaneda, Y. (2014). Seismic constraints of the formation process on the back-arc basin in the southeastern Japan Sea. *Journal of Geophysical Research: Solid Earth*, *119*, 1563–1579. https://doi.org/10.1002/2013JB010643
Sato, T., Shinohara, M., Karp, B. Y., Kulinich, R. G., & Isezaki, N. (2004). P-wave velocity structure in the northern part of the central Japan Basin, Japan Sea with ocean bottom seismometers and airguns. *Earth, Planets and Space*, *56*(5), 501–510. https://doi.org/10.1186/BF03352509
Sato, T., Takahashi, N., Miura, S., Fujie, G., Kang, D.-H., Kodaira, S., & Kaneda, Y. (2006). Last stage of the Japan Sea back-arc opening deduced from the seismic velocity structure using wide-angle data. *Geochemistry, Geophysics, Geosystems*, *7*, L07606. https://doi.org/10.1029/2005GC001135
Savostin, L., Zonenshain, L., & Baranov, B. (1983). Geology and plate tectonics of the Sea of Okhotsk. *Geodynamics of the Western Pacific-Indonesian Region*, 189–221. https://doi.org/10.1029/GD011p0189
Scheirer, D., Barth, G., Scholl, D., & Stern, R. (2016). Geophysical evidence for the origin of the Aleutian Basin, AGU Fall Meeting Abstracts.

Schellart, W. P. (2017). Andean mountain building and magmatic arc migration driven by subduction-induced whole mantle flow. *Nature Communications*, *8*(1), 2010. https://doi.org/10.1038/s41467-017-01847-z

Schellart, W. P., Jessell, M. W., & Lister, G. S. (2003). Asymmetric deformation in the backarc region of the Kuril arc, northwest Pacific: New insights from analogue modeling. *Tectonics*, *22*(5), 1047. https://doi.org/10.1029/2002TC001473

Schellart, W. P., Stegman, D. R., & Freeman, J. (2008). Global trench migration velocities and slab migration induced upper mantle volume fluxes: Constraints to find an Earth reference frame based on minimizing viscous dissipation. *Earth-Science Reviews*, *88*(1–2), 118–144. https://doi.org/10.1016/j.earscirev.2008.01.005

Schepers, G., Van Hinsbergen, D. J., Spakman, W., Kosters, M. E., Boschman, L. M., & McQuarrie, N. (2017). South-American plate advance and forced Andean trench retreat as drivers for transient flat subduction episodes. *Nature Communications*, *8*, 15,249. https://doi.org/10.1038/ncomms15249

Scholl, D. W. (2007). Viewing the tectonic evolution of The Kamchatka-Aleutian (KAT) connection with an Alaska crustal extrusion perspective. Volcanism and Subduction: The Kamchatka Region, 3–35.

Scholl, D. W., Buffington, E. C., & Marlow, M. S. (1975). Plate tectonics and the structural evolution of the Aleutian–Bering Sea region, GSA Special Papers. The Geological Society of America, pp. 1–31.

Sdrolias, M., Roest, W. R., & Müller, R. D. (2004). An expression of Philippine Sea plate rotation: The Parece Vela and Shikoku basins. *Tectonophysics*, *394*, 69–86.

Seama, N., & Isezaki, N. (1990). Sea-floor magnetization in the eastern part of the Japan Basin and its tectonic implications. *Tectonophysics*, *181*, 285–297.

Seton, M., Flament, N., Whittaker, J., Müller, R. D., Gurnis, M., & Bower, D. J. (2015). Ridge subduction sparked reorganization of the Pacific plate-mantle system 60–50 million years ago. *Geophysical Research Letters*, *42*, 1732–1740. https://doi.org/10.1002/2015GL063057

Seton, M., Müller, R. D., Zahirovic, S., Gaina, C., Torsvik, T., Shephard, G., et al. (2012). Global continental and ocean basin reconstructions since 200Ma. *Earth-Science Reviews*, *113*, 212–270.

Shapiro, M., Gladenkov, Y. B., & Shantser, A. (1996). Regional angular unconformities in the Cenozoic sequences of Kamchatka. *Stratigraphy and Geological Correlation*, *4*, 567–579.

Shapiro, M. N., & Solov'ev, A. V. (2009). Formation of the Olyutorsky–Kamchatka foldbelt: A kinematic model. *Russian Geology and Geophysics*, *50*, 668–681.

Shapiro, M. N., & Solov'ev, A. V. (2011). Cenozoic volcanic rocks of North Kamchatka: In search of subduction zones. *Geotectonics*, *45*, 210–224.

Shapiro, M., Solov'ev, A., Garver, G., Shcherbinina, E., Ledneva, G., & Brandon, M. (2004). Age of Terrigenous Rocks of Northeastern Karaginskiœ Island (Eastern Kamchatka). *Stratigraphy and Geological Correlation*, *12*, 188–198.

Shapiro, M. N., Solov'ev, A. V., & Hourigan, J. K. (2008). Lateral structural variability in zone of eocene island-arc-continent collision, Kamchatka. *Geotectonics*, *42*, 469–487.

Sharp, W. D., & Clague, D. A. (2006). 50-Ma initiation of Hawaiian-Emperor bend records major change in Pacific plate motion. *Science*, *313*, 1281–1284.

Sibuet, J.-C., Hsu, S.-K., Le Pichon, X., Le Formal, J.-P., Reed, D., Moore, G., & Liu, C.-S. (2002). East Asia plate tectonics since 15 Ma: constraints from the Taiwan region. *Tectonophysics*, *344*(1–2), 103–134. https://doi.org/10.1016/S0040-1951(01)00202-5

Sillitoe, R. (1977). Metallogeny of an Andean-type continental margin in South Korea: Implication for opening of the Japan Sea. Island arcs, deep sea trenches and back arc basins, 303–310.

Skolotnev, S. G., Tsukanov, N. V., & Sidorov, E. G. (2018). New data on the composition of ophiolite complexes on Karaginskii Island (Eastern Kamchatka). *Doklady Earth Sciences*. Springer, *479*(1), 290–294. https://doi.org/10.1134/S1028334X18030091

Solov'ev, A., & Palechek, T. (2004). New data on the age of the Andrianovka Formation, Sredinny Range in Kamchatka: Structure of metamorphic complexes in accretion zone, Proceedings of the Youth School-Conference of XXXVII Tectonic Conference, pp. 86–89.

Solov'ev, A., Brandon, M., Garver, J., & Shapiro, M. (2001). Kinematics of the Vatyn-Lesnaya Thrust Fault (Southern Koryakia). *Geotectonics*, *35*, 471–489.

Solov'ev, A. V., Garver, J. I., Shapiro, M. N., Brandon, M. T., & Hourigan, J. K. (2011). Eocene arc-continent collision in northern Kamchatka, Russian Far East. *Russian Journal of Earth Sciences*, *12*, 1–13.

Solov'ev, A., Hourigan, J., Brandon, M., Garver, J., & Grigorenko, E. (2004). The age of the Baraba Formation inferred from the U/Pb (SHRIMP) dating (Sredinnyi Range, Kamchatka): geological consequences. *Stratigraphy and Geological Correlation*, *12*, 418–424.

Solov'ev, A. V., Palechek, T. N., Shapiro, M. N., Johnston, S. A., Garver, J. I., & Ol'shanetskii, D. M. (2007). New data on the Baraba Formation age (the Sredinnyi Range of Kamchatka). *Stratigraphy and Geological Correlation*, *15*, 112–119.

Solov'ev, A., Shapiro, M., & Garver, J. (2002). Lesnaya nappe, northern Kamchatka. *Geotectonics*, *36*, 469–482.

Solov'ev, A., Shapiro, M., Garver, J., & Lander, A. (2004). Formation of the east Kamchatkan accretionary prism based on fission-track dating of detrital zircons from terrigene rocks. *Russian Geology and Geophysics*, *45*, 1237–1247.

Solov'ev, A., Shapiro, M., Garver, J., Shcherbinina, E., & Kravchenko-Berezhnoy, I. (2002). New age data from the Lesnaya Group: A key to understanding the timing of arc-continent collision, Kamchatka, Russia. *Island Arc*, *11*, 79–90.

Son, M., Song, C. W., Kim, M. C., Cheon, Y., Cho, H., & Sohn, Y. K. (2015). Miocene tectonic evolution of the basins and fault systems, SE Korea: Dextral, simple shear during the East Sea (Sea of Japan) opening. *Journal of the Geological Society*, *172*(5), 664–680. https://doi.org/10.1144/jgs2014-079

Spakman, W., Chertova, M. V., van den Berg, A., & van Hinsbergen, D. J. (2018). Puzzling features of western Mediterranean tectonics explained by slab dragging. *Nature Geoscience*, *11*(3), 211–216. https://doi.org/10.1038/s41561-018-0066-z

Spakman, W., Stein, S., van der Hilst, R., & Wortel, R. (1989). Resolution experiments for NW Pacific subduction zone tomography. *Geophysical Research Letters*, *16*, 1097–1100.

Steinberger, B., & Gaina, C. (2007). Plate-tectonic reconstructions predict part of the Hawaiian hotspot track to be preserved in the Bering Sea. *Geology*, *35*, 407.

Stern, R. J. (2004). Subduction initiation: Spontaneous and induced. *Earth and Planetary Science Letters*, *226*, 275–292.

Stern, R. J., & Bloomer, S. H. (1992). Subduction zone infancy: Examples from the Eocene Izu-Bonin-Mariana and Jurassic California arcs. *Geological Society of America Bulletin*, *104*, 1621–1636.

Stern, R. J., Reagan, M., Ishizuka, O., Ohara, Y., & Whattam, S. (2012). To understand subduction initiation, study forearc crust: To understand forearc crust, study ophiolites. *Lithosphere*, *4*, 469–483.

Sukhov, A. N., Chekhovich, V. D., Lander, A. V., Presnyakov, S. L., & Lepekhina, E. N. (2011). Age of the Shirshov submarine ridge basement (Bering Sea) based on the results of investigation of zircons using the U-Pb SHRIMP method. *Doklady Earth Sciences*, *439*, 926–932.

Sutherland, R., Collot, J., Bache, F., Henrys, S., Barker, D., Browne, G., et al. (2017). Widespread compression associated with Eocene Tonga-Kermadec subduction initiation. *Geology*, *45*, 355–358.

Takeuchi, A. (2004). Basement-involved tectonics in North Fossa Magna, central Japan. *Earth, Planets and Space*, *56*, 1261–1269.

Takeuchi, T., Kodama, K., & Ozawa, T. (1999). Paleomagnetic evidence for block rotations in central Hokkaido–south Sakhalin, Northeast Asia. *Earth and Planetary Science Letters*, *169*, 7–21.

Tamaki, M., Kusumoto, S., & Itoh, Y. (2010). Formation and deformation processes of late Paleogene sedimentary basins in southern central Hokkaido, Japan: Paleomagnetic and numerical modeling approach. *Island Arc*, *19*, 243–258.

Tamaki, K., Suyehiro, K., Allan, J., Ingle Jr., J. C., & Pisciotto, K. A. (1992). Tectonic synthesis and implications of Japan Sea ODP drilling, Proc. ODP Scientific Results. College Station, pp. 1333–1348.

Tanaka, H., Tsunakawa, H., Yamagishi, H., & Kimura, G. (1991). Paleomagnetism of the Shakotan Peninsula, West Hokkaido, Japan. *Journal of Geomagnetism and Geoelectricity*, *43*, 277–294.

Tang, J., Xu, W., Niu, Y., Wang, F., Ge, W., Sorokin, A., & Chekryzhov, I. (2016). Geochronology and geochemistry of Late Cretaceous–Paleocene granitoids in the Sikhote-Alin Orogenic Belt: Petrogenesis and implications for the oblique subduction of the paleo-Pacific plate. *Lithos*, *266*, 202–212.

Tararin, I. (2008). Granulites of the Kolpakovskaya Series in the sredinny range, Kamchatka: A myth or reality? *Petrology*, *16*, 193–209.

Tararin, I., Badredinov, Z., Markovsky, B., & Slyadnev, B. (2012). U-Pb SHRIMP dating of zircons from metamorphic complexes in eastern Kamchatka. *Russian Journal of Pacific Geology*, *6*, 114–130.

Tarduno, J., Bunge, H.-P., Sleep, N., & Hansen, U. (2009). The bent Hawaiian-Emperor hotspot track: Inheriting the mantle wind. *Science*, *324*, 50–53.

Tarduno, J. A., Duncan, R. A., Scholl, D. W., Cottrell, R. D., Steinberger, B., Thordarson, T., et al. (2003). The Emperor Seamounts: Southward motion of the Hawaiian hotspot plume in Earth's mantle. *Science*, *301*, 1064–1069.

Terekhov, E., Mozherovsky, A., Gorovaya, M., Tsoy, I., & Vashchenkova, N. (2010). Composition of the rocks of the Kotikovo Group and the main stages in the Late Cretaceous-Paleogene evolution of the Terpeniya Peninsula, Sakhalin Island. *Russian Journal of Pacific Geology*, *4*, 260–273.

Tikhomirov, P. L., Kalinina, E. A., Moriguti, T., Makishima, A., Kobayashi, K., Cherepanova, I. Y., & Nakamura, E. (2012). The Cretaceous Okhotsk–Chukotka Volcanic Belt (NE Russia): Geology, geochronology, magma output rates, and implications on the genesis of silicic LIPs. *Journal of Volcanology and Geothermal Research*, *221-222*, 14–32.

Torsvik, T. H., Doubrovine, P. V., Steinberger, B., Gaina, C., Spakman, W., & Domeier, M. (2017). Pacific plate motion change caused the Hawaiian-Emperor Bend. *Nature Communications*, *8*, 15,660.

Torsvik, T. H., Van der Voo, R., Preeden, U., Mac Niocaill, C., Steinberger, B., Doubrovine, P. V., et al. (2012). Phanerozoic polar wander, palaeogeography and dynamics. *Earth-Science Reviews*, *114*, 325–368.

Tsukanov, N. V., Kramer, W., Skolotnev, S. G., Luchitskaya, M. V., & Seifert, W. (2007). Ophiolites of the Eastern Peninsulas zone (Eastern Kamchatka): Age, composition, and geodynamic diversity. *Island Arc*, *16*, 431–456.

Tsukanov, N., Palechek, T., Soloviev, A., & Savelyev, D. (2014). Tectonostratigraphic complexes of the southern Kronotskii paleoarc (Eastern Kamchatka): Structure, age, and composition. *Russian Journal of Pacific Geology*, *8*, 233–246.

Tsukanov, N., Saveliev, D., & Kovalenko, D. (2018). Magmatic complexes of the Vetlovaya marginal sea paleobasin (Kamchatka): Composition and geodynamic setting. *Oceanology*, *58*, 92–106.

Tsukanov, N., Skolotnev, S., & Peyve, A. (2009). New data on the composition of ophiolites from the Kumroch-Valagin segment of the Achayvayam-Valagin paleoarc (Eastern Kamchatka). *Doklady Earth Sciences*. Springer, *427*(2), 934–938. https://doi.org/10.1134/S1028334X09060105

Ueda, H. (2016). Hokkaido. The Geology of Japan, 201–221.

Ueda, H., & Miyashita, S. (2005). Tectonic accretion of a subducted intraoceanic remnant arc in Cretaceous Hokkaido, Japan, and implications for evolution of the Pacific northwest. *Island Arc*, *14*, 582–598.

Valyashko, G., Chernyavsky, G., Seliverstov, N., & Ivanenko, A. (1993). Back-arc spreading in the Komandorsky Basin. *Papers of the Russian Academy of Sciences*, *338*, 212–216.

van de Lagemaat, S. H., van Hinsbergen, D. J., Boschman, L. M., Kamp, P. J., & Spakman, W. (2018). Southwest Pacific absolute plate kinematic reconstruction reveals major Cenozoic Tonga-Kermadec slab dragging. *Tectonics*, *37*, 2647–2674. https://doi.org/10.1029/2017TC004901

van der Hilst, R., Engdahl, R., Spakman, W., & Nolet, G. (1991). Tomographic imaging of subducted lithosphere below northwest Pacific island arcs. *Nature*, *353*, 37.

van der Meer, D. G., Spakman, W., van Hinsbergen, D. J., Amaru, M. L., & Torsvik, T. H. (2010). Towards absolute plate motions constrained by lower-mantle slab remnants. *Nature Geoscience*, *3*, 36.

van der Meer, D., Torsvik, T., Spakman, W., Van Hinsbergen, D., & Amaru, M. (2012). Intra-Panthalassa Ocean subduction zones revealed by fossil arcs and mantle structure. *Nature Geoscience*, *5*, 215.

van der Meer, D. G., van Hinsbergen, D. J. J., & Spakman, W. (2018). Atlas of the underworld: Slab remnants in the mantle, their sinking history, and a new outlook on lower mantle viscosity. *Tectonophysics*, *723*, 309–448.

van der Werff, W. (2000). Backarc deformation along the eastern Japan Sea margin, offshore northern Honshu. *Journal of Asian Earth Sciences*, *18*, 71–95.

van Hinsbergen, D. J. J., Peters, K., Maffione, M., Spakman, W., Guilmette, C., Thieulot, C., et al. (2015). Dynamics of intraoceanic subduction initiation: 2. Suprasubduction zone ophiolite formation and metamorphic sole exhumation in context of absolute plate motions. *Geochemistry, Geophysics, Geosystems*, *16*, 1771–1785. https://doi.org/10.1002/2015GC005745

van Hinsbergen, D. J., Steinberger, B., Doubrovine, P. V., & Gassmöller, R. (2011). Acceleration and deceleration of India-Asia convergence since the Cretaceous: Roles of mantle plumes and continental collision. *Journal of Geophysical Research*, *116*, B06101. https://doi.org/10.1029/2010JB008051

Van Horne, A., Sato, H., & Ishiyama, T. (2017). Evolution of the Sea of Japan back-arc and some unsolved issues. *Tectonophysics*, *710-711*, 6–20.

Vinogradov, V., Grigorev, V., & Leites, A. (1988). Age of metamorphism of Sredinnyi Ridges rocks of Kamchatka. *Izvestiya Akademii Nauk SSSR Seriya Geologicheskaya*, *9*, 30–38.

Wanke, M., Portnyagin, M., Hoernle, K., Werner, R., Hauff, F., van den Bogaard, P., & Garbe-Schonberg, D. (2012). Bowers Ridge (Bering Sea): An Oligocene-Early Miocene island arc. *Geology*, *40*, 687–690.

Wanke, M., Portnyagin, M., Werner, R., Hauff, F., Hoernle, K., & Garbe-Schönberg, D. (2011). *Geochemical evidence for subduction related origin of the Bowers and Shirshov Ridges (Bering Sea, NW Pacific)*. GEOMAR, Trier, Germany: KALMAR - Second Bilateral Workshop on Russian-German Cooperation on Kurile-Kamchatka and Aleutean Marginal Sea-Island Arc Systems.

Weaver, R., Roberts, A. P., Flecker, R., Macdonald, D. I. M., & Fot'yanova, L. M. (2003). Geodynamic implications of paleomagnetic data from Tertiary sediments in Sakhalin, Russia (NW Pacific). *Journal of Geophysical Research*, *108*(B2), 2066. https://doi.org/10.1029/2001JB001226

Whittaker, J. M., Muller, R. D., Leitchenkov, G., Stagg, H., Sdrolias, M., Gaina, C., & Goncharov, A. (2007). Major Australian-Antarctic plate reorganization at Hawaiian-Emperor bend time. *Science*, *318*, 83–86.

Woods, M. T., & Davies, G. F. (1982). Late Cretaceous genesis of the Kula plate. *Earth and Planetary Science Letters*, *58*, 161–166.

Worrall, D. M. (1991). Tectonic history of the Bering Sea and the evolution of Tertiary strike-slip basins of the Bering Shelf. *Geological Society of America*, *257*.

Worrall, D. M., Kruglyak, V., Kunst, F., & Kuznetsov, V. (1996). Tertiary tectonics of the Sea of Okhotsk, Russia: Far-field effects of the India-Eurasia collision. *Tectonics*, *15*(4), 813–826. https://doi.org/10.1029/95TC03684

Wright, N. M., Müller, R. D., Seton, M., & Williams, S. E. J. G. (2015). Revision of Paleogene plate motions in the Pacific and implications for the Hawaiian-Emperor bend. *Geology*, *43*, 455–458.

Wright, N. M., Seton, M., Williams, S. E., & Müller, R. D. (2016). The Late Cretaceous to recent tectonic history of the Pacific Ocean basin. *Earth-Science Reviews*, *154*, 138–173.

Yang, Y.-T. (2013). An unrecognized major collision of the Okhotomorsk Block with East Asia during the Late Cretaceous, constraints on the plate reorganization of the Northwest Pacific. *Earth-Science Reviews*, *126*, 96–115.

Yogodzinski, G. M., Rubenstone, J. L., Kay, S. M., & Kay, R. W. (1993). Magmatic and tectonic development of the western Aleutians: An oceanic arc in a strike-slip setting. *Journal of Geophysical Research*, *98*(B7), 11,807–11,834. https://doi.org/10.1029/93JB00714

Yoon, S. H., Sohn, Y. K., & Chough, S. K. (2014). Tectonic, sedimentary, and volcanic evolution of a back-arc basin in the East Sea (Sea of Japan). *Marine Geology*, *352*, 70–88.

Yoshida, T., Kimura, J.-I., Yamada, R., Acocella, V., Sato, H., Zhao, D., et al. (2014). Evolution of late Cenozoic magmatism and the crust–mantle structure in the NE Japan Arc. *Geological Society, London, Special Publications*, *385*, 335–387.

Zahirovic, S., Seton, M., & Müller, R. (2014). The Cretaceous and Cenozoic tectonic evolution of Southeast Asia. *Solid Earth*, *5*, 227.

Zhao, P., Alexandrov, I., Jahn, B.m., & Ivin, V. (2018). Timing of Okhotsk sea plate collision with Eurasia plate: Zircon U-Pb age constraints from the Sakhalin Island, Russian Far East. *Journal of Geophysical Research: Solid Earth*, *123*, 8279–8293. https://doi.org/10.1029/2018JB015800

Zharov, A. E. (2005). South Sakhalin tectonics and geodynamics: A model for the Cretaceous-Paleogene accretion of the East Asian continental margin. *Russian Journal of Earth Sciences*, *7*, 1–31.

Zinkevich, V., Kolodyazhny, S. Y., Bragina, L., Konstantinovskaya, Y. A., & Fedorov, P. (1994). Tectonics of the eastern edge of Kamchatka's Sredinny metamorphic massif. *Geotectonics*, *28*, 75.

Zinkevich, V., & Tsukanov, N. (1993). Accretionary tectonics of Kamchatka. *International Geology Review*, *35*, 953–973.

Zonenshain, L. P. (1990). Geology of the USSR: A plate-tectonic synthesis. Amer. Geophys. Union, Geodynamic Ser. 21, 242.

Zyabrev, S. (2011). Stratigraphy and structure of the central East Sakhalin accretionary wedge (Eastern Russia). *Russian Journal of Pacific Geology*, *5*, 313.

References From the Supporting Information

Baba, A. K., Matsuda, T., Itaya, T., Wada, Y., Hori, N., Yokoyama, M., et al. (2007). New age constraints on counter-clockwise rotation of NE Japan. *Geophysical Journal International*, *171*(3), 1325–1341. https://doi.org/10.1111/j.1365-246X.2007.03513.x

Harbert, W., Heiphetz, A., & Savostin, L. (1994). Reconnaissance paleomagnetism of the Olyutorsky superterrane, northeast Russia, Proceedings, International Conference on Arctic Margins, MMS 94–0040. University of Pittsburgh, pp. 223–228.

Harbert, W., Tsukanov, N., Alexeiev, D., Gaedicke, C., Freitag, R., Baranov, B., et al. (2009). Paleomagnetism of the Cretaceous rocks from Cape Kronotskiy, East Kamchatka and reconstruction of terrane trajectories in the NE Pacific area. *Stephan Mueller Special Publication Series*, *4*, 313–327.

Hayashida, A. (1986). Timing of rotational motion of Southwest Japan inferred from paleomagnetism of the Setouchi Miocene Series. *Journal of Geomagnetism and Geoelectricity*, *38*, 295–310.

Hayashida, A., & Ito, Y. (1984). Paleoposition of Southwest Japan at 16 Ma: Implication from paleomagnetism of the Miocene Ichishi Group. *Earth and Planetary Science Letters*, *68*(2), 335–342. https://doi.org/10.1016/0012-821X(84)90164-X

Hiroki, Y., & Matsumoto, R. (1999). Magnetostratigraphic correlation of Miocene regression-and-transgression boundaries in central Honshu. *Journal of the Geological Society of Japan*, *105*, 87–107.

Hirooka, K., Sakai, H., Takahashi, T., Kinoto, H., & Takeuchi, A. (1986). Tertiary tectonic movement of central Japan inferred from paleomagnetic studies. *Journal of Geomagnetism and Geoelectricity*, *38*, 311–323.

Hirooka, K., Yamada, R., Yamashita, M., & Takeuchi, A. (1990). Paleomagnetic evidence of the rotation of central Japan and the paleoposition of Japan. *Palaeogeography, Palaeoclimatology, Palaeoecology*, *77*(3–4), 345–354. https://doi.org/10.1016/0031-0182(90)90185-A

Hoshi, H., Kato, D., Ando, Y., & Nakashima, K. (2015). Timing of clockwise rotation of Southwest Japan: constraints from new middle Miocene paleomagnetic results. *Earth, Planets and Space*, *67*, 92.

Hoshi, H., & Matsubara, T. (1998). Early Miocene paleomagnetic results from the Ninohe area, NE Japan: Implications for arc rotation and intra-arc differential rotations. *Earth, Planets and Space*, *50*, 23–33.

Hoshi, H., & Sano, M. (2013). Paleomagnetic constraints on Miocene rotation in the central Japan Arc. *Island Arc*, *22*(2), 197–213. https://doi.org/10.1111/iar.12022

Hoshi, H., & Takahashi, M. (1997). Paleomagnetic constraints on the extent of tectonic blocks and the location of their kinematic boundaries: Implications for Miocene intra-arc deformation in Northeast Japan. *The Journal of the Geological Society of Japan*, *103*(6), 523–542. https://doi.org/10.5575/geosoc.103.523

Hoshi, H., & Takahashi, M. (2013). *Refined paleomagnetic direction of the Miocene Motegi Formation*. Central Honshu: Tochigi Prefecture.

Hoshi, H., Tanaka, D., Takahashi, M., & Yoshikawa, T. (2000). Paleomagnetism of the Nijo Group and its implication for the timing of clockwise rotation of southwest Japan. *Journal of Mineralogical and Petrological Sciences*, *95*(8), 203–215. https://doi.org/10.2465/jmps.95.203

Hoshi, H., & Teranishi, Y. (2007). Paleomagnetism of the Ishikoshi Andesite: A Middle Miocene paleomagnetic pole for northeastern Japan and tectonic implications. *Earth, Planets and Space*, *59*(7), 871–878. https://doi.org/10.1186/BF03352749

Hoshi, H., & Yokoyama, M. (2001). Paleomagnetism of Miocene dikes in the Shitara basin and the tectonic evolution of central Honshu, Japan. *Earth, Planets and Space*, *53*(7), 731–739. https://doi.org/10.1186/BF03352401

Hosoi, J., Okada, M., Gokan, T., Amano, K., & Martin, A. J. (2015). Early to Middle Miocene rotational tectonics of the Ou Backbone Range, northeast Japan. *Island Arc*, *24*(3), 288–300. https://doi.org/10.1111/iar.12109

Ishikawa, N. (1997). Differential rotations of north Kyushu Island related to middle Miocene clockwise rotation of SW Japan. *Journal of Geophysical Research*, *102*(B8), 17,729–17,745. https://doi.org/10.1029/97JB01343

Itoh, Y. (1988). Differential rotation of the eastern part of southwest Japan inferred from paleomagnetism of Cretaceous and Neogene rocks. *Journal of Geophysical Research*, *93*(B4), 3401–3411. https://doi.org/10.1029/JB093iB04p03401

Itoh, Y., Doshida, S., Kitada, K., & Danhara, T. (2001). Paleomagnetism and fissiontrack ages of the Mt. Wasso moonstone rhyolitic welded tuff in the Ishikawa Prefecture, central Japan. *Bulletin of the Geological Survey of Japan*, *52*(11–12), 573–579. https://doi.org/10.9795/bullgsj.52.573

Itoh, Y., & Hayakawa, H. (1988). Magnetostratigraphy of neogene rocks around the Yatsuo area in Toyama prefecture, Japan. *The Journal of the Geological Society of Japan*, *94*, 515–525.

Itoh, Y., & Ito, Y. (1989). Confined ductile deformation in the Japan arc inferred from paleomagnetic studies. *Tectonophysics*, *167*(1), 57–73. https://doi.org/10.1016/0040-1951(89)90294-1

Itoh, Y., & Kitada, K. (2003). Early Miocene rotational process in the eastern part of south-west Japan inferred from paleomagnetic studies. *Island Arc*, *12*(4), 348–356. https://doi.org/10.1046/j.1440-1738.2003.00402.x

Kojima, T., Okada, M., Ohira, H., Tokieda, K., Komuro, H., & Amano, K. (2001). Paleomagnetism and fission-track ages of Oki-Dogo Island in Southwest Japan. *Earth, Planets and Space*, *53*(1), 45–54. https://doi.org/10.1186/BF03352361

Kovalenko, D. (1992). Paleomagnetism in the Paleogene Suites of the Il'pinskiy Peninsula, Kamchatka. *Geotectonics*, *26*, 408–421.

Kovalenko, D. (1993). Paleomagnetism of Paleogene complexes at the Ilpinsky Peninsula (the South Koryak Plateau). *Fizika Zemli*, *5*, 72–80.

Kovalenko, D. (1996). Paleomagnetism and kinematics of the Central Olyutorsky Range, Koryak Highland. *Geotectonics*, *30*, 243.

Kovalenko, D., Chernov, E., & Kurilov, D. (2002). Paleomagnetism of Upper Cretaceous and Cenozoic geological complexes in the western and eastern Kamchatka areas. *Fizika Zemli*, *38*, 469–484.

Kovalenko, D., & Kravchenko-Berezhnoy, I. (1999). Paleomagnetism and tectonics of Karaginsky Island, Bering Sea. *Island Arc*, *8*, 426–439.

Kovalenko, D., & Remizova, L. (1997). Paleomagnetism of the Northwestern Olyutorskii Zone, Southern Koryak Upland. *Izvestiya Physics of the Solid Earth*, *33*, 589–598.

Levashova, N. M., Bazhenov, M. L., & Shapiro, M. N. (1997). Late Cretaceous paleomagnetism of the East Ranges island arc complex, Kamchatka: Implications for terrane movements and kinematics of the northwest Pacific. *Journal of Geophysical Research*, *102*(B11), 24,843–24,857. https://doi.org/10.1029/97JB00780

Levashova, N. M., Shapiro, M. N., & Bazhenov, M. L. (1998). Late Cretaceous paleomagnetic data from the Median Range of Kamchatka, Russia: Tectonic implications. *Earth and Planetary Science Letters*, *163*(1–4), 235–246. https://doi.org/10.1016/S0012-821X(98)00190-3

Nakajima, T., & Hirooka, K. (1986). Clockwise rotation of Southwest Japan inferred from paleomagnetism of Miocene rocks in Fukui Prefecture. *Journal of Geomagnetism and Geoelectricity*, *38*, 513–522.

Otofuji, Y.-I., Itaya, T., & Matsuda, T. (1991). Rapid rotation of southwest Japan—Palaeomagnetism and K-Ar ages of Miocene volcanic rocks of southwest Japan. *Geophysical Journal International*, *105*(2), 397–405. https://doi.org/10.1111/j.1365-246X.1991.tb06721.x

Otofuji, Y.-I., & Matsuda, T. (1983). Paleomagnetic evidence for the clockwise rotation of Southwest Japan. *Earth and Planetary Science Letters*, *62*(3), 349–359. https://doi.org/10.1016/0012-821X(83)90005-5

Otofuji, Y.-I., & Matsuda, T. (1984). Timing of rotational motion of Southwest Japan inferred from paleomagnetism. *Earth and Planetary Science Letters*, *70*(2), 373–382. https://doi.org/10.1016/0012-821X(84)90021-9

Otofuji, Y.-I., Nishizawa, Y., Tamai, M., & Matsuda, T. (1997). Palaeomagnetic and chronological study of Miocene welded tuffs in the northern part of Central Japan: Tectonic implications for the latest stage of arc formation of Japan. *Tectonophysics*, *283*(1–4), 263–278. https://doi.org/10.1016/S0040-1951(97)00065-6

Pechersky, D. M., Levashova, N. M., Shapiro, M. N., Bazhenov, M. L., & Sharonova, Z. V. (1997). Palaeomagnetism of Palaeogene volcanic series of the KamchatskyMys Peninsula, East Kamchatka: The motion of an active island arc. *Tectonophysics*, *273*(3–4), 219–237. https://doi.org/10.1016/S0040-1951(97)00002-4

Sawada, Y., Mishiro, Y., Imaoka, T., Yoshida, K., Inada, R., Hisai, K., et al. (2013). K-Ar ages and paleomagnetism of the Miocene in the Izumo Basin, Shimane Prefecture. *Journal of the Geological Society of Japan*, *119*(4), 267–284. https://doi.org/10.5575/geosoc.2012.0044

Takahashi, M., Hoshi, H., & Yamamoto, T. (1999). Miocene counterclockwise rotation of the Abukuma Mountains, Northeast Japan. *Tectonophysics*, *306*, 19–31.

Tamaki, M., Itoh, Y., & Watanabe, M. (2006). Paleomagnetism of the Lower to Middle Miocene Series in the Yatsuo area, eastern part of southwest Japan: Clockwise rotation and marine transgression during a short period. *Bulletin of the Geological Survey of Japan*, *57*, 73–88.

Yamaji, A., Momose, H., & Torii, M. (1999). Paleomagnetic evidence for Miocene transtensional deformations at the eastern margin of the Japan Sea. *Earth, Planets and Space*, *51*, 81–92.